

GOLD ANOMALY FORMATION IN AREAS OF COVER AT KARARI AND NORTHERN LEONORA, AND IMPLICATIONS FOR EXPLORATION

*M. Cornelius, B. Singh, I.D.M. Robertson, R.R. Anand,
R. Hough, A. Cornelius*

CRC LEME OPEN FILE REPORT 152

December 2006

CRCLEME

(CRC LEME Restricted Report 214R December, 2004.
2nd Impression 2006.)

GOLD ANOMALY FORMATION IN AREAS OF COVER AT KARARI AND NORTHERN LEONORA, AND IMPLICATIONS FOR EXPLORATION

*M. Cornelius, B. Singh, I.D.M. Robertson, R.R. Anand,
R. Hough, A. Cornelius*

CRC LEME OPEN FILE REPORT 152

December 2006

(CRC LEME Restricted Report 214R December, 2004.
2nd Impression 2006.)

© CRC LEME 2006

CRC LEME is an unincorporated joint venture between CSIRO-Exploration & Mining, and Land & Water, The Australian National University, Curtin University of Technology, University of Adelaide, Geoscience Australia, Primary Industries and Resources SA, NSW Department of Primary Industries and Minerals Council of Australia.

Headquarters: CRC LEME c/o CSIRO Exploration and Mining, PO Box 1130, Bentley WA 6102, Australia

This report summarizes research completed as a collaborative project between CRC LEME and Sons of Gwalia Ltd. The report was originally published in December 2004 and had a one-year confidentiality limitation from that date, which has since expired.

Copies of this publication can be obtained from:

The Publications Officer, CRC LEME, c/- CSIRO Exploration & Mining, PO Box 1130, Bentley WA 6102, Australia. Information on other publications in this series may be obtained from the above, or from <http://crlceme.org.au>. Electronic copies of this publication may be obtained in pdf format from <http://clw.csiro.au/publications/>

Cataloguing-in-Publication:

Gold anomaly formation in areas of cover at Karari and Northern Leonora, and implications for exploration.

ISBN 1921 039 523

1. Regolith-landforms – Yilgarn 2. Geochemistry - Yilgarn 3. Gold – Yilgarn 4. Calcrete 5. Biogeochemistry 6. Lag 7. Laser ablation ICPMS

I. Cornelius M.

II. Title

CRC LEME Open File Report 152.

ISSN 1329-4768

Addresses and affiliations of all authors

CRC LEME
c/- CSIRO Exploration and Mining
P.O. Box 1130,
Bentley
WA 6102.

The user accepts all risks and responsibility for losses, damages, costs and other consequences resulting directly or indirectly from using any information or material contained in this report. To the maximum permitted by law, CRC LEME excludes all liability to any person arising directly or indirectly from using any information or material contained in this report.

© Cooperative Research Centre for Landscape Environments and Mineral Exploration 2006.

CONTENTS

1. Key findings and implications for exploration
2. Introduction
3. Approach
4. Work completed in 2004
5. Summary of activities at McGrath
 - 5.1 Introduction
 - 5.2 Regolith-landform setting
 - 5.3 Ridge sampling
 - 5.4 Ferruginous granules in transported cover
 - 5.5 Soil gas survey
 - 5.6 Lag survey and other work
 - 5.7 Ferruginous gravel in colluvium
 - 5.8 Vegetation sampling
 - 5.9 Selective extractions of soil
 - 5.10 Partial extractions of basal sediments
6. Summary of activities at Whirling-Dervish
 - 6.1 Introduction
 - 6.2 Geomorphology and drainage
 - 6.3 Regolith stratigraphy
 - 6.4 Logging, patrography and mineralogy of WDDD001
 - 6.5 Distinction between transported and *in situ* material
 - 6.6 Soil geochemical survey
 - 6.7 Biogeochemical survey
 - 6.8 Calcrete analyses
 - 6.9 Laser ablation ICPMS and microprobe study
 - 6.10 Regolith geochemistry and statistical analysis
 - 6.11 Geophysical surveys
7. Summary of research outcomes
8. Acknowledgements
9. References

Annual report on the collaborative project

GOLD ANOMALY FORMATION IN AREAS OF COVER AT KARARI AND NORTHERN LEONORA, AND IMPLICATIONS FOR EXPLORATION

for period ending 31st December 2004

Matthias Cornelius, Balbir Singh, Ian Robertson, Ravi Anand, Rob Hough and Amanda Cornelius

CSIRO/CRC LEME, P.O. Box 1130, Bentley, WA 6102

1. KEY FINDINGS AND IMPLICATIONS FOR EXPLORATION

- In the Carosue Dam mine corridor, pedogenic carbonate (calcrete) is an effective regional surface exploration medium for Au. Samples should be taken selectively from 0 to 4 m depth, ideally from a specific depth interval, and should be tested using diluted HCl to avoid ferruginous or non-carbonated materials.
- Biogeochemical sample media may assist in delineating drill targets within larger Au-in-calcrete anomalies using pathfinder elements such as Mo and Bi. At McGrath, Au in biogeochemical samples appears to indicate the presence of Au mineralization under cover.
- In areas of thick transported cover, ferruginous materials, in particular magnetic detrital gravel beds at or near the base of the cover, may indicate the presence of regional geochemical anomalies e.g., of As and Sb. Ferruginous gravels near the base of transported cover, overlying Au mineralization in fresh rock, may also act as a sink for transported Au, Cd, Hg and other pathfinder elements and thus show the signature of underlying and nearby mineralization. Selective sampling of ferruginous nodules and pisoliths, either by magnet or by visual separation after sieving, is recommended.
- Laser ablation ICPMS analysis using both transects and spot analysis, can determine the location of Au and pathfinder elements within the regolith and improve the understanding of anomaly formation.

2. INTRODUCTION

This report summarises progress during 2004, the first year of a three-year project, subject to annual review and extension by both CRC LEME and Sons of Gwalia Ltd (SOG).

The objective of the project is to investigate processes that lead to the formation of pathfinder and target element signatures within, and on transported cover that blanket mineral deposits located in the eastern Yilgarn Craton. The project forms part of the larger CRC LEME umbrella project 'Yilgarn Field Studies' and is in close collaboration with the CRC LEME 'Mineral and Biological Hosts' Project (aimed at identifying the mineral and biological hosts of target and pathfinder elements) and the CRC LEME 'Objective Logging Project' (aimed at identifying petrophysical characteristics of the regolith). Results of the input from all three projects are summarised in this report.

The research with Sons of Gwalia was initially aimed at investigating the Karari pit, building on earlier work by CSIRO/CRC LEME (Gray *et al.*, 2000). Following field visits and 3D photogrammetric visualisation of the pit (Sirovision), planned pit face sampling could not proceed due to safety concerns. An alternative site was suggested and, in February 2004, work commenced at the Whirling-Dervish Prospect, approximately 1.5 km N of Karari pit. Later, in June 2004, work commenced on a second site, McGrath pit, N of Leonora, following reconnaissance field visits by CSIRO staff.

Biogeochemical and soil extraction studies at McGrath and Whirling-Dervish and soil gas studies at

McGrath, were pilot studies. Further work is to be completed on specific aspects only, e.g., vegetation sampling at McGrath North. Without additional data, i.e., background and infill sampling, the existing data sets are too small for satisfactory conclusions and therefore should only be a guide.

Ongoing research includes microanalysis of ferruginous gravels from the McGrath area, microbial work at McGrath and Whirling-Dervish, and laser ablation work on specific samples from both sites to identify the mineral hosts of specific target and pathfinder elements. This will continue into the first half of 2005, with all results published in 2006.

3. APPROACH

Following field visits and consultation with SOG exploration staff, two principal study sites were selected for the project:

1) The McGrath Au pit, approximately 20 km N of Leonora, is an example of the fresh ground-water environment of the N Yilgarn Craton and facilitates studies on the formation of geochemical signatures in areas of medium (10-20 m) to thick (>60 m) cover. Various geochemical approaches were tested to investigate their potential for exploration in this terrain.

2) The Whirling-Dervish Au prospect near the Karari Mine, in the Carosue Dam mine corridor, is approximately 130 km E of Kalgoorlie in a saline ground water environment (Gray *et al.*, 2000) S of the Menzies Line (Butt *et al.*, 1977; Butt, 1988). The bedrock lithology is mainly felsic. Kaolin-group minerals dominate the residual regolith and much of the transported cover. The geochemical signature of the deposit is very weak due to the lack of Fe-oxides in the regolith and the thickness of transported cover, and this provides an impediment to regional exploration.

Research in 2004 comprised various orientation surveys and collection of base-line data. On this information, more specific studies and follow-up work are suggested for the second project year; the extent of this is being reviewed.

4. WORK COMPLETED IN 2004

- Based on surface mapping and drill hole logging, 3D regolith frameworks were established for both sites and will be discussed within the context of anomaly formation and dislocation.
- Petrographic, mineralogical and geochemical characterisation of the dominant regolith materials.
- Identification of surface, near-surface and intra-sedimentary geochemical signatures of the bedrock mineralization.
- Process interpretation and its importance to exploration.

Some aspects of the work at the time of reporting are still in progress and cannot be included; in particular, the outcome of microbiological studies (both sites), soil gas analyses (McGrath) and laser ablation analyses (McGrath).

5. SUMMARY OF ACTIVITIES AT McGRATH

5.1 Introduction

McGrath is a mafic- and ultramafic-hosted Au deposit with a resource of approximately 200 000 oz being worked as a small open-cut mine. The site was selected as a research site for the following reasons:

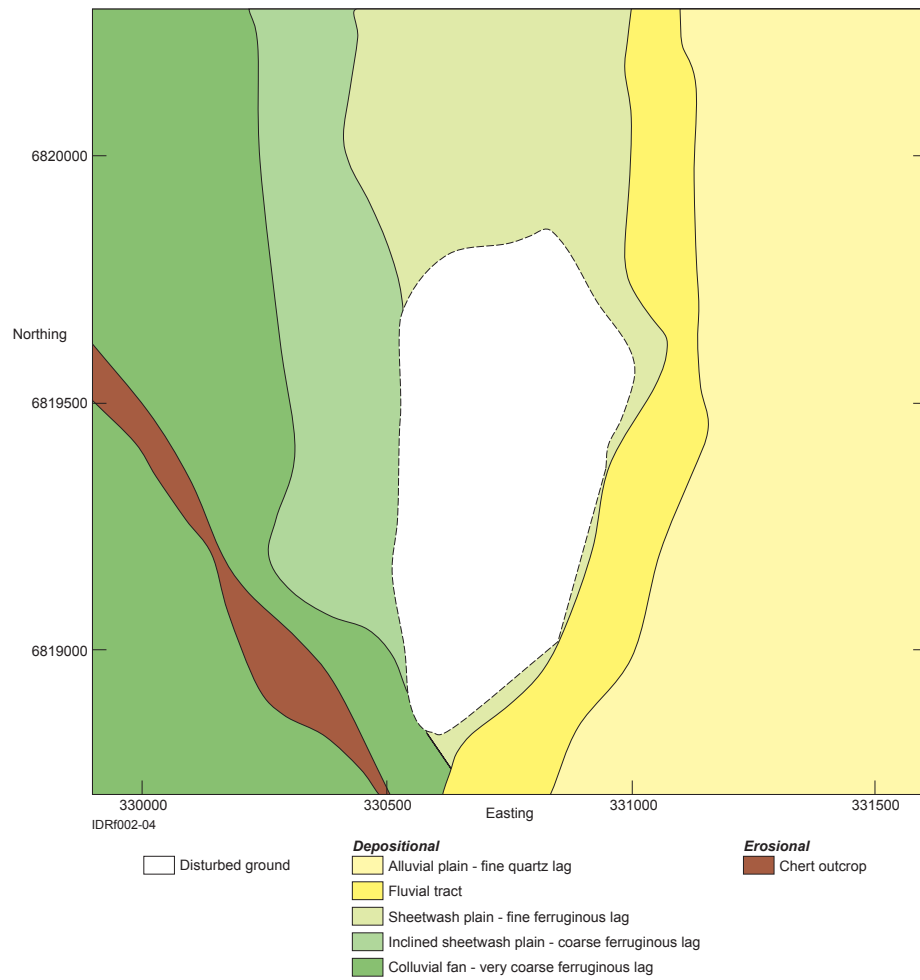


Figure 1. Outline of the mapped units and observation sites.

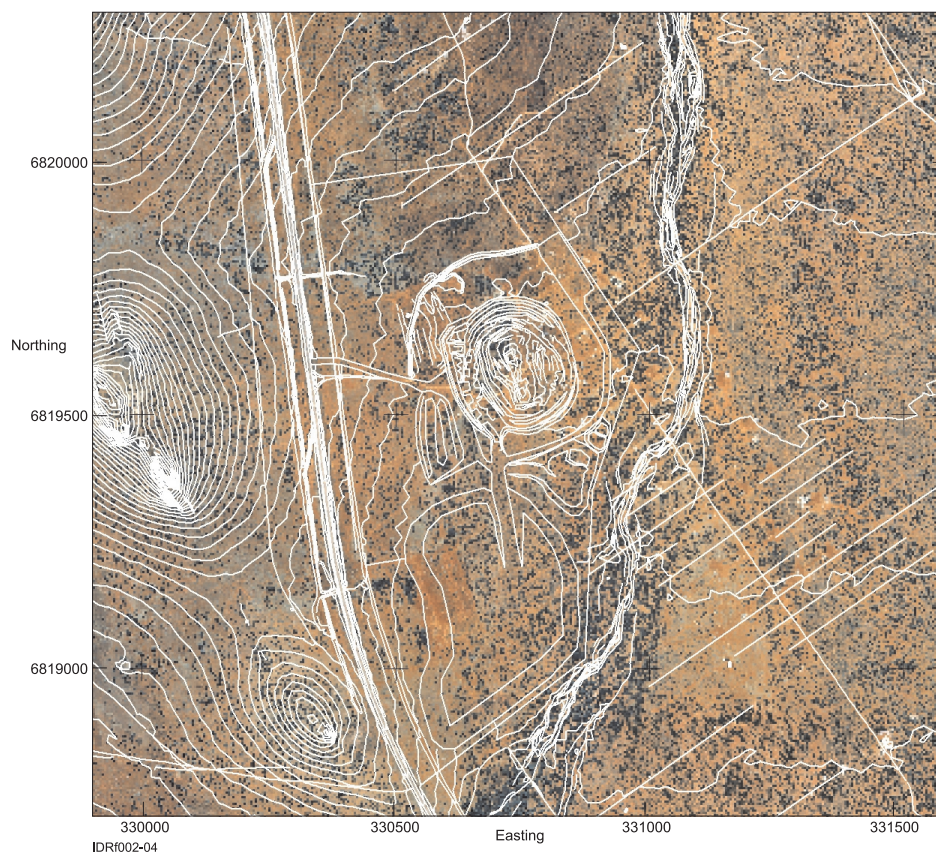


Figure 2. Aerial photograph with contours and mining infrastructure.

- Gold mineralization is associated with a wide range of pathfinder elements (Au-As-Sb-Hg-Cd-Bi-Mo);
- Mineralization extends from an area of shallow cover (N of McGrath pit) to thick cover (S of the pit, with the sediment thickness exceeding 60 m);
- The regolith is well exposed in the open pit. Drill spoil from RC drill holes is still on site and in good condition.

The specific research objectives at McGrath were to:

- Identify geochemical surface signatures (biota, partial or selective extraction, gas, lag) in areas of medium to thick cover (McGrath North at 9400N and McGrath South at 8000N-8400N).
- Identify any intra-sedimentary signatures that can enhance the search halos of drill holes and, hence, the geochemical footprint of the mineralization, particularly in areas of deep cover, (i.e., at McGrath South).

5.2 Regolith-landform setting

Purpose and Method

Surface mapping at McGrath gives an overview of the exposed regolith and its surface dynamics. Eight E-W traverses at 200 m intervals (Figure 1) were used to map the area surrounding the McGrath pit (1.6 x 1.7 km). A steady course (± 20 m N or S of line, avoiding obstructions) was kept by GPS and observations were made against GPS coordinates (Appendix A). Photos were taken of critical areas and typical materials were sampled. A map was produced from these observations (Figure 1). This may be compared to the air photo of the area (Figure 2).

Regolith-landform units

The ground immediately surrounding the pit and waste dump had been scraped off mechanically in preparation for mining and the original surface has been lost. This area was mapped as disturbed ground. Much of the remaining area is nearly pristine, except for the main road and access tracks.

Chert ridge

A major topographic feature is a ridge of chert (Figure 3), striking NNW across the SW corner of the mapped area. The best outcrop is a narrow but steep ridge (Figure 4) with saddles of low outcrop and scree. The chert is fine-grained, greenish and strongly sheared with mangiferous dendrites on fracture surfaces. In places it is brecciated with hematite.

Colluvial fan

Sloping out to the ENE and WSW from the chert ridge are colluvial slopes or fans (Figure 5). These are partly covered by a coarse (>40 mm), blocky black to brown dominantly lithic lag (Figure 6) from which most of the fine lag has been washed, on a brown soil or hardpanised colluvium (Figure 7). A few small, linear outcrops of schistose basement rocks protrude through it.

Inclined sheetwash plain

The colluvial slopes merge with an inclined sheetwash plain. The toe of the slope follows the road for much of its length. Here the lag is finer (mostly 15-40 mm). It, in turn, merges to the E with the sheetwash plain where the lag is finer still.

Sheetwash plain

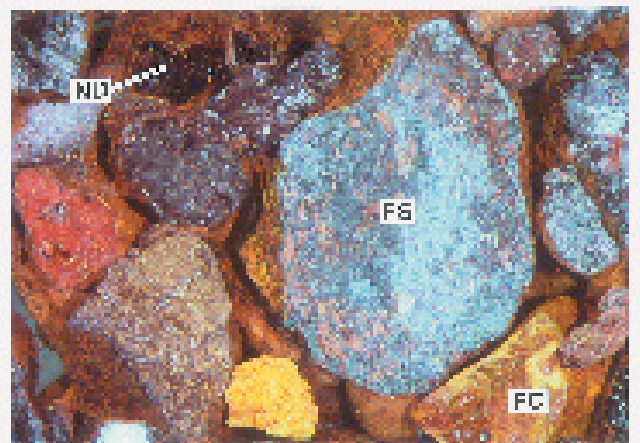
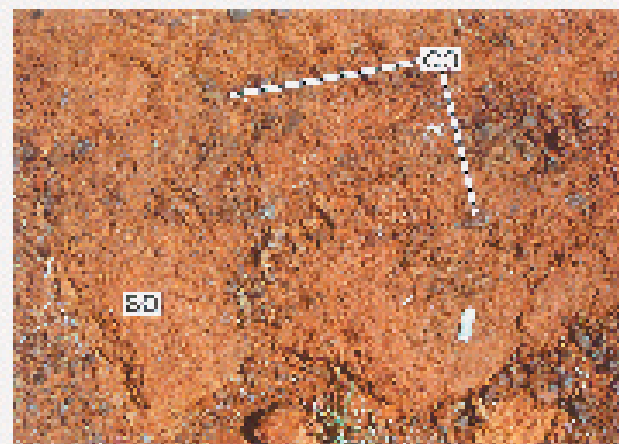
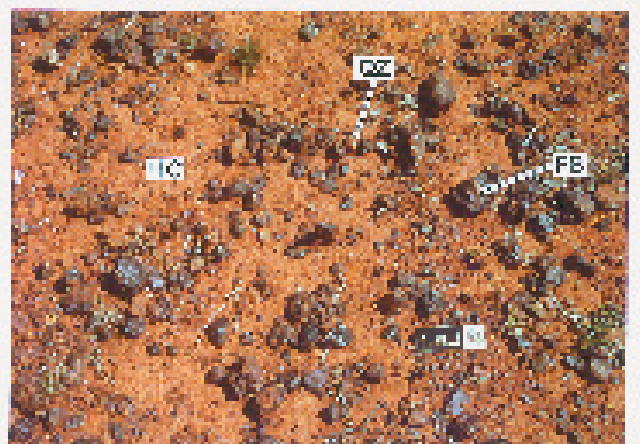
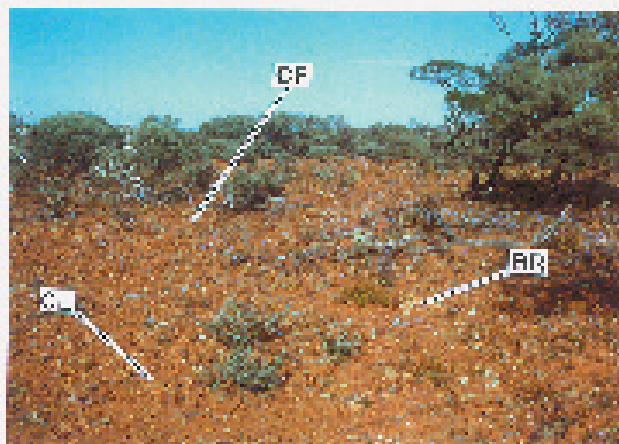
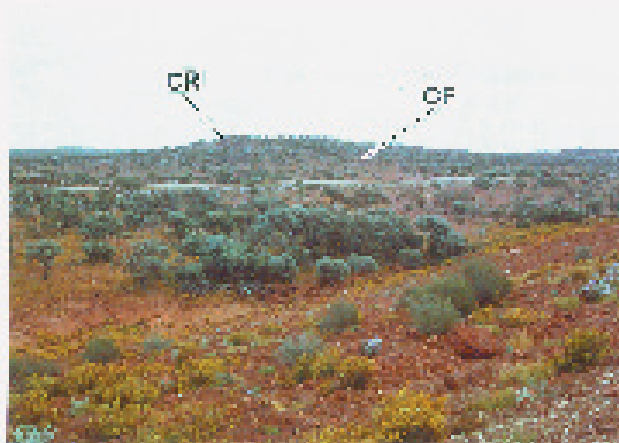
This nearly flat sheetwash plain is dominated by a partial mantle of fine lag (Figure 8) on a brown soil. The polymictic lag is largely brown and lithic but partly black and nodular. Most of the lag is <15 mm although a few larger clasts occur (25-40 mm; Figure 9). It consists mainly of ferruginous clasts (Figure 10) of spongy to massive hematite but some are goethite with contained pseudomorphs after mica and one had a structure reminiscent of a spinifex fabric. Some ferruginous clasts contain chert and remnants of quartz veining.

Alluvial tract

A broad alluvial tract is in abrupt contact with the sheetwash plain in the W and an alluvial plain in the E. The contact with the lag-covered plains to the E and W is marked by the first appearance of channelled concentrations of lag and other erosive structures. The alluvial tract is also marked by the appearance of a small everlasting flower *Rhodanthe chasleyae*, at the time of mapping. Within this

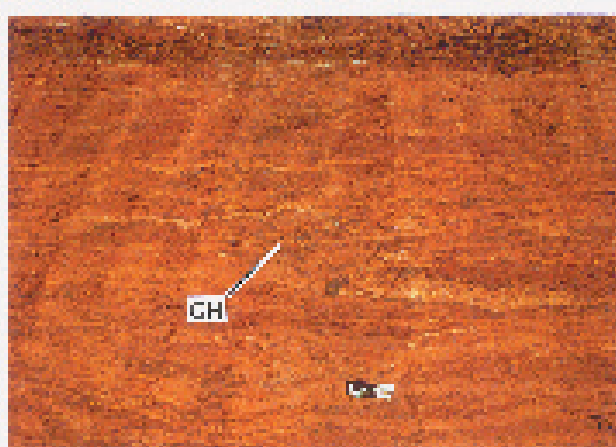
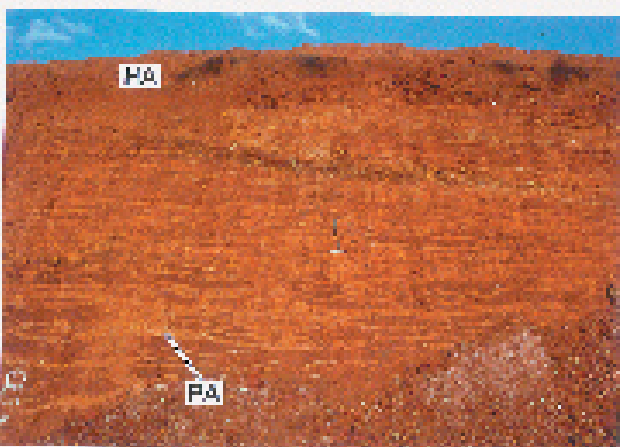
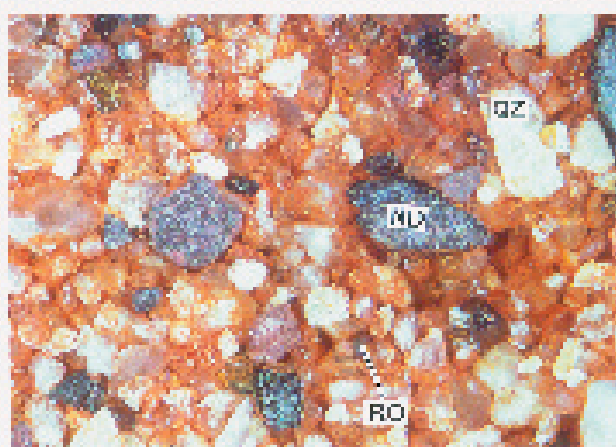
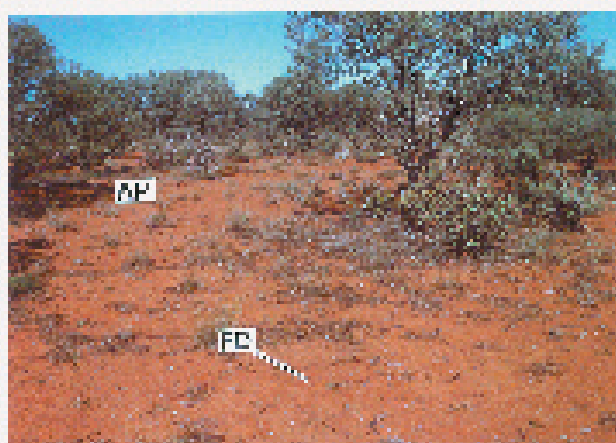
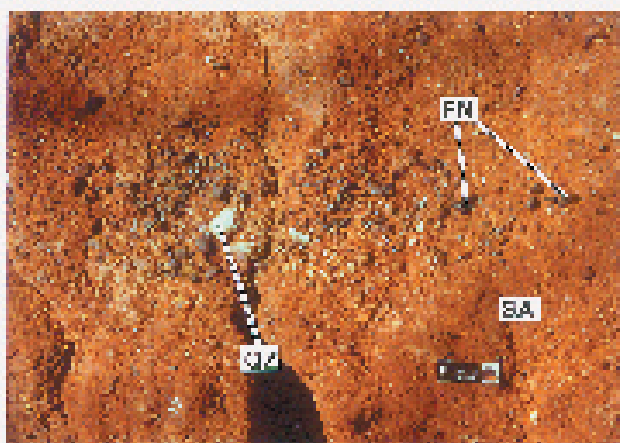
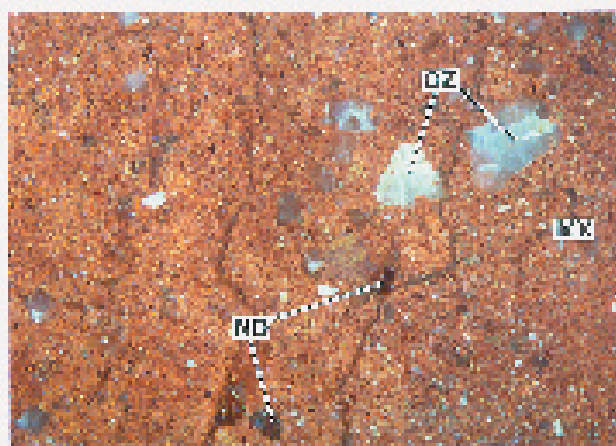
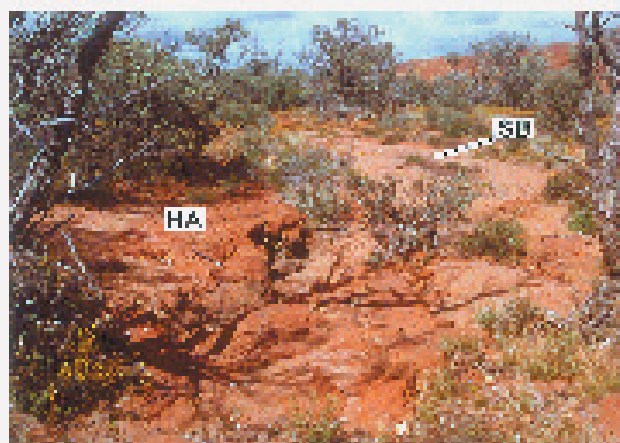
FIGURES 3-10

<p>Figure 3. The low chert ridge (CR) to the W of the road flanked by fans of colluvium (CF).</p>	<p>Figure 4. Blocky outcrops of chert (BC) form the spine of the ridge. McGrath waste dump (WD) in the background.</p>
<p>Figure 5. Coarse lag (CL) developed on gently sloping colluvial fan (CF) with a few small bedrock outcrops (BR) at 330074mE, 6819978mN.</p>	<p>Figure 6. Cobbles of ferruginous saprolite (FS) and minor quartz (QZ) on hardpanized soil and colluvium (HC) at 330074mE, 6819978mN.</p>
<p>Figure 7. Outcrop of hardpanized soil (SO) cementing a colluvium (CO) of angular lithic fragments in a gully beside the road. Scale 30 mm.</p>	<p>Figure 8. Fine lag (FL) on sheetwash plain (SP). Actively mobile lag is concentrated into recent vehicle tracks (TR).</p>
<p>Figure 9. Detail of lag on sheetwash plain. Most fragments are tabular lithic fragments (TL), though some are nodules (ND) and fragments of nodules (FN).</p>	<p>Figure 10. Detail of a polished section of fine polymictic lag, consisting of ferruginous saprolite (FS) with a variety of internal fabrics, ferruginous clay nodules (FC) and broken goethite-rich nodules (ND).</p>



FIGURES 11-18

<p>Figure 11. Bars of eroded hardpanized alluvium (HA) exposed in sandy bed (SB) and banks of stream.</p>	<p>Figure 12. Poorly-sorted hardpanized alluvium, consisting of matrix-supported angular vein quartz (QZ) and minor ferruginous nodules (ND) in a sandy-silty matrix (MX).</p>
<p>Figure 13. A lens of gravel in the hardpanized sandy alluvium (SA), consisting of ferruginous nodules (FN) and vein quartz fragments (QZ).</p>	<p>Figure 14. Alluvial plain (AP) underlain by hardpanized alluvium and mantled by a fine quartz-rich deflation lag (FD).</p>
<p>Figure 15. Fine deflation lag of alluvial plain derived from hardpanized alluvium.</p>	<p>Figure 16. Polished section of fine deflation lag, which is rich in angular to subrounded quartz (QZ) and polymictic ferruginous nodules (ND) with a variety of internal fabrics. Some quartz grains show rounding (RO).</p>
<p>Figure 17. Top part of hardpanized colluvium valley-fill exposed in McGrath pit entry ramp showing subhorizontal partings (PA) and an upper thin layer (200-300 mm) of hardpanized sandy alluvium (HA).</p>	<p>Figure 18. Detail of figure 17 showing gravel-filled channels (CH)</p>



tract lies a braided stream with 1-3 channels with a bed of ferruginous saprolite gravel, sand and low bars and exposures of hardpanised alluvium (Figure 11). The upper 300 mm of the alluvium are fine-grained, poorly sorted and consist of sub-angular quartz (2 mm) in a lacy matrix of silicified clay and silt (Figure 12). There are a few small lenses (Figure 13) of polymictic coarser material (<25 mm) (vein quartz, ferruginous nodules and lithic blocks of ferruginous saprolite). The lower 300 mm are much coarser (<60 mm), lenseoid and have a similar composition to the lenses in its upper part.

The hardpanized alluvium consists of poorly sorted sand-sized (0.04-3.0 mm), strained quartz, some round, ferruginous granules, minor chert and traces of microcline, tourmaline and epidote. This is matrix supported by a red-brown, Fe-stained mass of clay with weathered mica remnants. Voids have been partly filled with, and lined, by deep red-brown, delicately banded aluminosilicate cement. Probably the provenance was dominantly granitic (quartz, microcline, tourmaline, mica) with some input of chert but also deeply weathered (angular, shardy quartz, ferruginous granules, clay and lacking significant feldspar). Since deposition, it has suffered partial matrix dissolution and deposition of a neofomed banded aluminosilicate cement by percolating groundwaters.

Alluvial plain

This plain surface (Figure 14) is covered with a brown soil with a partial mantle of fine quartz-rich deflation lag (Figure 15). The lag largely consists of equant but angular quartz (80%) and some ferruginous lithic fragments (Figure 16) and broken nodules (20%) up to 20 mm across but generally less than 5 mm with lesser chert and a trace of microcline. Some of the quartz grains contain inclusions of feldspar and mica. The ferruginous granules are largely of spongy hematite but there is some goethite and ferruginous clay. The quartz (80%) is largely white and 1-5 mm in size. Although it is subangular to angular, the edges are slightly rounded and frosted, implying transport. A very few quartz grains are highly rounded. This lies on a thin red, hematite-stained sand of clear quartz that is, in part, aeolian. Beneath lies a hardpanized alluvial grit (see above) from which the lag was clearly derived.

Hardpanized colluvium and alluvium

The only significant 3D exposure is in the McGrath pit, where several metres of colluvium-alluvium are exposed (Figure 17), covering the palaeochannel clays and the residual profile beneath. The lower part of this transported layer is coarse, massive and probably colluvial. The upper part is strongly hardpanized, shows subhorizontal partings and consists of silty-sandy layers alternating with gravel-

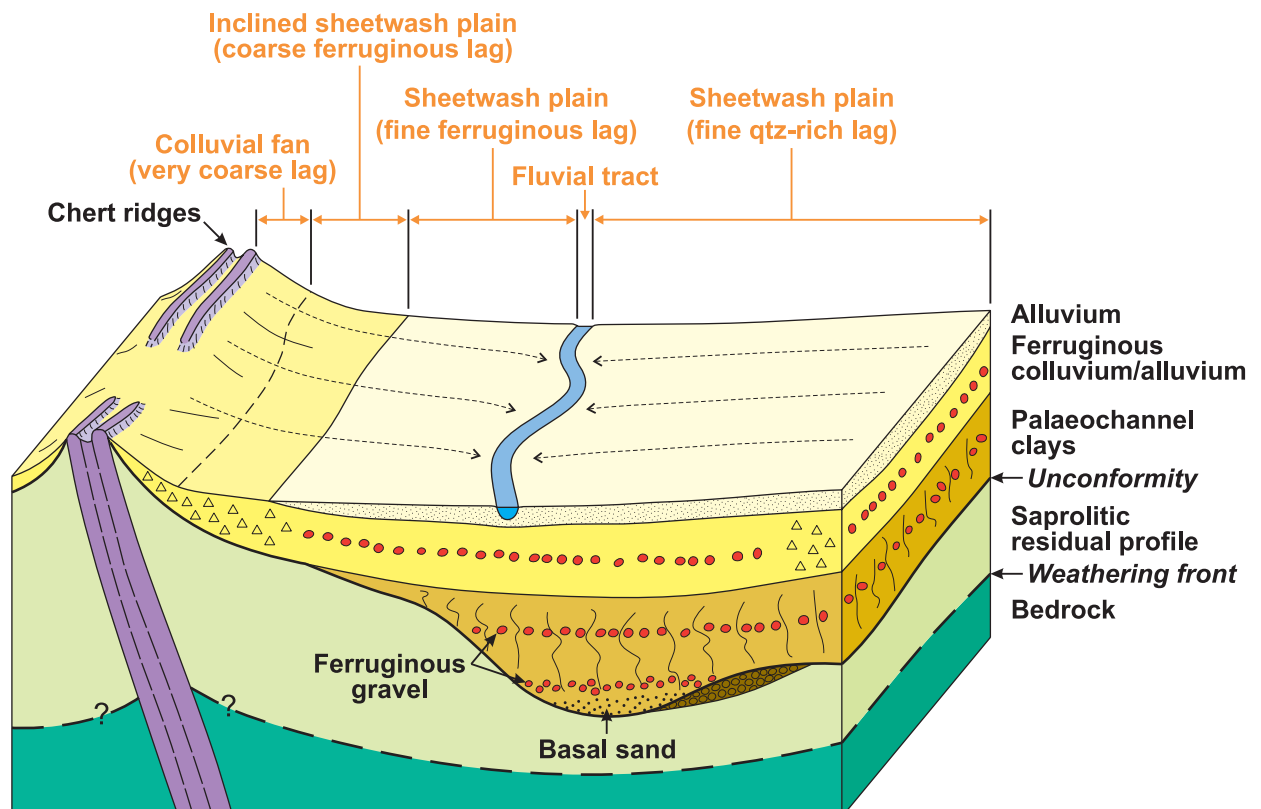


Figure 19. 3D landscape model for McGrath.

TABLE 1
LOCATIONS OF RIDGE SAMPLES

Sample	From			To			Notes
	Easting	Northing	Height	Easting	Northing	Height	
MGI005	330148	6819543	411	330136	6819537	411	Chip sample
MGI006	330016	6819459	416	330001	6819451	417	Chip sample
McGNRidge001	329937	6820268	416	329853	6820270	420	A Hard, B soft
McGNRidge002	329811	6820277	424	329730	6820301	427	A Hard, B soft

filled channels (Figure 18) and is largely fluvial. This is overlain by about 200 mm of hardpanized more recent alluvium (Figure 17), similar to that found in the bed of the fluvial tract.

Surface dynamics

The hardpanized alluvium in the bed of the fluvial tract underlies the alluvial plain and forms a thin layer over the hardpanized colluvium-alluvium in the McGrath pit. It is unlikely that the braided fluvial tract has always occupied its current position, but has probably migrated laterally (Figure 19) across areas now occupied by the alluvial and sheetwash plains (but not the inclined sheetwash plain).

The highly mobile, ferruginous, fine lag, which appears to the W of the fluvial tract and characterises the sheetwash plain, is not developed significantly on the alluvial plain. This is probably a dynamic phenomenon. The lag has probably migrated down-slope from the inclined sheetwash plain, and is carried away when it reaches the stream. Little of it has been moved by bioturbation of underlying ferruginous colluvial-alluvial materials, although it is possible that a small proportion of this fine lag could have been brought to the surface, through the layer of hardpanized alluvium, by ants.

5.3 Ridge sampling

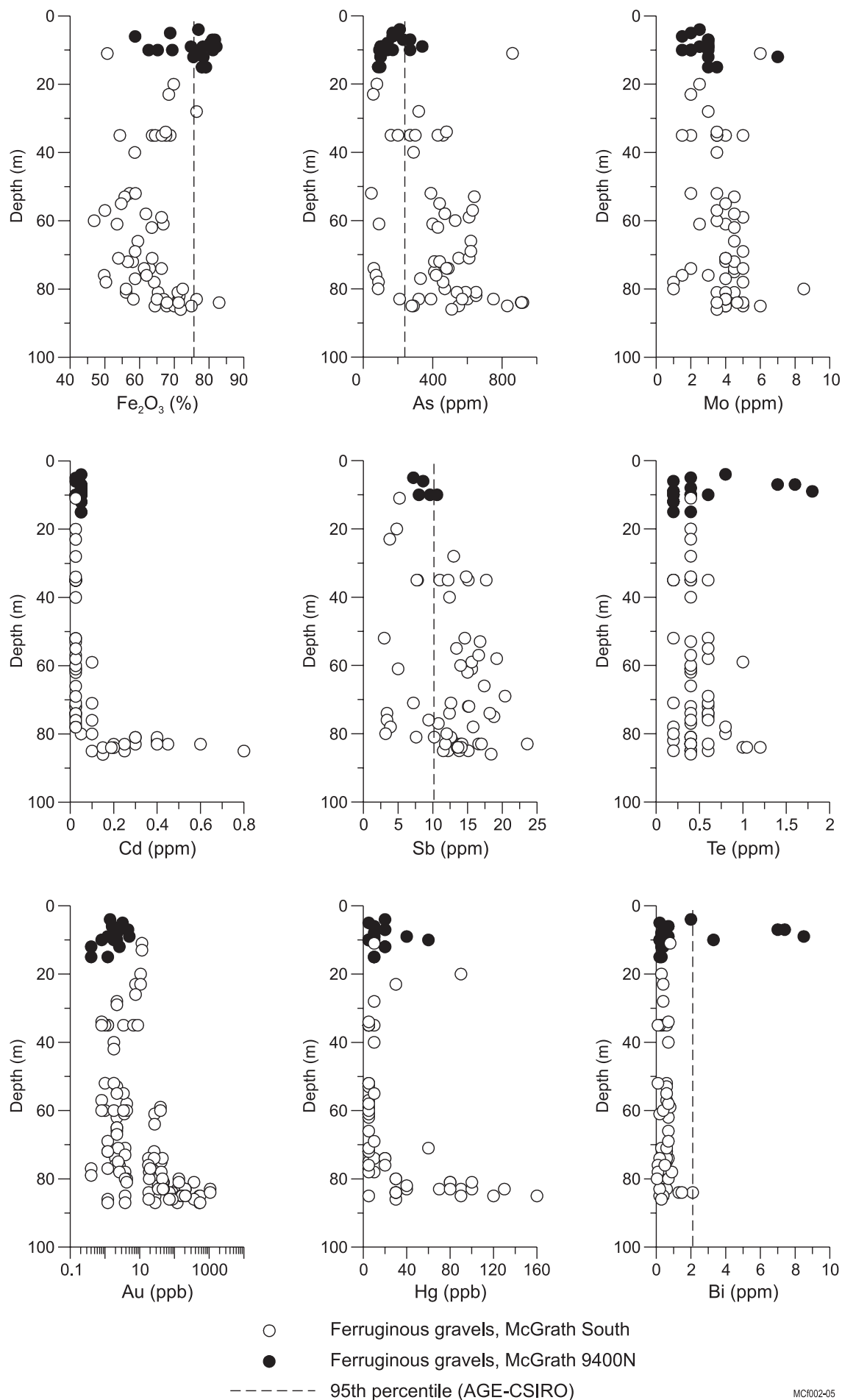
Small outcrops of green cherty materials on the ridge to the W of McGrath North were chip-sampled (Table 1) on traverses approximately normal to the strike, in order to obtain geochemical information of the probable lag source material. Darker, cherty rocks were similarly chip-sampled to the W of the McGrath pit. (MGI05 and MGI06; Table 1). Some of the materials were hard, ferruginous and siliceous (A sample) and likely to have contributed to the lag; others were soft and schistose (B sample) and more likely to have contributed to the soil. The samples were subdivided accordingly, pulped and analysed (Appendices B and C, rock chips).

The cherts from W of McGrath are siliceous but do not show any unusual geochemistry, apart from carrying some As. The ferruginous cherts (Fe 37-40%) from McGrath North are relatively enriched in Hg (60-80 ppb), As (230-960 ppm) and slightly enriched in Cu (130-155 ppm), Ni (475-520 ppm), Zn (105-215 ppm) and Mn (400-1200 ppm), probably reflecting their contained Fe-oxides. The soft outcropping, schistose materials are relatively enriched in Si (27-31 %), Al (7-8 %), K (4600-7100 ppm) and Rb (25 ppm). Their Cr and Ti geochemistry indicates these schistose rocks are probably mafic and are deeply weathered.

5.4 Ferruginous gravel in transported cover

Work by CSIRO and CRC LEME, over the past 20 years, has intensively investigated the use of lateritic residuum, preserved either at surface or under transported overburden. In particular, palaeo-lag (at the interface between the residual weathered profile and the transported cover) is a useful sample medium beneath transported overburden (Robertson and King, 1998). If preserved, it provides a broader and more consistent, though generally weaker, expression of residual profile mineralization than the top of the residual profile itself. However, palaeo-lag is either not preserved or may not have been formed in some places. Also, the unconformity can be difficult to identify and sample.

In many parts of the Yilgarn Craton, the colluvial-alluvial sediments that fill old valleys also contain gravel layers, up to several metres thick, that lie a few metres above the unconformity and further up in the sedimentary sequence (Anand and Paine, 2001). Much of the upper gravel layers may have formed within the sediment before reworking and accumulation, and is therefore unlikely to provide information on the local bedrock composition. However, gravel near the base of the transported



MC1002-05

Figure 20. Element concentrations in ferruginous gravel from McGrath South and North (9400N) versus drill depth. For some elements, 95th percentiles of Yilgarn laterite composition are given for comparison.

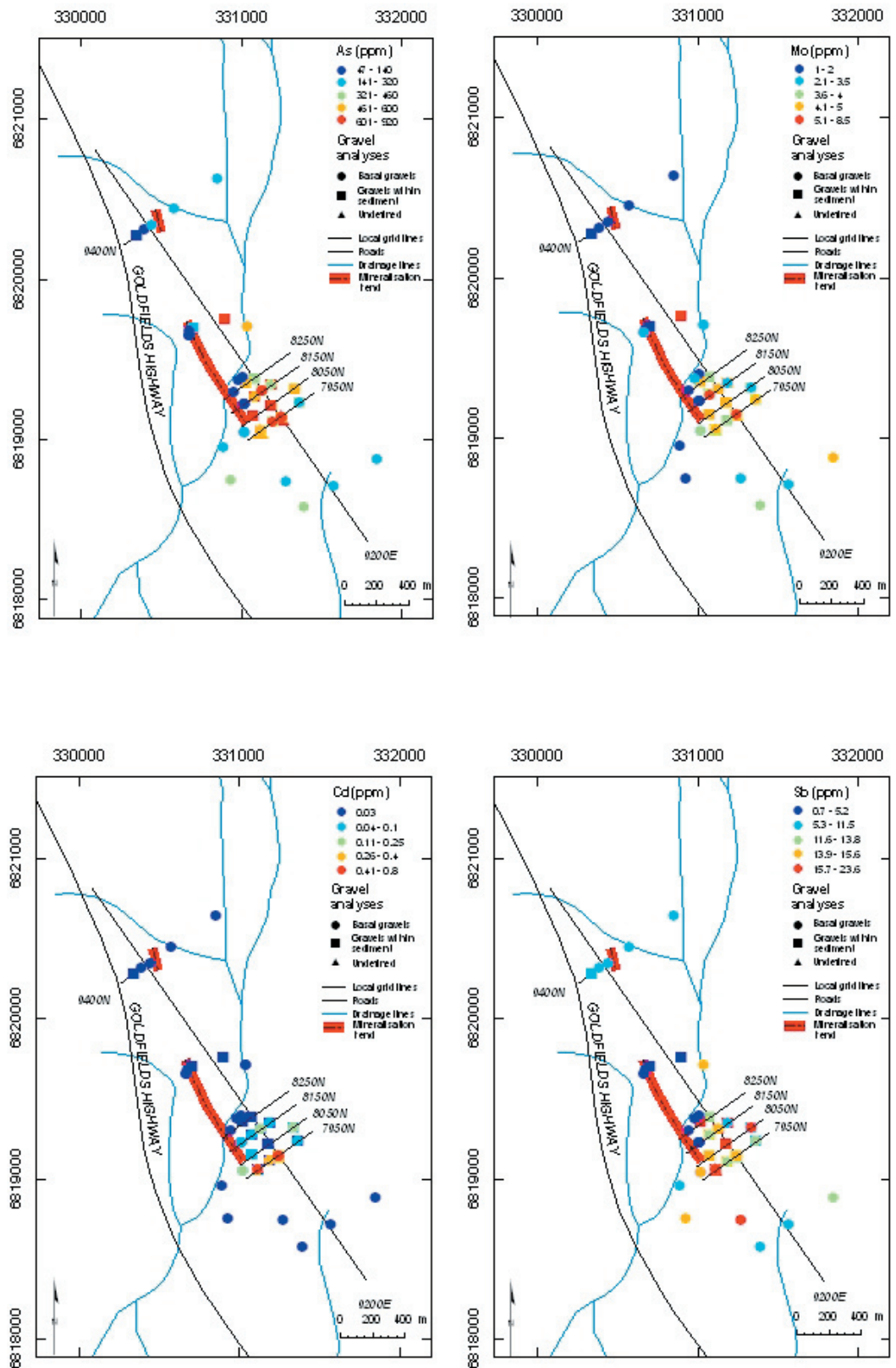


Figure 21A-D Element concentration maps with contoured base of transported overburden.

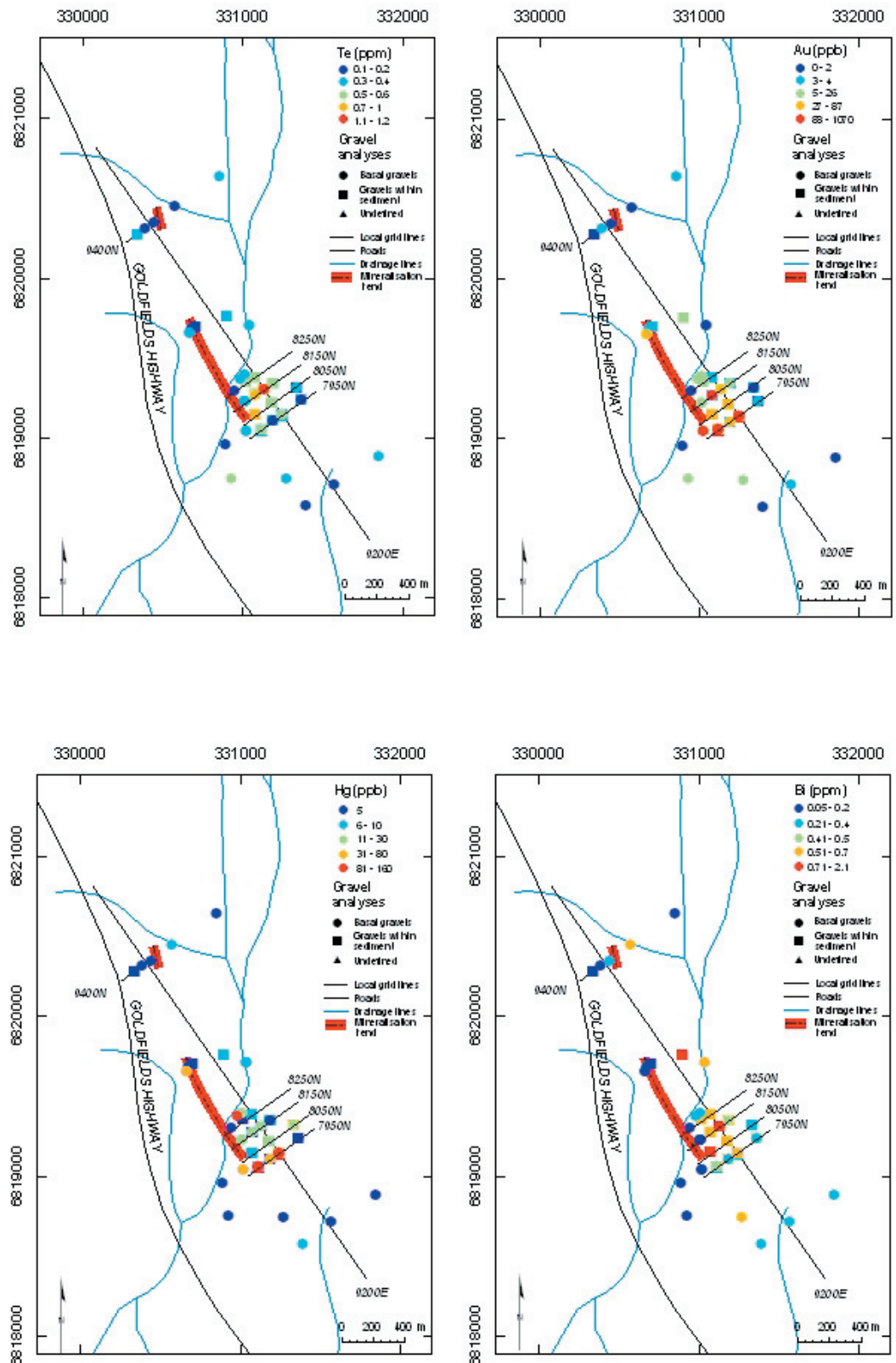


Figure 21E-H Element concentration maps with contoured base of transported overburden.

sequence not only contains lithic components but also detrital ferruginous, often magnetic clasts, that may have been derived from erosion of nearby weathering surfaces after the valley was formed; in essence, another form of palaeo-lag. These materials may show a geochemical signature of the bedrock they formed on and can add considerable value to a deep reverse circulation (RC) or aircore (AC) drill hole by detecting the signature of Au mineralization that could otherwise be overlooked due to the limited size of its primary halo.

Commonly, gravel layers are obvious in drill spoil and can be further identified by their strong magnetic susceptibility (abundant magnetite). Concentration can be achieved by handheld magnet and sieving; hand picking can concentrate non-magnetic gravels.

Drill spoil from RC, rotary airblast (RAB) or AC holes is well preserved at surface around McGrath pit and offers an opportunity to investigate the use of transported ferruginous materials for prospect-scale exploration.

In addition to detrital geochemical signatures in gravel (e.g., As and Sb), the ferruginous gravel at McGrath may have also retained metals that were hydromorphically dispersed from the bedrock (in groundwater or even as gaseous phases) during post-depositional weathering. In particular, Au, As, Hg and Cd concentrations are elevated in basal gravel above or close to bedrock mineralization along line 7950N whereas, in near-basal gravel along 9400N (McGrath North), Te, Hg, Bi and, to a lesser degree, As and Mo are high (Figure 20).

Analytical work

Approximately 75 samples of ferruginous gravel were collected from RC drill holes S and E of McGrath pit. Samples were also collected from AC or RAB holes several hundred metres away to provide a geochemical background. The samples were analysed by XRF, ICP-MS and ICP-OES for a suite of 52 elements (Appendix C, Ferruginous gravel). Several samples were also separated into magnetic, non-magnetic and lithic components, which were then analysed separately. Microprobe and laser ablation investigation for Au, Cd, Hg and other pathfinder elements on polished blocks will be completed in early 2005 to identify the siting of these elements, e.g., in the cutans or throughout the clasts.

At McGrath South, the regolith comprises the following units: -

0 - 5 m	Pinkish weakly calcareous hardpanized colluvium containing magnetic gravel
5 - 13 m	Reddish brown coarse, highly magnetic colluvium/alluvium
13 - 20 m	Red clay with minor magnetic gravel
20 - 32 m	Megamottled clays with minor magnetic gravel

TABLE 2
MAGNETIC AND NON-MAGNETIC GRAVEL GEOCHEMISTRY - McGRATH S

Sample no		1601567_2		1601568_2		1601552_2		1601689_2		1601690_2	
Hole		SSC877		SSC877		SSD868		SSD905		SSD905	
Grid E		9046		9046		9200		9205		9205	
Grid N		7950		7950		8150		7950		7950	
From		83		85		84		81		83	
To		85		87		86		83		85	
Analyte	Units	non magn	magnetic	non magn	magnetic	non magn	magnetic	non magn	magnetic	non magn	magnetic
TiO ₂	%	0.87	1.15	0.73	1.28	0.76	1.05	1.2	1.14	0.82	1.1
Fe ₂ O ₃	%	65.2	76.4	64.4	74.9	67.9	82.9	56.1	71	58.2	66.9
V	ppm	950	1220	1050	1310	960	1240	930	1040	920	1070
Cr	ppm	1090	1150	930	1460	2730	3050	850	1180	1190	1620
As	ppm	600	320	550	290	910	920	590	540	750	570
Zr	ppm	130	170	120	150	140	180	210	180	150	180
Mo	ppm	4.5	4	4	4	5	3.5	3.5	4	4	4
Cd	ppm	0.45	0.3	0.25	0.15	0.2	0.15	0.3	0.3	0.6	0.4
Sb	ppm	16.6	17	11.5	12.2	13.5	14.1	7.6	10.2	11.8	14
Te	ppm	0.4	0.4	0.4	0.6	1	1.2	0.4	0.4	0.4	0.6
Au	ppb	153	164	519	25.5	76.4	18.2	48.6	46.6	207	185
Hg	ppb	100	40	120	90	30	30	80	80	130	70
Bi	ppm	0.3	0.5	0.3	0.4	1.3	2.1	0.3	0.5	0.3	0.6
(Zr/V)100	<16 in basal gravel	14	14	11	11	15	15	23	17	16	17

32 – 45 m	Puggy clays with <u>magnetic, spheroid pisoliths</u> and granules
45 – 55 m	Silty clay without gravel
55 – 60 m	Slightly puggy, yellowish clays with magnetic gravel
60 – 65 m	<u>Magnetic gravel layer</u> with a little red matrix; gravel clasts 10-15 mm
65 – 71 m	Reddish clay with few magnetic gravels
71 – 73 m	Yellow clay with dolocrete
73 – 74 m	Yellow sandy clay
74 – 77 m	<u>Magnetic gravel layer</u>
77 – 79 m	<u>Magnetic gravel layer</u> with quartz clasts
79 – 80 m	Lower saprolite, slightly talcose, possibly with magnetite, rock fragments
80 – 82 m	Yellow lower saprolite with many rock fragments
82 – 84 m	Saprock, abundant rock fragments

Throughout the McGrath South area, gravel layers occur at approximately 75 m, 60 m and 40 m vertical depth. The origin of these gravel accumulations is uncertain. Deeper gravel layers may be lateritic residuum and lithic fragments washed into the valley from nearby hills. These materials are mixed with authigenic gravel formed within the sediments. The generally magnetic (maghemite) character of the ferruginous gravel indicates it was once exposed at surface. Other gravel components, mainly from 40 m depth, have concentric cutans, are well rounded (pisoliths). At other locations, similar gravel clasts have been shown to be authigenic (Anand and Paine, 2001).

Results

Geochemical signature of the Au mineralization in fresh rock

Five fresh rock RC chip samples from the McGrath prospect with Au concentrations of 4.5-40 ppm

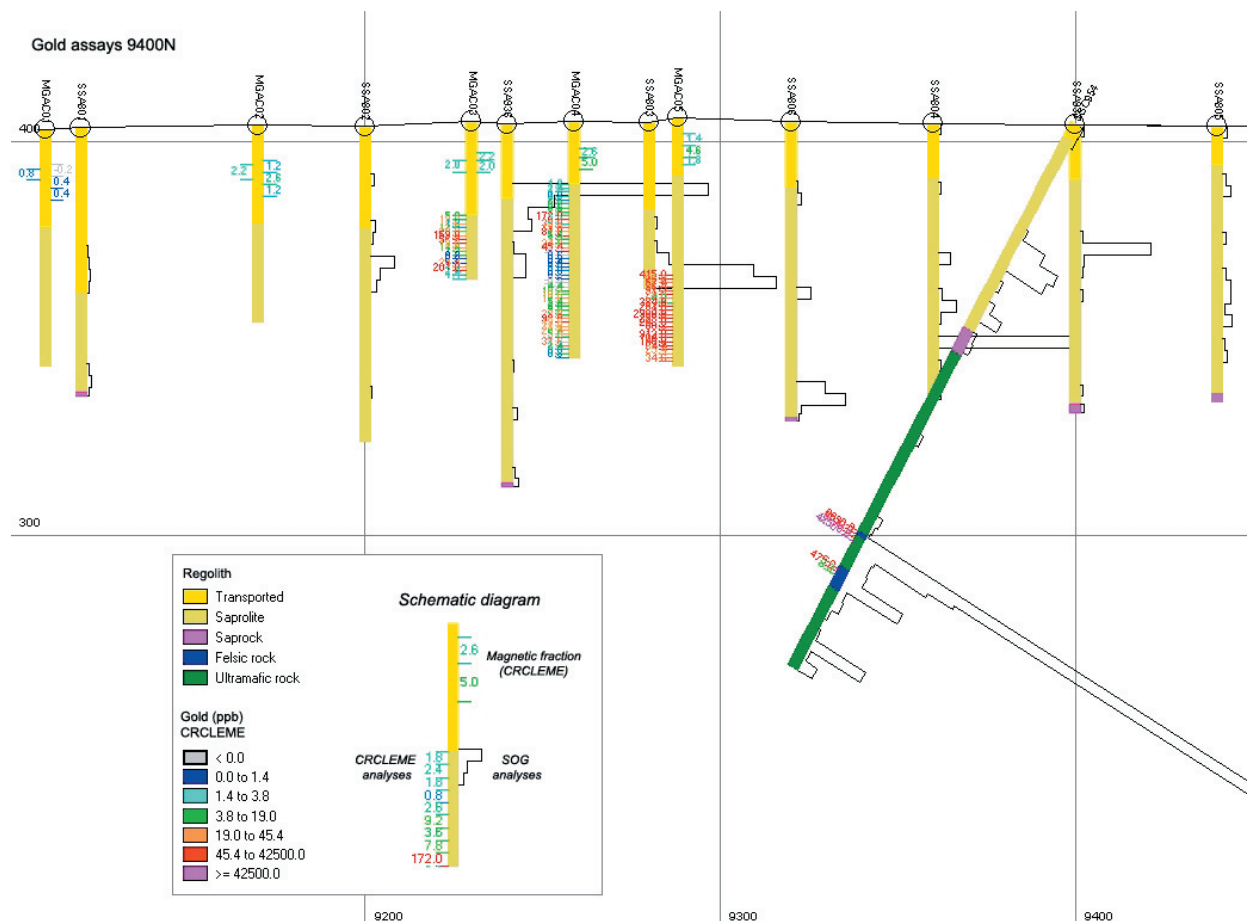


Figure 22. Drill section 9400N showing Au concentrations in ppb and regolith/rock units.

and four samples with <0.5 ppm Au are listed in Appendix C (Fresh rock). Although the number of samples is small, it seems that Bi, Cd, Cs, Cu, Hg, Mo, Rb, Te and Tl may indicate >0.5 ppm Au mineralization. The magnesium concentrations imply all samples are of mafic-ultramafic composition.

Ferruginous gravel within the sedimentary cover

The geochemical compositions of ferruginous gravel from three different gravel lenses within the valley fill in the McGrath South area, and the compositions of ferruginous gravel (exact depths unknown but less than 40 m) from percussion holes several hundred meters to one km S of McGrath are given in Appendix C, Ferruginous gravel.

Arsenic and Sb concentrations in ferruginous gravel (Figure 21A, D) within a 400x600 m area are greater than the 95th percentiles (>230 ppm and >10 ppm respectively) for the Yilgarn Craton, based on data from the CSIRO-AGE database (GSWA, 1998). This seems to outline a prospect-scale geochemical halo around the mineralized zone.

South-east of the mineralization and down-stream in the palaeodrainage, high concentrations of Au, Hg, Cd and P (maxima 1.039, 0.160, 0.800 and 1500 ppm respectively) occur in the basal or near basal

TABLE 3
COMPONENTS OF LAG - McGRATH NORTH

Sample No	Coordinates (m)		Notes	Percentages <5 mm		ΔPercent (all fractions)			Appearance		
	Easting	Northing		% Magnetic	% Nonmagnetic	%>5 mm	%<5 mm Magnetic	%<5 mm Nonmagnetic	>5 mm	<5 mm Nonmagnetic	<5 mm Magnetic
1	330722	6820556		70.5	29.5	39.0	43.0	18.0	L=N	L>G	G
2	330620	6820443		62.3	37.7	50.6	30.8	18.6	L=N	L>G	G
3	330566	6820416		62.8	37.2	31.3	43.1	25.6	L=N	L>G	G
4	330500	6820360	DH5	57.8	42.2	30.7	40.0	29.3	L=N	L=G	G
5	330478	6820370		44.8	55.2	29.9	31.4	38.7	L=N	L>G	G
6	330466	6820366	DH4	41.3	58.7	26.4	30.4	43.2	L=N	L>G	G
7	330451	6820364		46.4	53.6	45.5	25.3	29.2	L=N	G>L	G
8	330433	6820357	DH3	37.5	62.5	24.0	28.5	47.4	L=N	G>L	G
9	330407	6820340		37.9	62.1	52.6	18.0	29.4	L=N	G=L	G
10	330383	6820324	DH2	34.7	65.3	56.6	15.0	28.3	L=N	L>G	G
11	330349	6820307		15.0	85.0	60.0	6.0	34.0	L=N	L>G	G
12	330333	6820284	DH1	10.6	89.4	60.3	4.2	35.5	L=N	L>G	G
13	330288	6820257	Between fence and road	17.4	82.6	33.1	11.6	55.2	L=N	L>G	G

Appearance: L - Lithic G - Granular N - Nodular

gravel. These are associated with As, Bi, Te and Mo (maxima 900, 2.1, 1.2 and 8.5 ppm respectively) (Figure 21B, C, E-H).

Although there are slightly greater concentrations of indicator elements in the non-magnetic components of some of the gravel (Table 2), the differences are small. As magnetic nodules are so easily extracted from the drill spoil, sieving and manual separation of non-magnetic nodules is thought to be unwarranted.

5.5 Soil gas survey

Seventeen soil samples were taken along line 7950N and submitted to SDP Pty Ltd, Queensland, for soil gas analyses to test the application of this method in an area of thick transported cover. Results are unavailable to date.

5.6 Lag survey and other work

Introduction

High-grade Au mineralization (>40 g/t) was intersected in earlier RC drilling on line 9400N at approximately 100 m vertical depth. The mineralization appears to extend up-dip and was recently tested by SOG using AC drilling (5 holes totalling 273 m) which also provided material for CRC LEME studies. Results show a small dispersion halo in the regolith with Au concentrations less than 2.5 ppm (Figure 22).

Thirteen surface lag samples were collected along the principal drill section to test for any useful response through about 16-28 m of colluvial cover. Likely mechanical dispersion mechanisms are sheetwash from higher ground and vertical movement by ants, termites and burrowing animals that may have penetrated the colluvium and reached the residual profile. In this situation, the best responses from depth are likely to be in the finer lag fractions. Possible chemical dispersion mecha-

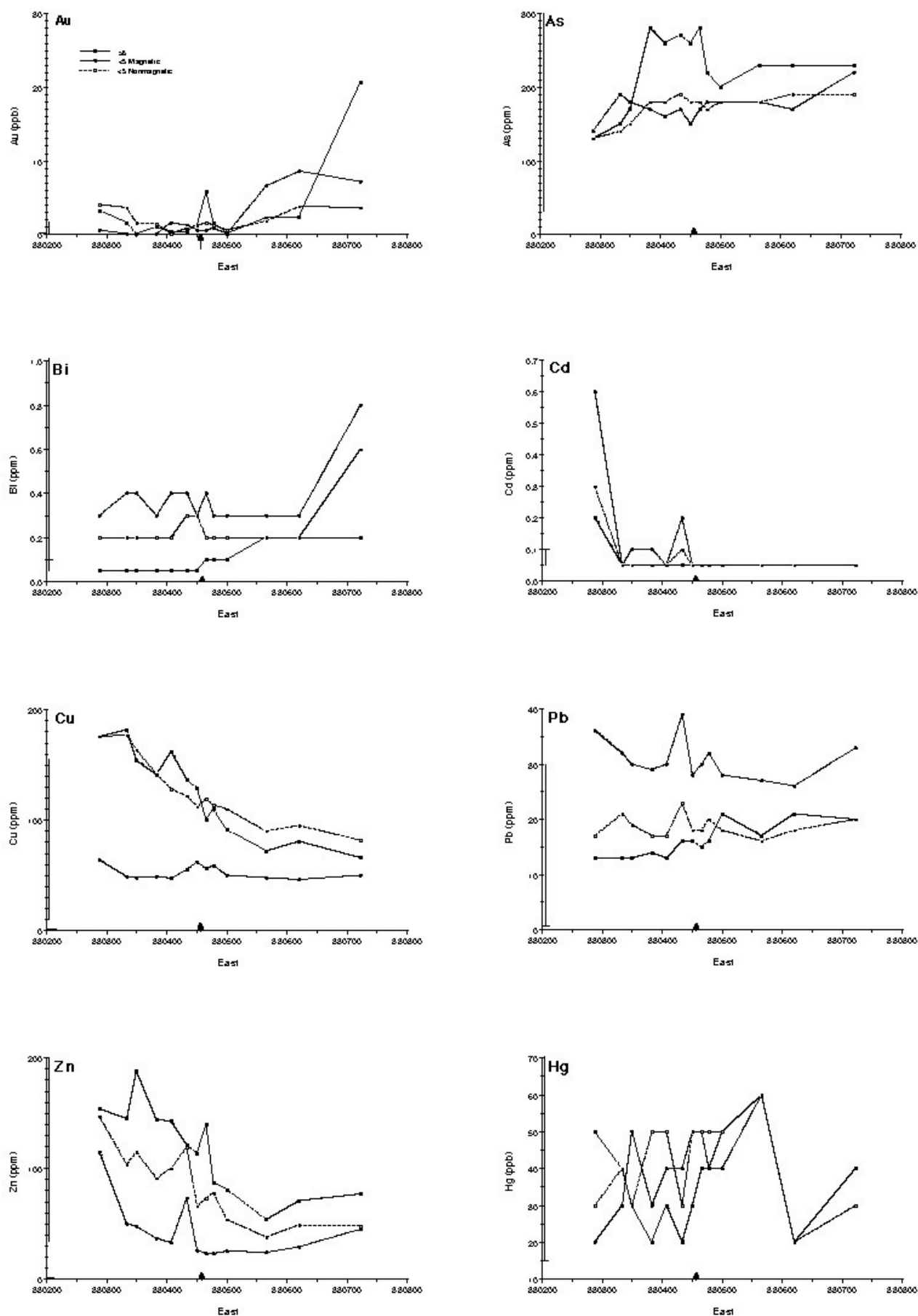


Figure 23. Lag geochemistry along drill line 9400N (local grid) showing the mineralisation as an arrow at 330460mE (UTM). This is compared with the detection limits and the ranges of ridge sampling to place the lag data in context.

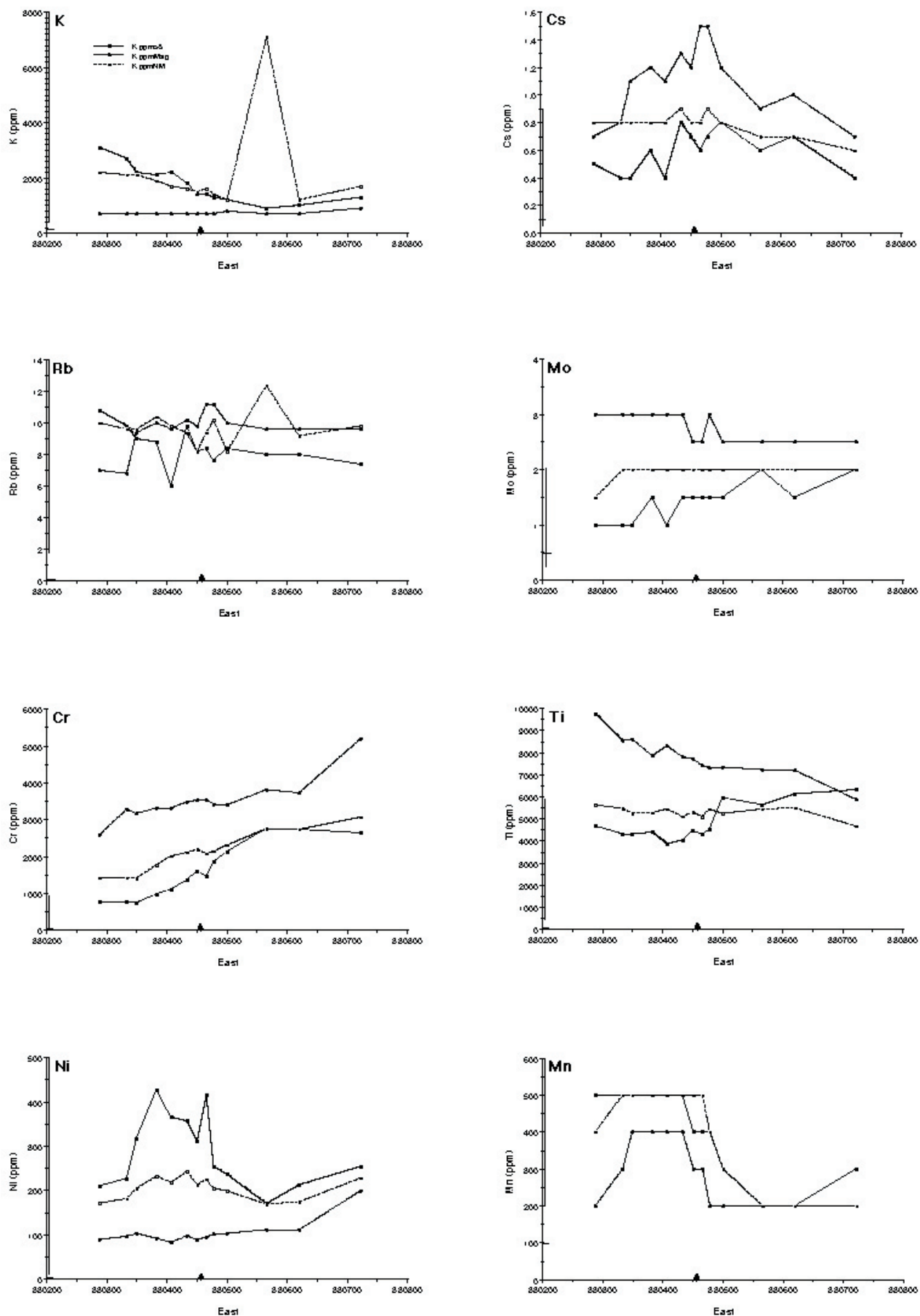


Figure 23 (contd). Lag geochemistry along drill line 9400N (local grid) showing the mineralisation as an arrow at 330460mE (UTM). This is compared with the detection limits and the ranges of ridge sampling to place the lag data in context.

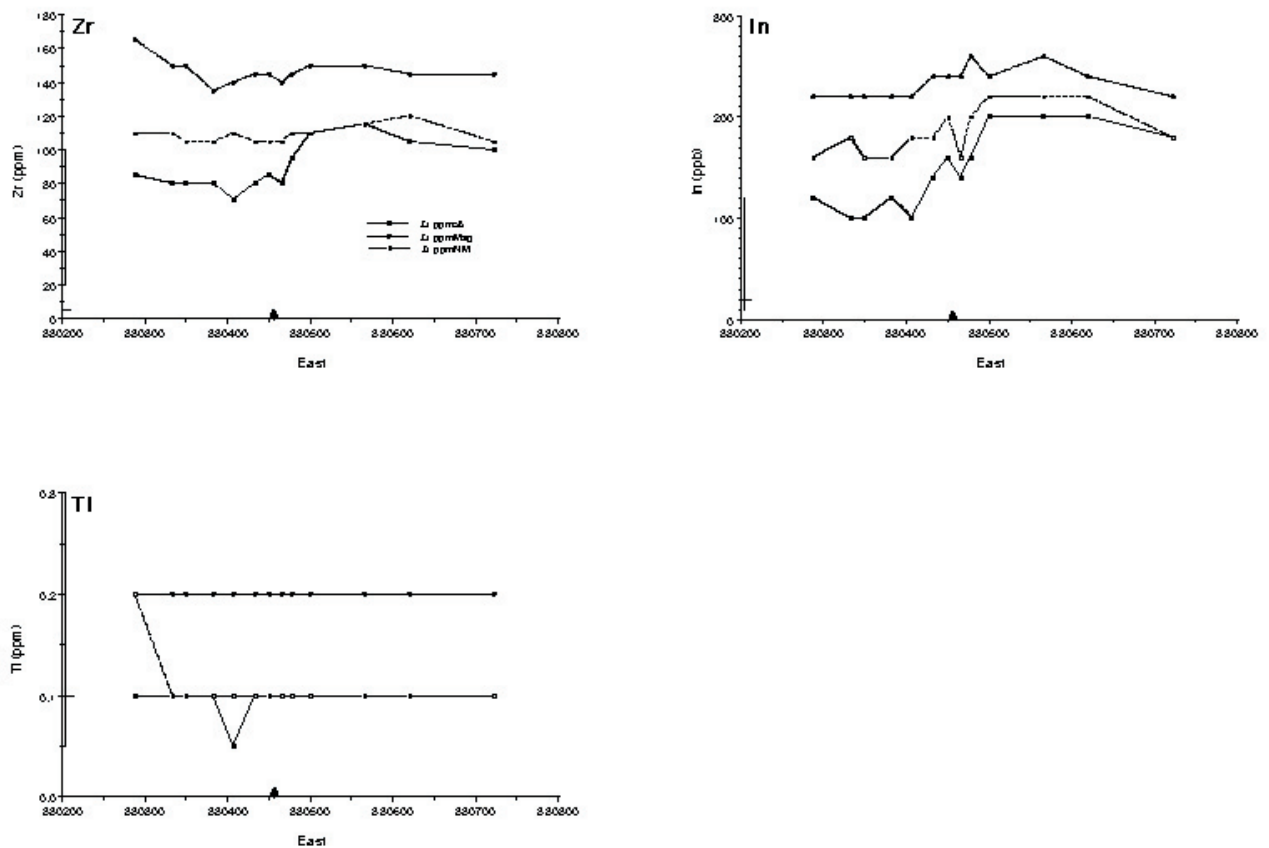


Figure 23 (contd). Lag geochemistry along drill line 9400N (local grid) showing the mineralisation as an arrow at 330460mE (UTM). This is compared with the detection limits and the ranges of ridge sampling to place the lag data in context.

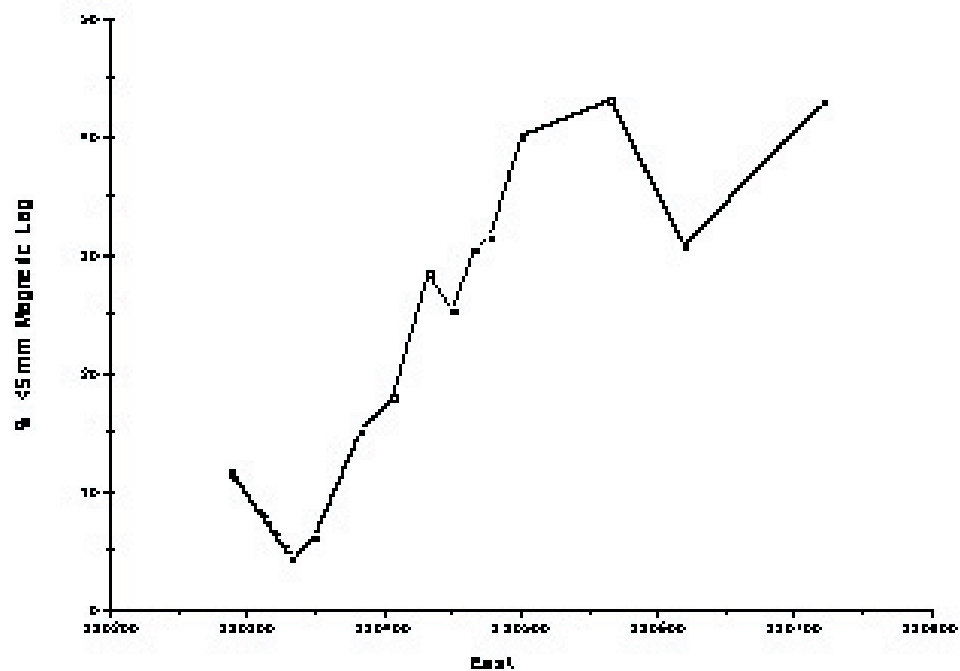


Figure 24. The proportion of magnetic component in the fine lag (<5mm) increases to the E.

nisms are less well defined and include cycling by vegetation and trapping by suitable materials. Thus, size fractions and magnetic and mineralogically and texturally different non-magnetic fractions were examined separately.

Method

Field: Samples of the complete lag, weighing about 2 kg, were brushed from the surface into a plastic dustpan and bagged in calico from 5-6 sub-sample sites within 4 m of each sample site. Sites were chosen where the probability of contamination by drilling activities was thought to be minimal. Sites proximally down slope from new or old drill-spoil sites were specifically avoided. The sample spacing was decreased close to mineralization to ensure sufficient definition.

Laboratory: The lag sample was agitated by hand in a stream of tap water in a plastic bucket to remove dust, phyllodes, twigs and fecal pellets. It was further agitated in a stream of water on a 710 μm sieve to remove fines and any remaining twigs and phyllodes. About 200 g of red sand passed the sieve and was discarded. This consists of about half (visually estimated) hematite-stained quartz (35% angular and 10% rounded) and half ferruginous granules (20% black to dark brown lithic ferruginous clasts, 5% black ferruginous granules, 20% red ferruginous clay granules and 5% yellow ferruginous clay granules). The $>710\ \mu\text{m}$ fraction was dried at 50°C for 15 hours in a stream of air (this temperature is no greater than would be expected on a dark lag surface on a hot summer's day in the Yilgarn).

The dry samples were separated quantitatively into $>5\ \text{mm}$ and $<5\ \text{mm}$ fractions using a plastic sieve. The magnetic material was separated from the $<5\ \text{mm}$ fraction with a powerful rare-earth magnet. All three fractions were weighed and examined (Table 3). i) The $>5\ \text{mm}$ fraction consists of brown, tabular lithic fragments and fragments of broken brown to black nodules. Nearer the ridge, the proportion of lithic fragments is dominant, but, out in the plain, the proportions of broken nodules and lithic fragments were approximately equal. Most of this is $<20\ \text{mm}$ with a few reaching 50 mm in size. ii) The non-magnetic fraction consists largely of brown to black lithic fragments with a lesser proportion of broken granules, lacking cutans although, near the traverse centre, the proportion of broken granules approximately equals the lithic fragments (This was not determined simply from angularity but from observed internal structure - broken nodules are angular.). iii) The magnetic fraction consists of black to dark-brown pisolitic to nodular granules, some broken, but all lacking a cutan. After removal of reference materials, the lag samples were pulped in low Cr steel and analysed (Appendix B).

Results

The lag traverse followed a drill section 9400mN (including drilling from 9110-9290mE) which is oblique to the UTM grid. The data are plotted against UTM eastings (Figure 23, Table 3). The location of the up-dip projection of the mineralization onto the unconformity is indicated at UTM 330460mE. The detection limits are shown by a small horizontal tick against the vertical axis. The range of all the ridge samples is shown as a vertical bar beside the vertical axis. The rocks exposed on the chert ridges are the most probable source of the lag. These two statistics help to place the plots in context.

The data for Cd, Bi, Hg, Mo, Tl and Mn are too close to detection limits to be reliable and are unduly influenced by noise and reporting intervals. Of the remaining elements, many fall within the noise envelope of the ridge samples, particularly As, Cu, Pb, Zn, K, Cs, Rb, Ti and Ni. Elements that might indicate mineralization are As and Ni, and only occur in the coarse lag. That this is not reflected in the fine lag (neither magnetic nor non-magnetic) suggests the coarse lag 'anomaly' is probably a coincidence coupled with the close sampling interval used near mineralization. The magnetic fraction in the fine lag shows a Cs peak over mineralization, but this is not reflected in the coarse lag or the non-magnetic component of the fine lag. As both K and Rb are not anomalous, it is unlikely that the Cs anomaly is the only manifestation of a phyllic halo. Gradients are apparent in some of the data with increasing Cu and Zn to the W and As, In and Cr increasing to the E. These probably represent systematic provenance changes in the lag and probably in the underlying colluvium. The magnetic lag fraction appears to be enriched in Bi, Pb, Cs, Mo, Cr, Ti, Zr and In, relative to the non-magnetic component, probably related to enhanced Fe concentrations. The progressive increase in the proportion of magnetic lag to the E in the $<5\ \text{mm}$ fraction (Figure 24) suggests longer exposure in the soil for the conversion of hematite and goethite to maghemite.

TABLE 4
MAGNETIC GRAVEL GEOCHEMISTRY - McGRATH 9400N

CSIRO No	HoleID	Grid E	Grid N	From	To	Analyte Unit Digest Method DL	Fe2O3 % Fusion XRF 0.01	As ppm 4-acid ICP-MS 1	Te ppm 4-acid ICP-MS 0.2	Au ppb Aqua regia ICP-MS 0.2	Hg ppb Aqua regia ICP-MS 10	Bi ppm 4-acid ICP-MS 0.1
1601674	MGAC01	9110	9400	9	12		82.1	100	0.2	-0.2	-10	0.7
1601675				12	15		78.4	100	0.2	0.4	20	0.4
1601676				15	18		79.1	98	0.4	0.4	-10	0.2
1601677	MGAC02	9170	9400	9	12		74.8	110	0.2	1.2	-10	0.3
1601678				12	15		75.5	100	0.2	2.6	20	0.3
1601679				15	18		77.9	86	0.2	1.2	10	0.3
1601680	MGAC03	9230	9400	8	10		80.4	140	0.4	2.2	10	0.3
1601681				10	13		81.1	140	0.4	2	10	0.6
1601682	MGAC04	9260	9400	7	9		80.9	230	1.6	2.6	20	7.4
1601683				9	12		78.2	340	1.8	5	40	8.5
1601684	MGAC05	9290	9400	4	7		76.9	210	0.8	1.4	20	2
1601685				7	10		81.7	270	1.4	4.6	20	7
1601686				10	12		77.5	270	0.6	1.8	60	3.3
Rpt1601686				10	12		77.2	280	0.6		60	3.3

5.7 Ferruginous gravel in colluvium

At McGrath North, the AC drilling on line 9400N intersected ferruginous, magnetic gravelly lenses at 4-18 m depth. The dominantly small (1-10 mm), worn nodules and pisoliths were sampled using a rare earth hand magnet. In the laboratory, the dry samples were separated into >5 mm and <5 mm fractions using a plastic sieve, and only the <5 mm fraction was analysed. The results show a weak to moderate As-Te-Au-Hg-Bi signature (Table 4) in gravel from holes MGAC04 and MGAC05, directly above the mineralization. There is no dispersion halo extending to the W, possibly because the palaeo-surface apparently slopes SE. It is unknown, how far the geochemical signature extends to the SE.

Compared with the surface lag, buried ferruginous gravels show a geochemical signature of the underlying mineralization and therefore are a useful additional sample medium in percussion drilling. Similar to the McGrath South area, it appears Hg gas may have ascended and was captured by Fe-oxides as it only appears in the lowermost ferruginous gravel layers. The relative efficiency of hydrous Fe oxides to adsorb Hg (Andersson, 1979) has been stressed by Carr and Wilmschurst (2000) who therefore see Fe oxides as the dominant host in most exploration samples.

5.8 Vegetation sampling

A pilot study was conducted along line 9400N to investigate the use of plants as an exploration sample medium for identifying the signature of a narrow, high-grade Au zone in an area of thin to medium cover thickness (approx. 15 m).

Results from four sample sites show a good response in litter (As, Au and Bi) and bark (Au) (Table

TABLE 5
BARK AND LITTER GEOCHEMISTRY - McGRATH 9400N

CSIRO No	Grid E	Grid N	SampleType	Analyte Unit Digest Method DL	As ppm HNO3, Aqua regia ICP-MS 0.1	Au ppb HNO3, Aqua regia ICP-MS 0.2	Bi ppm HNO3, Aqua regia ICP-MS 0.02
07-7202	9164	9358	Bark		0.7	0.6	0.01
07-7196	9227	9408	Bark		0.9	1.2	0.02
07-7208	9255	9408	Bark		0.4	1.8	0.01
07-7214	9319	9428	Bark		0.4	1.2	0.01
07-7201	9164	9358	Litter		0.5	1.1	0.01
07-7195	9227	9408	Litter		1.1	2	0.02
07-7207	9255	9408	Litter		2.2	3.8	0.04
07-7213	9319	9428	Litter		5.7	1.4	0.02

5). Samples taken above the surface expression of the mineralized zone (9260E, 9400N) show an anomaly to background ratio of 2-3. Additional sampling is needed to substantiate the preliminary findings, however, the sparse vegetation cover along the traverse due to clearing limits the number of available sites.

5.9 Selective extractions of soil

Parallel to the biogeochemical survey, the application of several partial/selective extraction methods was tested across the Au mineralization at McGrath North (9400N). The extractants were: -

- Sodium dithionite
- Hydroxylamine hydrochloride 0.1M
- Hydroxylamine hydrochloride 0.25M

Sodium dithionite targets crystalline Fe oxides and shows a single point Au-As-Bi-Mo-W anomaly over part of the mineralized zone. A 0.25M hydroxylamine extraction, targeting amorphous Fe, shows an As-Mo response over the mineralization. None of the extractions shows a geochemical signal over the western up-dip end of the mineralization. Geochemical data are listed in Appendix C, partial extractions 9400N.

5.10 Partial extractions of basal sediments

Partial extractions of basal sandy sediment from drill spoil S of McGrath (8050N), from approximately 80-90 m depth, were used to investigate hydromorphic dispersion processes at the base of the transported cover and the top of the residual profile. Two size fractions (<75 µm and 250-1000 µm) were analysed after extraction with dilute and concentrated HCl. Results (Appendix C, partial extractions, basal sediment) show Au concentrations are greater in the 250-1000 µm than in the <75 µm fraction. The strength of the HCl appears to have little influence on the Au extracted; some samples yielding more Au to the dilute acid, others more to the concentrated acid.

TABLE 6
BASAL SEDIMENT GEOCHEMISTRY BY PARTIAL DIGEST

HoleID	Grid E	Grid N	From	To	Lithology	CSIRONo	Analyte Unit Digest Method	Cd ppb ICP-MS Partial 10	Sb ppm ICP-MS Partial 0.005	Te ppb ICP-MS Partial 10	Au P ppb ICP-MS Partial 0.5	Au ppb ICP-MS Total 0.5	Hg ppb ICP-MS Partial 2	Tl ppb ICP-MS Partial 1	Bi ppb ICP-MS Partial 1
SSC870	9125	8050	83	84	Sand, quartz, lithic gravel, angular and subrounded	1601473		260	1820	50	16.5	80	206	9	61
			84	85		1601474		40	440	-10	2.5	30	72	3	18
			85	86		1601475		30	650	50	-0.5		34	1	93
			86	87		1601476		120	2460	170	1		32	28	310
			87	88		1601477		150	1870	120	3	130	64	36	175
			88	89	Saprolite and quartz	1601478		330	940	90	4		52	14	113
			83	84		1601483		40	485	-10	8	81	56	7	28
			84	85		1601484		30	385	20	2.5	20	58	5	28
			85	86		1601485		40	1190	70	13		20	6	173
			86	87		1601486		120	3920	110	24		18	102	249
SSD871	9180	8050	87	88	Red sand, silt, qz, lithic, angular	1601487		150	345	30	2.5	290	18	56	18
			88	89		1601488		270	260	-10	93.5		18	75	13
			89	90		1601489		400	1300	-10	76		4	21	49
			90	91		1601490		350	1360	-10	67	60	-2	9	31
			85	86	Yellow, sand/saprolite	1601493		30	145	-10	3	20	26	2	7
			86	87		1601494		50	1340	80	15		32	9	120
			87	88		1601495		100	4030	120	79.5	50	20	36	254
			88	89		1601496		90	1690	50	459		16	18	134
			89	90		1601497		90	2810	110	411		38	21	159
			90	91	Saprolite	1601498		100	2530	40	227	70	30	19	112
SSD872	9260	8050	91	92		1601499		130	3420	40	84.5		26	13	102
			92	93		1601500		150	3210	40	87		54	12	108

250-1000 µm fraction by concentrated HCl extraction
Total Au by aqua regia digest

A comparison between total digest (Aqua regia) and partial digest (HCl) generally shows poor recovery in the partial digests. This suggests there are small grains of lithic auriferous material in the basal sediments. Other elements, e.g., Bi, Sb, Te and Tl show high concentrations in the lower 1-4 m of the sediment (Table 6) that, in most cases, do not correspond to similarly high concentrations in the underlying saprolite. These enrichments are thought to be of hydromorphic origin. Mercury concentrations appear to increase in the upper part of the basal sands of the sedimentary sequence, possibly indicating ascendant dispersion through the sedimentary sequence. A similar trend is not apparent for Cd. The variability of the pathfinder concentrations within the basal sediments and between holes makes this sample medium less promising for exploration.

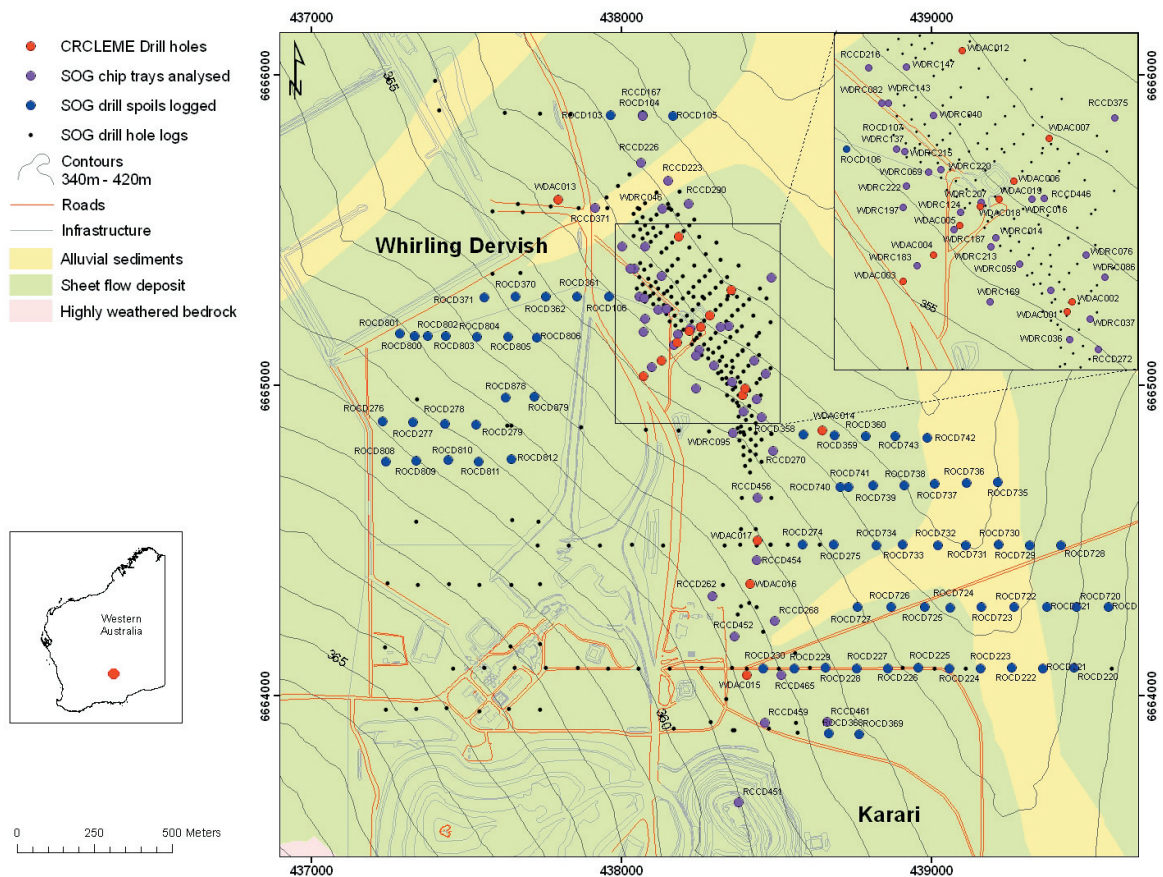


Figure 25. A map of Whirling-Dervish prospect showing locations of CRC LEME and company drill holes.

6. SUMMARY OF ACTIVITIES AT WHIRLING-DERVISH

6.1 Introduction

The Whirling-Dervish deposit is 1.5 km N of the Karari open pit, approximately 120 km NE of Kalgoorlie in the Eastern Goldfields Province of the Yilgarn Craton.

The deposit, together with the Karari mine, Montie's Dam, Luvironza and Elliot's Lode, is located in a syntectonic sedimentary basin dominated by volcanoclastic sedimentary rocks and associated with subvolcanic intrusives comprising monzonite, syenite and related porphyries, and lamprophyre (W. Witt, written comm., 2004). The Whirling-Dervish deposit is just S of the Menzies Line (Butt et al., 1977; Butt, 1988), in a saline groundwater environment.

The area was selected as a study site because of the dominantly felsic character of its host rocks that contrasts with the commonly mafic to ultramafic character of many other Au deposits in the Yilgarn Craton. Therefore, it poses different challenges to geochemical exploration. The generally Fe-poor bedrock weathers to a kaolin-rich and Fe-oxide poor regolith that is covered by medium to thick alluvium and colluvium. Despite the transported cover, the deposit shows a good surface signature (Au in calcrete) that had not been fully recognised and utilised by previous explorers. Sampling of calcareous materials in the upper 3 m of the regolith outlines a geochemical footprint of the deposit that is approximately 50 m offset towards the drainage to the NE and E.

In January 2004, a 719 m AC program was completed at Whirling-Dervish. Thirteen holes were drilled (Figure 25) to obtain samples of various regolith materials for mineralogical and geochemical studies. Holes were generally drilled to blade refusal with the exception of three holes (WDAC015 to 017) that were drilled to investigate the transported regolith between the Karari pit and Whirling-Dervish, and were stopped in upper saprolite. Results of 374 analyses of AC material, initially analysed for Au, Hg and Cd by ICP-MS (after aqua regia digest; detection limits of 0.00002, 0.01 and 0.05 ppm respectively) are listed in Appendix D.

A further three holes (WDAC018, WDAC019A and WDRC019B) tested the surface expression of

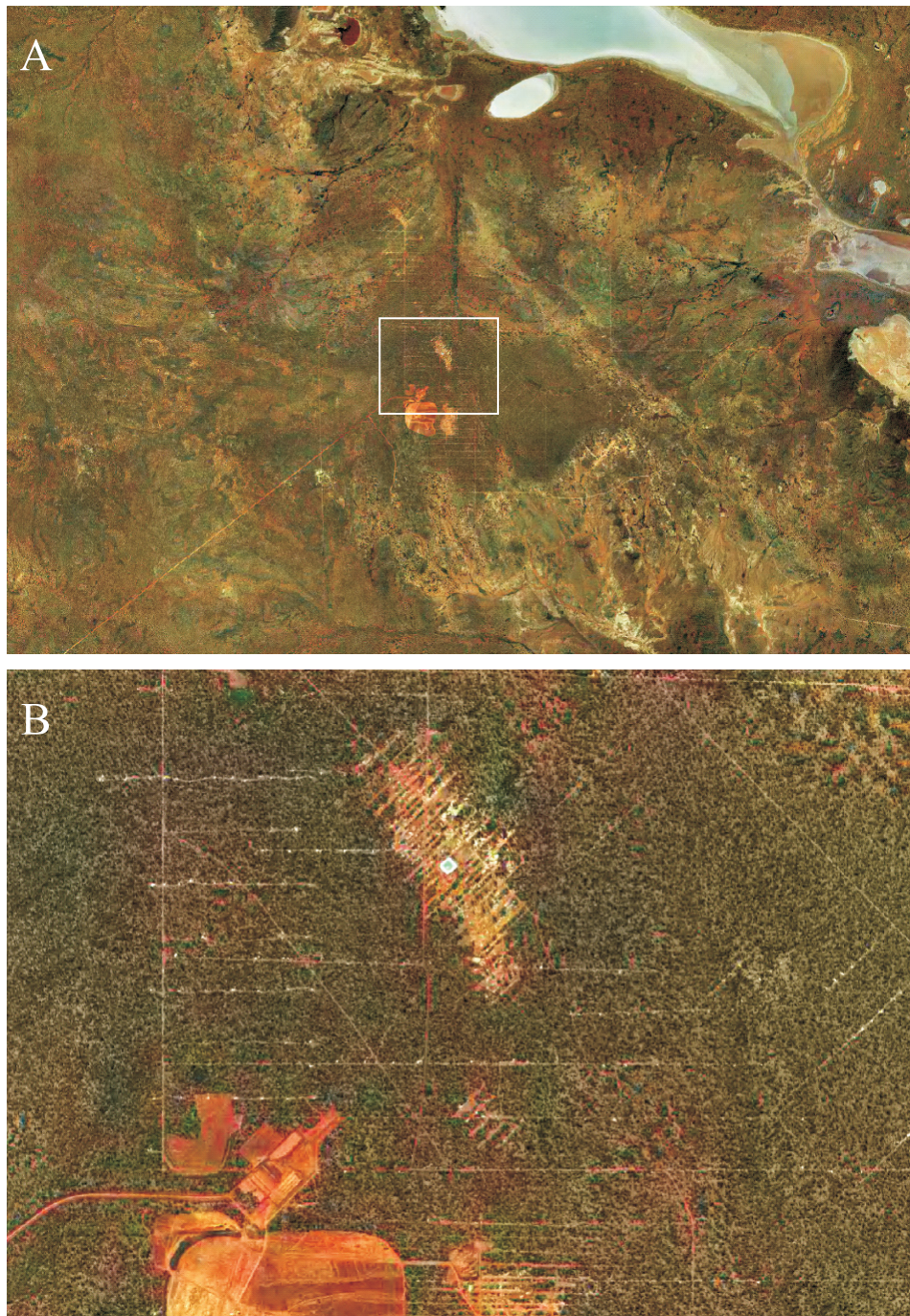


Figure 26. Aerial photograph of the Whirling-Dervish prospect showing Lake Rebecca to north and a breakaway system to the south. Size of box in A is 3x2.5 km and B is an enlargement of the boxed area in A.

the Whirling-Dervish mineralized zone along section 49600N and provided samples of high grade mineralization within the regolith. In addition to the AC drilling, samples were taken from diamond drill core (WDDD01) for geochemical, mineralogical and petrophysical studies.

6.2 Geomorphology and drainage

The Whirling-Dervish Prospect lies on a relatively flat, undissected plateau (350-370 m AMSL) bound by an extensive breakaway to the S and SE and gentle slopes to the N (Figure 25). The area drains to the adjacent Lake Rebecca to the N through a system of weakly developed channels (Figure 26). At a local scale, the Whirling-Dervish prospect gently slopes to the NE, with sheet wash also in that direction.

6.3 Regolith stratigraphy

The 3D regolith stratigraphy of the area was established using 15 CRC LEME drill holes and the logs of 382 SOG drill holes. In addition, drill spoil of 194 SOG holes were logged in the field, and

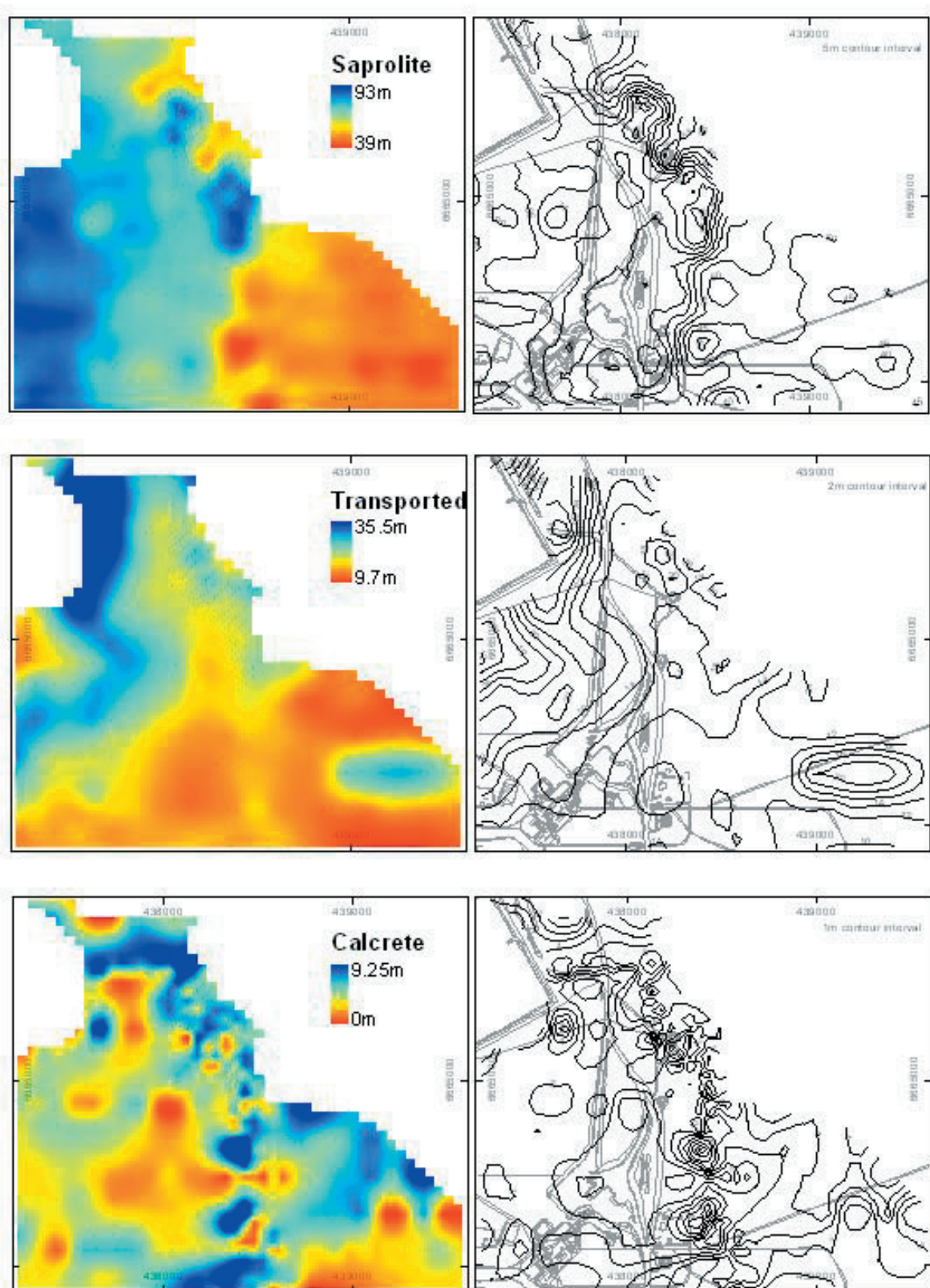


Figure 27. Depths of three main regolith units in the Whirling-Dervish area.

chip tray materials of 45 SOG drill holes were analysed by ASD to accurately determine the boundary between transported material and *in situ* regolith. Locations of all these drill holes are shown in Figure 25.

The regolith at Whirling-Dervish consists broadly of three main units: i) a surface layer of calcrete, ii) transported material and iii) *in situ* weathered material (Figure 27). The thickness of the calcrete layer varies from 1-6 m, with a few places where it is as deep as 9 m. It tends to be relatively deeper in the NE part of the prospect. The depth of transported material below the calcrete horizon gener-

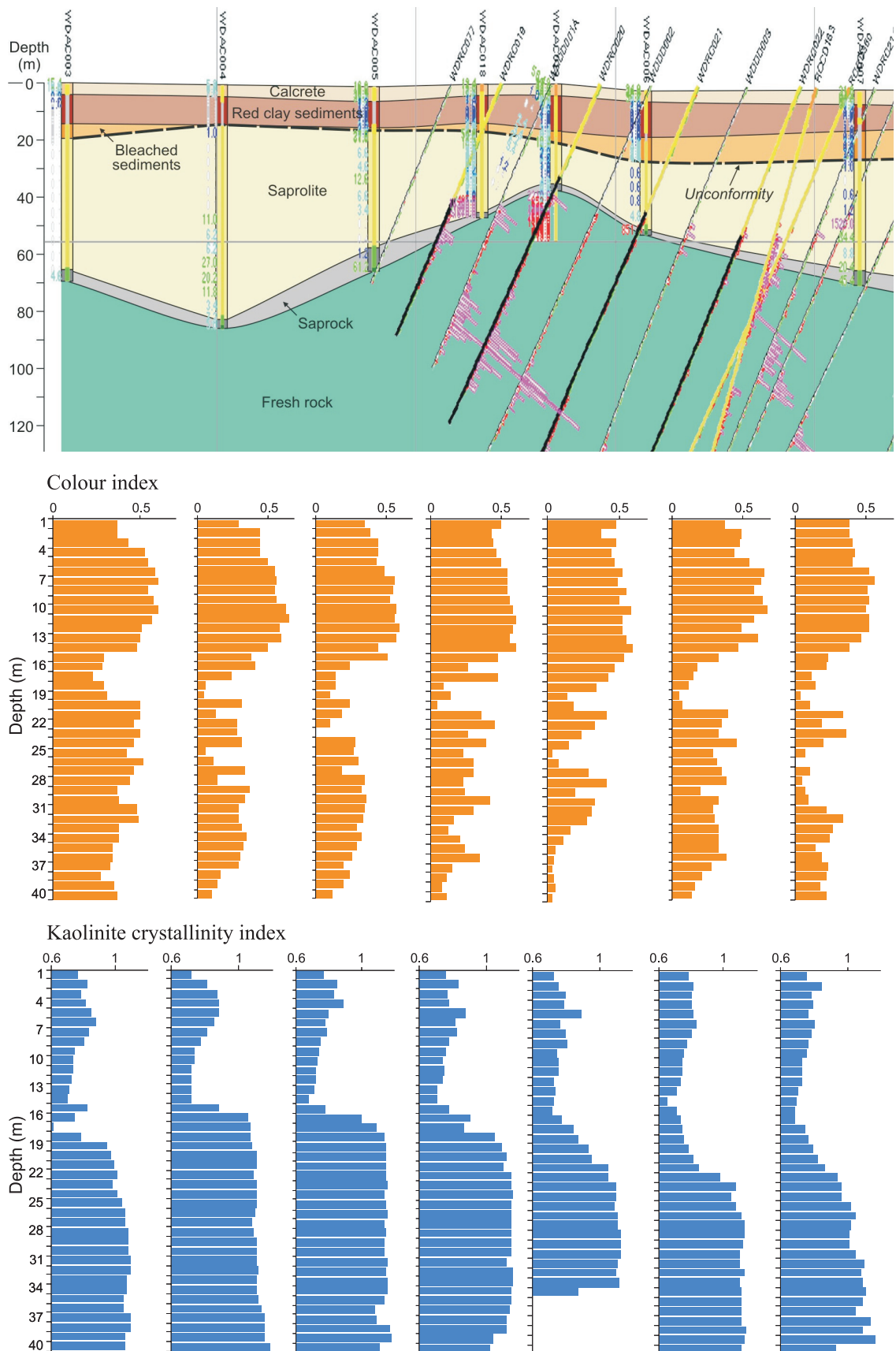


Figure 28. A schematic representation of regolith stratigraphy and Au grades (SOG data), colour and kaolinite crystallinity index profiles of CRC LEME AC drill traverse 49600N, Whirling-Dervish.

ally extends to 23 m, with isolated depths of up to 35 m. It mainly consists of red clay with lenses of magnetic nodules. In places, upper parts of the transported material also contain colluvium-derived lateritic nodules of various sizes. The *in situ* material underlying the transported material is generally truncated to saprolite with loss of the mottled zone. The depth of weathering varies from 39-93 m and is deepest in the western part of the area (Figure 27).

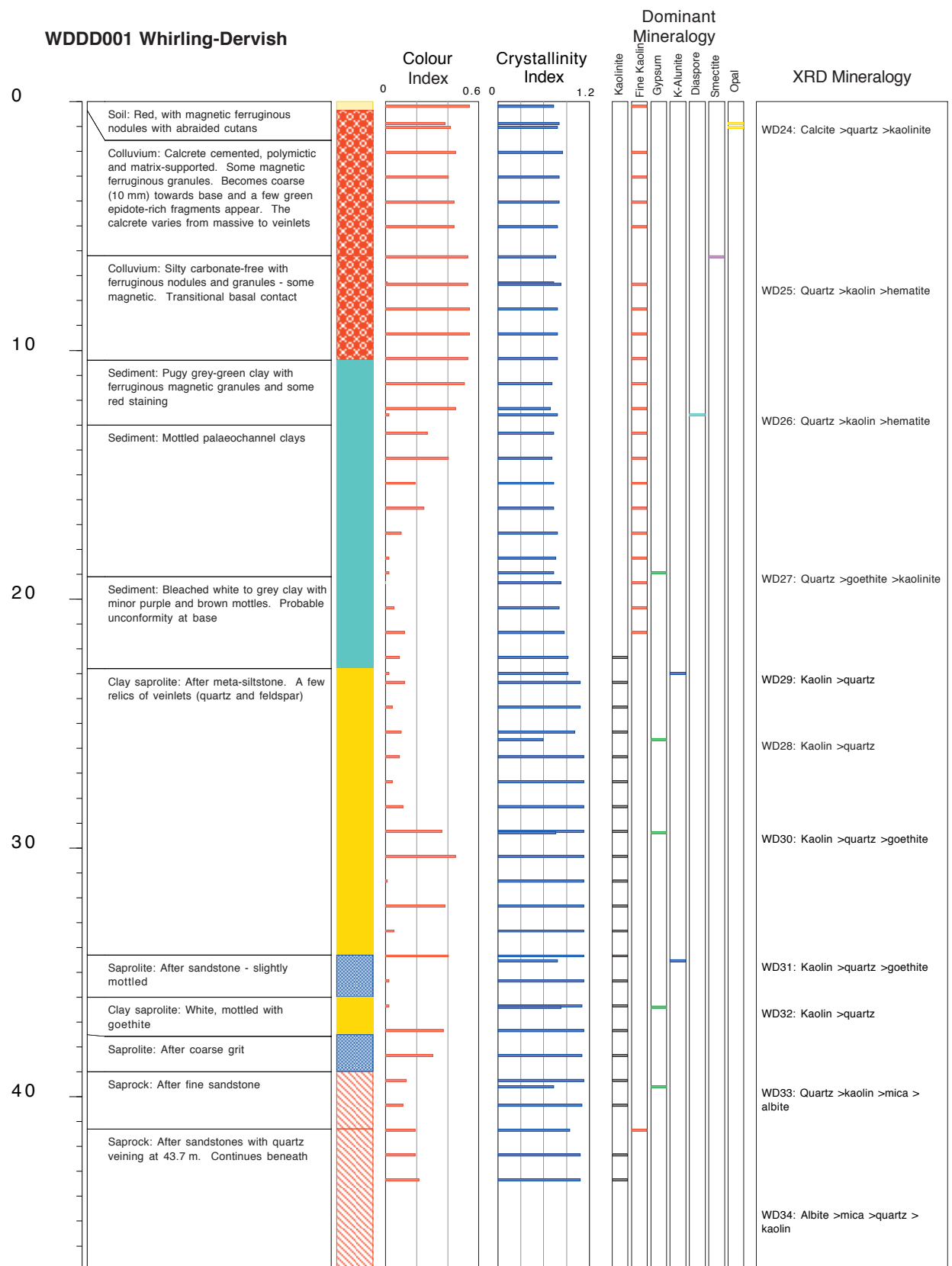


Figure 29. Log of WDDD001 with ASD parameters colour index, clay crystallinity index, ASD perceived dominant mineralogy and XRD mineralogy of described specimens.

The regolith stratigraphy of the CRC LEME drill traverse over the centre of the mineralization (extending NE from 438070E, 6665030N to 438355E, 6665308N) is shown in Figure 28. A uniform horizon of calcrete covers sediments of varying thickness. The sediments are shallow on the SE end of the traverse and gradually increase in thickness to the NE. A significant lower portion of the deeper sediment in the NE is bleached and closely resembles the underlying saprolite. The nature of this bleached zone was established using a combination of particle size analysis and electron microscopy as discussed below. The depth of weathering is variable within the traverse and is at a minimum at drill hole WDAC019, close to the centre of mineralization.

WDDD001

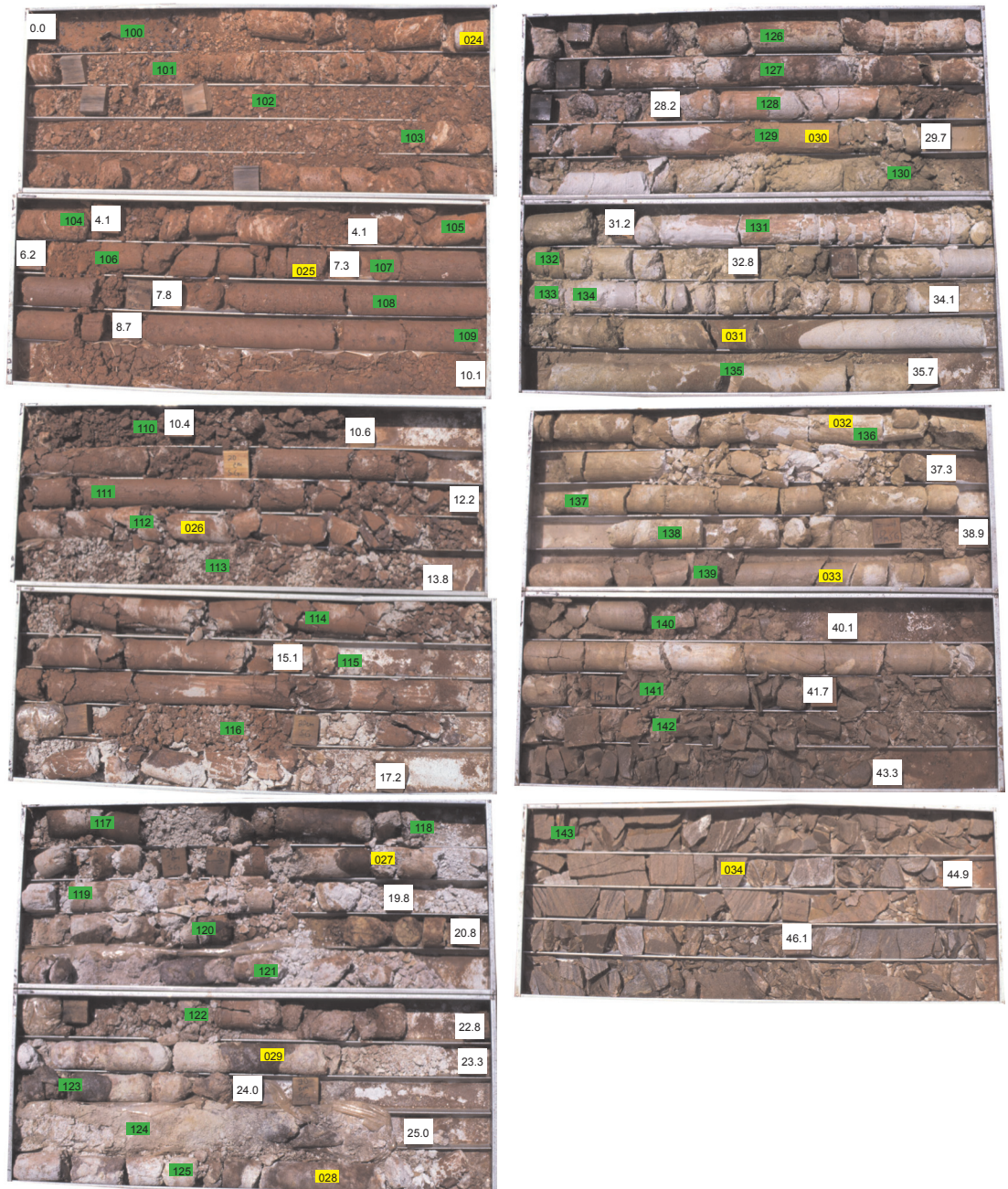


Figure 30. WDDD001 - photographic log with white depth markers, yellow petrographic specimens and green ASD specimens.

6.4 Logging, petrography and mineralogy of WDDD001

Core logging

The diamond core was logged (Figure 29) and photographed (Figure 30) to the weathering front, where the lithology could be distinguished easily. The top 0.35 m consists of red soil containing abraded magnetic, ferruginous nodules. Below this, lies a red-brown polymictic colluvium with an Fe-stained silty-sandy matrix and clasts of ferruginous nodules and lithic clasts. The top part is cemented by calcrete and the lower part (below 6.2 m) has been hardpanized by an opaline, alumino-silicate cement. Its base, at about 10.4 m, is transitional to a grey-green valley-fill clay sediment, with a few ferruginous granules that is highly mottled in places (Figure 30) and massive to puggy in others. The base of these sediments and their contact with the residual profile, at 22.8 m, was particularly difficult to determine, even from diamond core. It appears that the top of the residual profile has been re-textured by pedoplasation. However, the accurate determination of the top of the residual profile

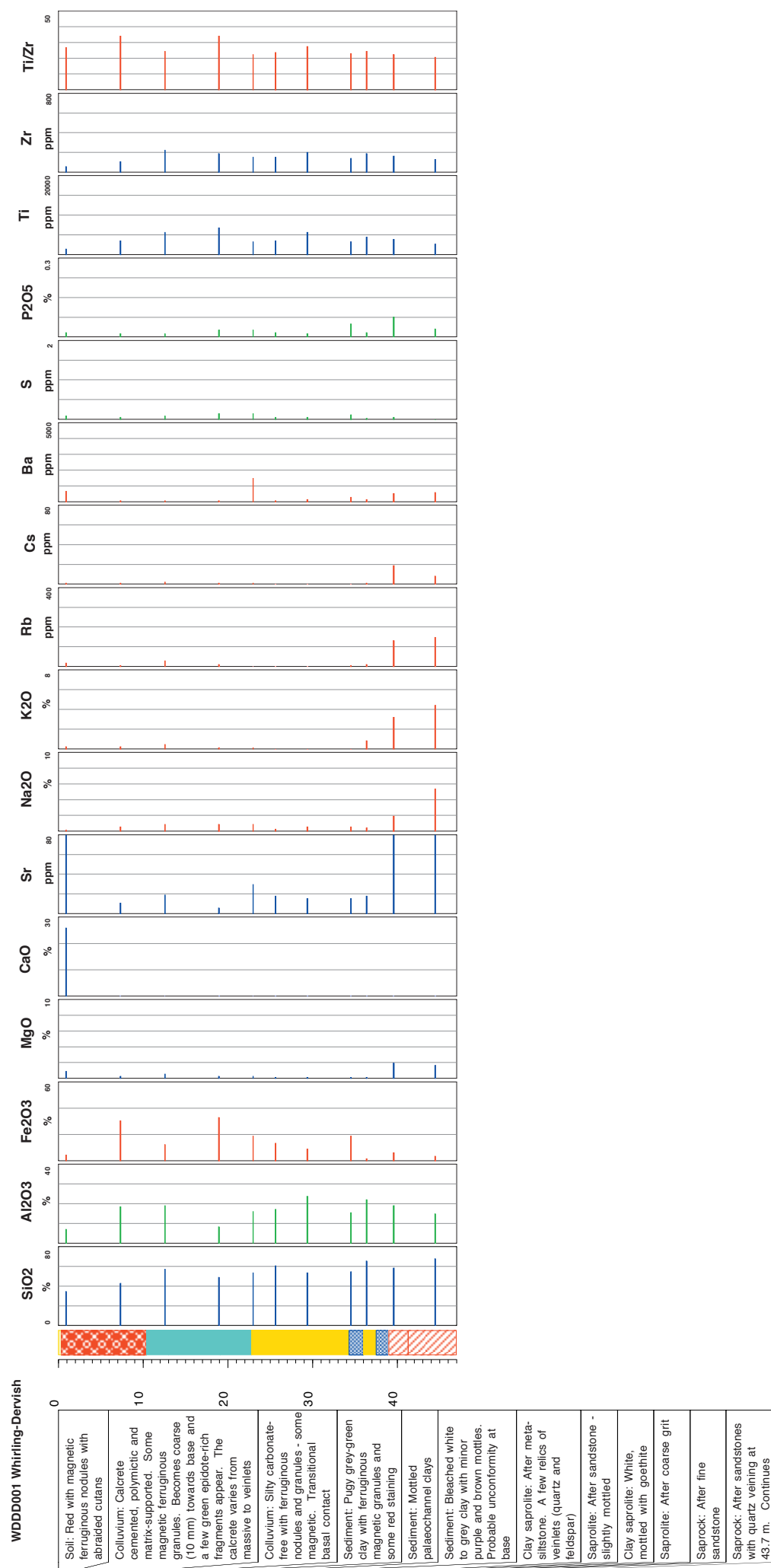


Figure 31. Log of WDDD001 with geochemistry.

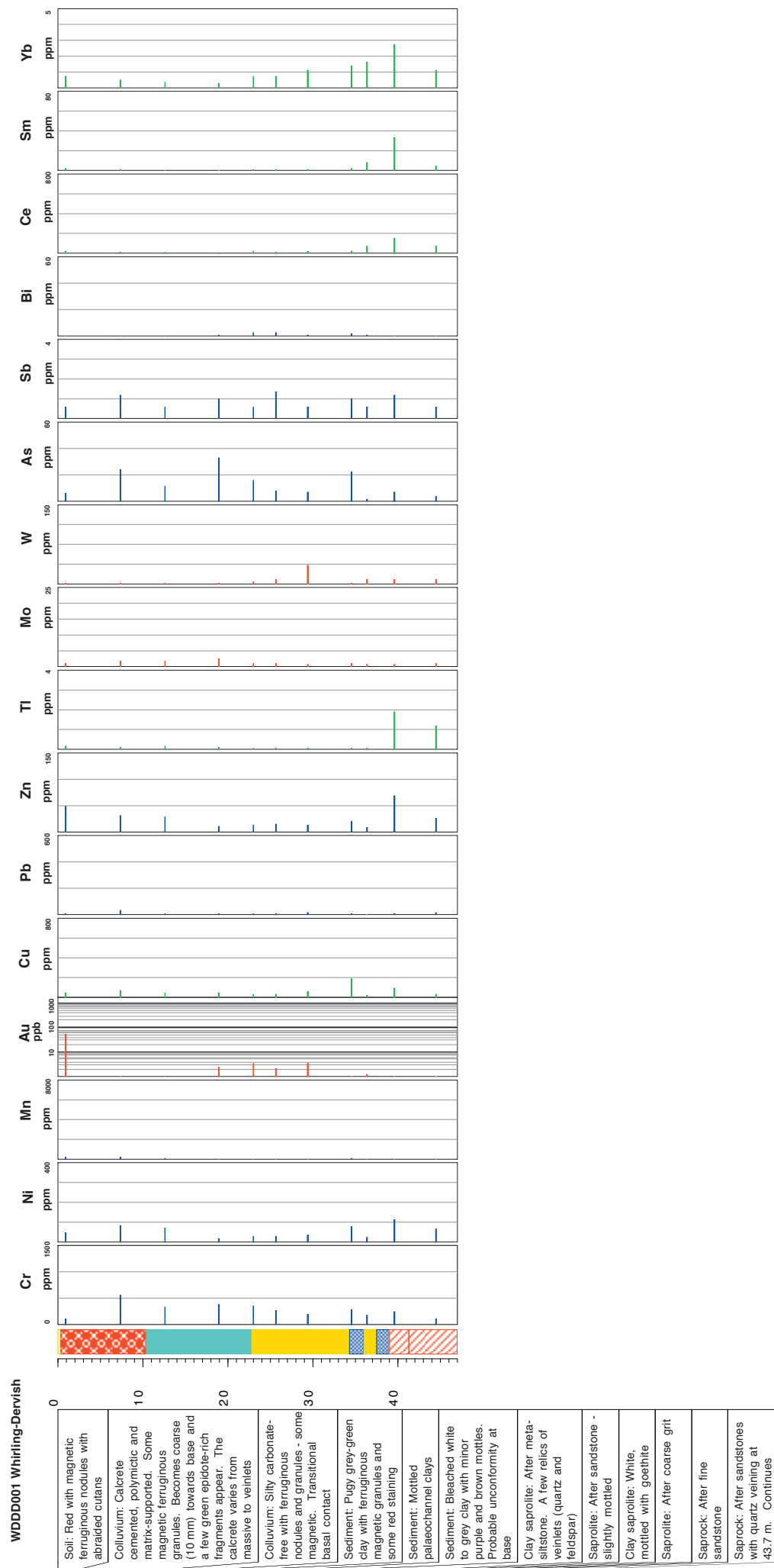


Figure 31 (contd). Log of WDDD001 with geochemistry.

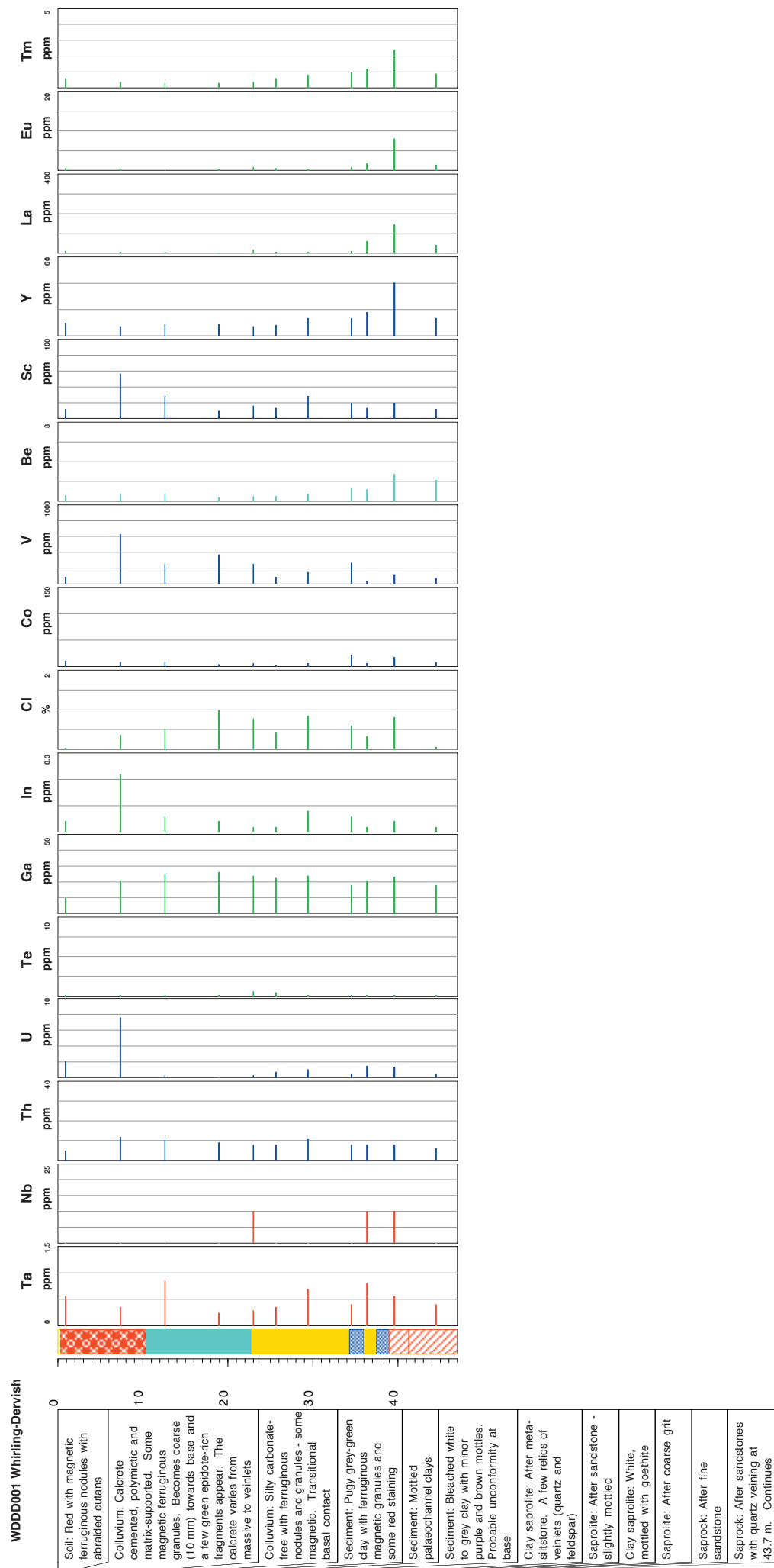


Figure 31 (contd). Log of WDDD001 with geochemistry.

is crucial to exploration in the regolith. The appearance and fabrics of clay and quartz were the final core-logging determinants.

Below the unconformity, the clay saprolite or pedolith contains a few relict veinlets of quartz (largely re-textured), confirming a residual profile but these were not sufficiently abundant to mark the unconformity by abrupt appearance or absence. Mottling is variable. It was only below 34.3 m that saprolitic fabrics, after metamorphic structures, could be distinguished, passing finally into very slightly weathered quartzo-feldspathic metasedimentary bedrock at 45 m (Figure 30).

Sampling and analysis

Eleven relatively coherent specimens were taken at 2.5-7.0 m intervals to represent the major materials of the drill profile. Two were from the colluvium, two from the clay sediment, four were various probable pedolithic materials of the upper residual profile and two were recognizable saprolites. The deepest specimen was of saprock. These were sectioned, examined by petrographic microscope and analysed for major and minor elements of lithological importance (Figure 31) and subjected to XRD analysis (Figure 29). The petrography, although difficult to interpret in places, was broadly consistent with the core logging. However, the interval between specimens was not sufficiently close to accurately locate the unconformity.

Additional specimens (37) were collected at roughly metre intervals and added to the petrographic specimens for spectroscopic analysis by ASD (Figure 29). There is a sharp and consistent increase in clay crystallinity (structural order) at or very close (± 0.5 m) to the logged unconformity, which provides an independent confirmation of the unconformity. The clays of the saprolite are significantly more structurally ordered than those of the overlying clay-rich sediment. A decrease in the colour index, indicating a decrease in the 'redness' of the materials, occurs about 5 m above the unconformity (Figure 29).

Petrography

Details of the petrographic studies are given below and illustrated on Figures 32, 33 and 34 by close-up photographs of the drill core slabs (left) and photomicrographs of thin sections (right). Primary fabrics have been extensively destroyed by pedoplasation and are difficult to interpret.

WD24. 0.9 m: Carbonate-cemented colluvial sediment - Figures 32A and B.

A wide variety of clasts, consisting of brown ferruginous saprolite and minor goethite nodules are set in a matrix of smaller clay-rich saprolite clasts, carbonate and clay. Veins of coarse, late, pedogenic carbonate penetrate the rock. Internally, the larger clasts (10 mm) consist of angular, strained quartz grains coated and bound together by a slightly banded orange-brown ferruginous alumino-silicate cement and red, fibrous ferruginous clay. Voids are filled with fine-grained granular carbonate and opaline silica. Quartz grains in the matrix have coats or partial coats of ferruginous alumino-silicate. Voids in the matrix are filled or lined with a slightly fibrous carbonate.

WD25. 7.3 m: Colluvial sediment - Figures 32C and D.

A variety of subangular to subrounded to nodular black goethite and hematite clasts, angular strained vein or granitic quartz, rounded saprolite clay balls and lithic clasts are loosely packed in a matrix of smaller quartz grains and orange-brown goethite-stained clay. Internally, some of the ferruginous nodules are massive, others contain quartz grains but a few are lithic and even bedded or foliated. The lithic clasts consist of yellow saprolites, probably after ultramafic rocks, some weathered BIF and some deeply weathered sediments. This implies a broad provenance from various levels in a mature lateritic profile developed on a broad suite of Archaean rocks.

WD26. 12.6 m: Mottled clay sediment - Figures 32E and F.

A very fine mat of flaky kaolinite is loosely scattered with larger subrounded and smaller angular to shardy quartz clasts and goethite nodules. One grain consists of a cherty mosaic of quartz grains, implying a weakly polymictic clast composition. This has been mottled by hematite that has developed as patches in the matrix or spread from cracks and ped boundaries in the clay. This has left the quartz fabric unaltered. There are a few arcuate structures which may be burrows that may have developed during mottling, as they cut across the mottled structures, but are themselves partly mottled.

WD27. 18.95 m: Mottled clay sediment - Figures 32G and H.

Fine-grained, anhedral quartz grains are packed in a matrix of flaky kaolinite. The proportion of quartz, the size of the quartz grains and the kaolinite flakes vary, suggesting a possible bedded struc-

FIGURE 32

<p>A. WD24. 0.9 m. Carbonate-cemented colluvium. Clasts of brown ferruginous saprolite (FS) and goethite nodules (GN) are surrounded by a matrix (MX) of small clay saprolite clasts, carbonate and clay. A coarse, late carbonate (CA) penetrates the rock as veinlets. Close up photograph of cut block in oblique reflected light.</p>	<p>B. WD24. 0.9 m. Detail of clasts of quartz (QZ) and Goethite nodules (GN) with a coating of ferruginous aluminosilicate (FA). Other clasts are ferruginous saprolite (FS). All are set in a matrix of granular to fibrous carbonate (CA). Photomicrograph of thin section in transmitted light under crossed polarizers.</p>
<p>C. WD25. 7.3 m. Hardpanized colluvium. Polymictic subround to subangular lithic saprolitic clasts (LL), some pieces of probable weathered metasediment (SD), nodules of goethite (GO) and grains of quartz (QZ) are loosely packed into a similar matrix (MX) of finer-grained materials.</p> <p>Close up photograph of cut block in oblique reflected light.</p>	<p>D. WD25. 7.3 m. Clasts of weathered metasediment (SD), goethite nodules (GO), fragments of yellow saprolite (YS) after ultramafic rocks and quartz (QZ), packed into a matrix of quartz and goethite-stained clay (GC). Internally, some goethite nodules are massive (MV). Derived from a broad, provenance of variably exposed regolith. Photomicrograph of thin section in transmitted plane polarized light.</p>
<p>E. WD26. 12.60 m. Mottled, clay-rich sediment. A matrix of fine kaolinite (KA) contains scattered quartz clasts (QZ) and minor goethite nodules (GN). The matrix has been mottled by hematite (HE). Close up photograph of cut block in oblique reflected light.</p>	<p>F. WD26. 12.60 m. Detail of quartz clasts (QZ) set in a fine-grained kaolinite matrix (KA) that has been mottled by hematite (HE). Photomicrograph of thin section in transmitted plane polarized light.</p>
<p>G. WD27. 18.95 m. Mottled, clay-rich sediment. White kaolinite (KA) has been strongly mottled and stained by goethite (GT). Close up photograph of cut block in oblique reflected light.</p>	<p>H. WD27. 18.95 m. Detail of the kaolinite-rich matrix (KA) scattered with small quartz grains (QZ). The ratio of quartz and clay varies in the section, possibly reflecting bedding. Voids are developed along cracks that are now filled with weakly banded fine-grained clay (VO). Photomicrograph of thin section in transmitted plane polarized light.</p>

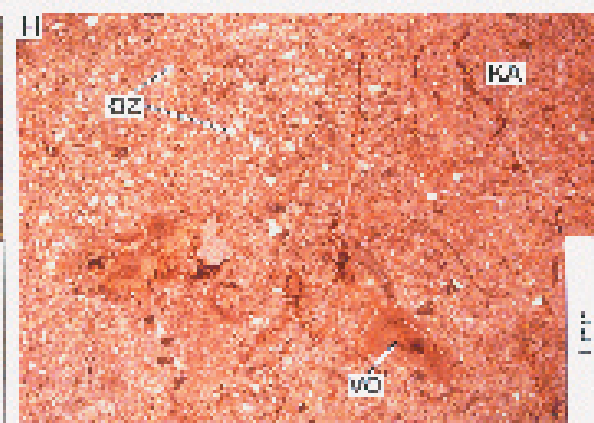
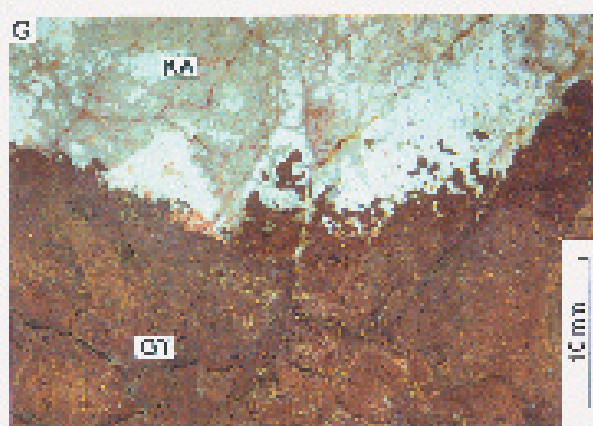
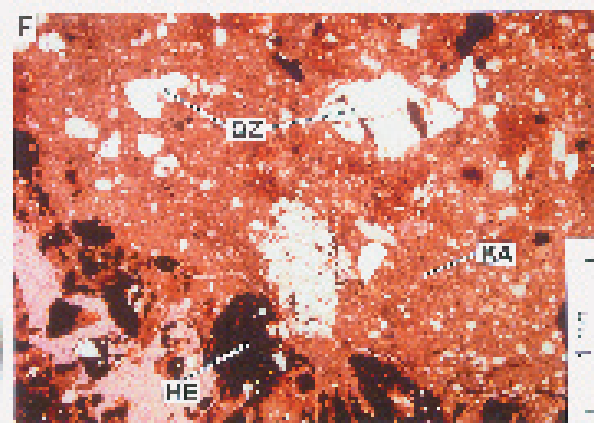
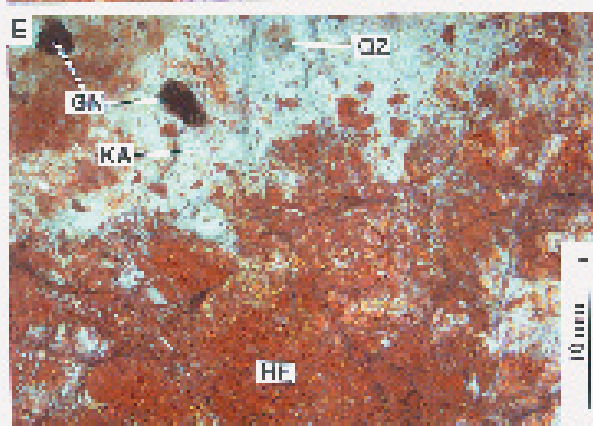
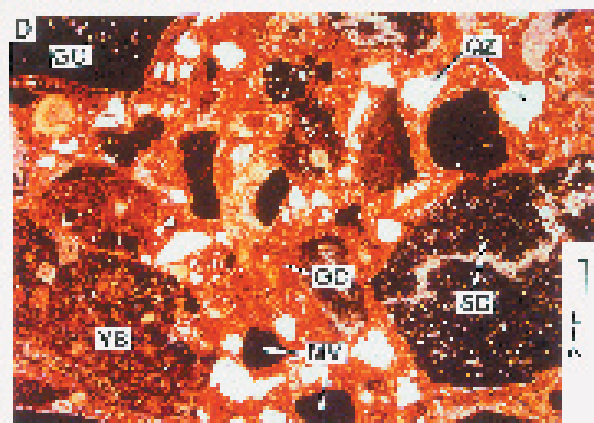
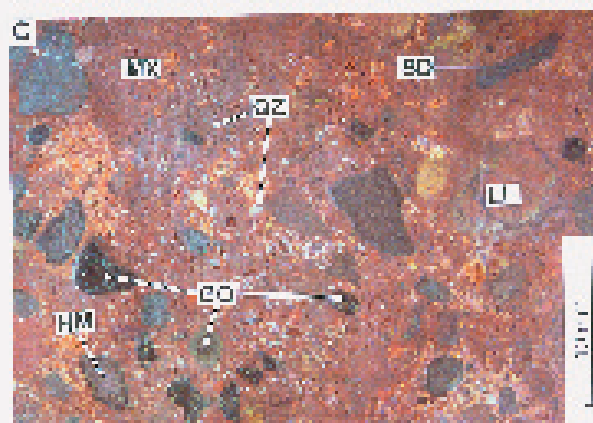
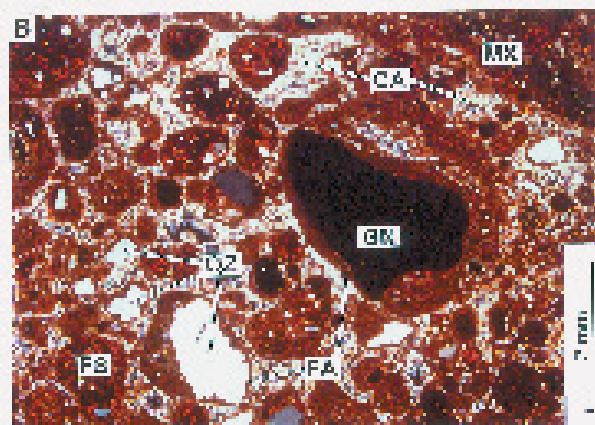
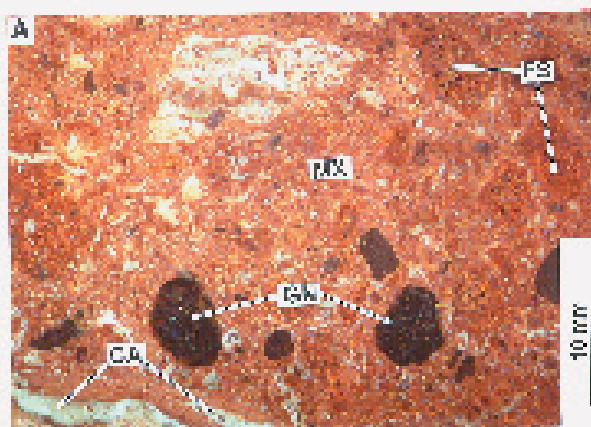


FIGURE 33

<p>A. WD29. 23.00 m. Mottled saprolite or pedolith. Quartz grains (QZ) and patched of coarse flaky kaolinite, possibly after feldspars are packed in a fine-grained kaolinite matrix (KA). This has been mottled and veined with hematite (HM). Close up photograph of cut block in oblique reflected light.</p>	<p>B. WD29. 23.00 m. Equant crystals of quartz (QZ) and patches of coarse, flaky kaolinite, probably after feldspars (FS) are surrounded by a groundmass of fine-grained kaolinite (KA). Ped-like cracks are filled with hematite and goethite (HG). Photomicrograph of thin section in transmitted plane polarized light.</p>
<p>C. WD28. 25.65 m. Mottled pedolith. Scattered grey anhedral quartz grains (QZ) are surrounded by a mat of white kaolinite (KA) that has been cracked and mottled by hematite (HM). The grains of patches of granular vein quartz (VQ) have been separated by clay and Fe oxides. Close up photograph of cut block in oblique reflected light.</p>	<p>D. WD28. 25.65 m. Quartz grains (QZ) are surrounded by a groundmass of flaky kaolinite (KA) with relict structures possibly indicating weathered feldspars (FS) in a fine-grained groundmass. Hematite (HM) has penetrated the groundmass along ped boundaries. Photomicrograph of thin section in transmitted plane polarized light.</p>
<p>E. WD30. 29.40 m. Pedolith. Brown-stained quartz grains (QZ) are loosely scattered in fine-grained kaolinite that has been largely stained yellow by goethite (KG) and a coarser-grained flaky kaolinite (KH) that has been stained pink by hematite. Close up photograph of cut block in oblique reflected light.</p>	<p>F. WD30. 29.40 m. Grains of quartz (QZ) and cherty patches of quartz granules (CH) are scattered in a goethite- and hematite-stained clay matrix (MX). The grains of remnants of veins and patches of metamorphic quartz (QV) have been separated by clays (CL) stained by Fe oxides. Photomicrograph of thin section in transmitted plane polarized light.</p>
<p>G. WD31. 34.55 m. Saprolite of quartzo-feldspathic schist. Braided yellow ribbons of clay (KR) pseudomorph a schistose fabric surrounding grains of stained quartz (QZ) and pink-stained flaky clays (KP). Close up photograph of cut block in oblique reflected light.</p>	<p>H. WD31. 34.55 m. Detail of braided ribbons of Fe-stained kaolinite (KA) veined with goethite (GT) set with quartz grains (QZ) and ribbons of granular metamorphic quartz (QV). Photomicrograph of thin section in transmitted plane polarized light.</p>

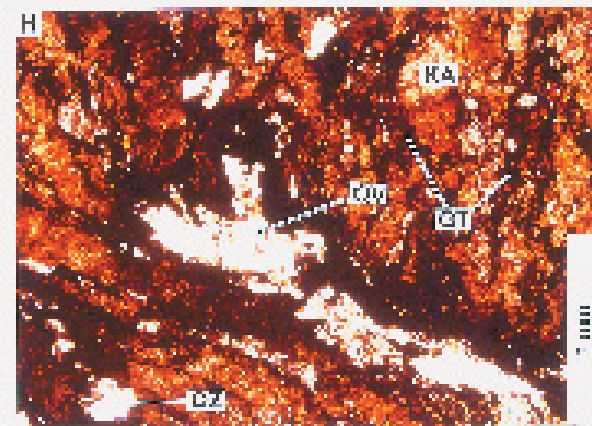
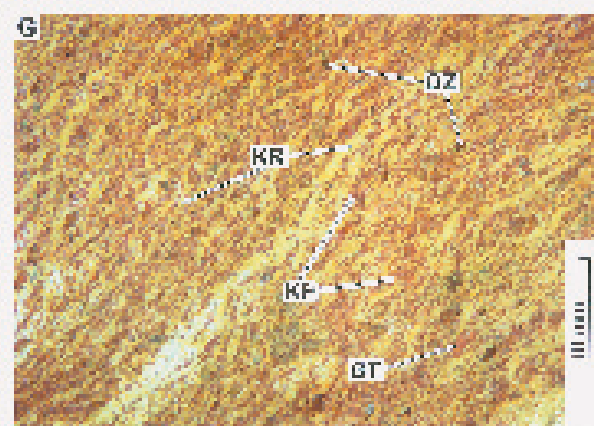
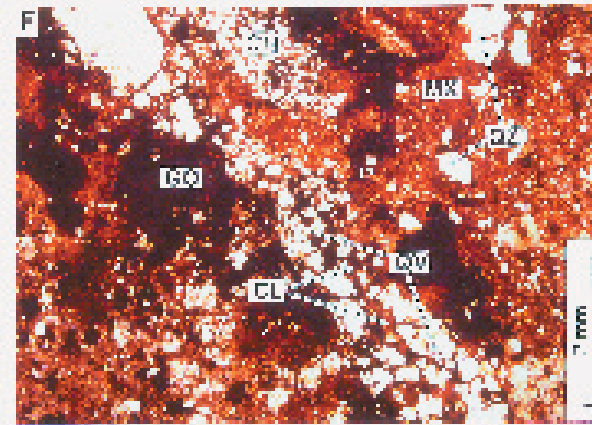
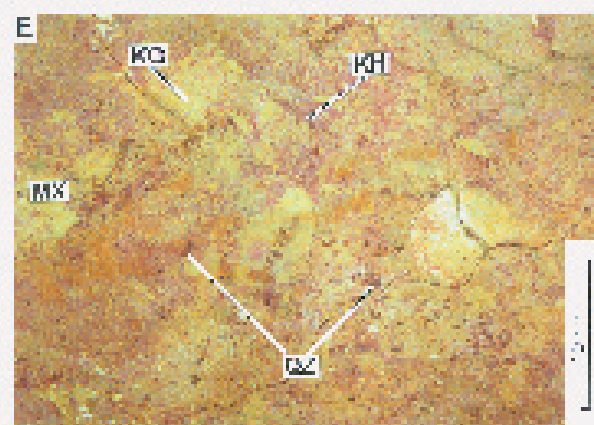
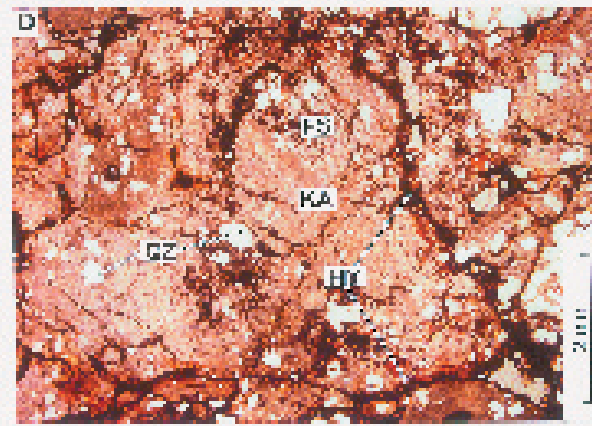
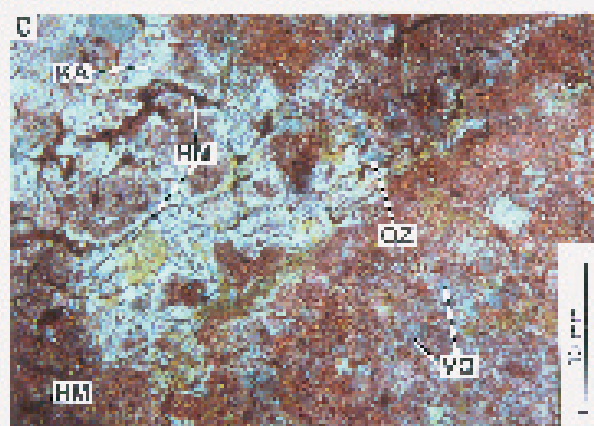
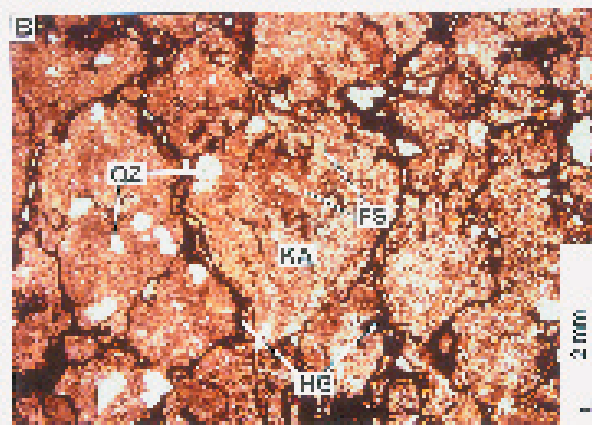
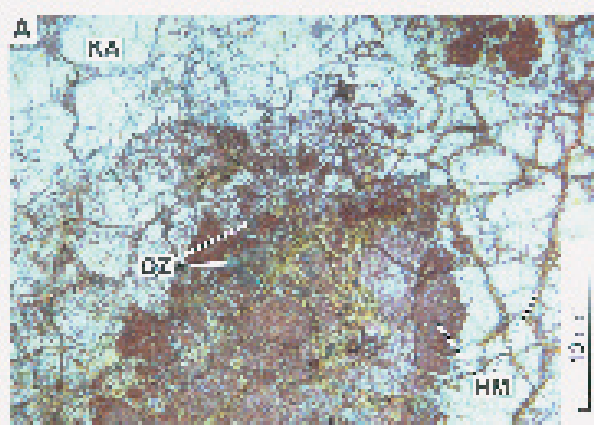
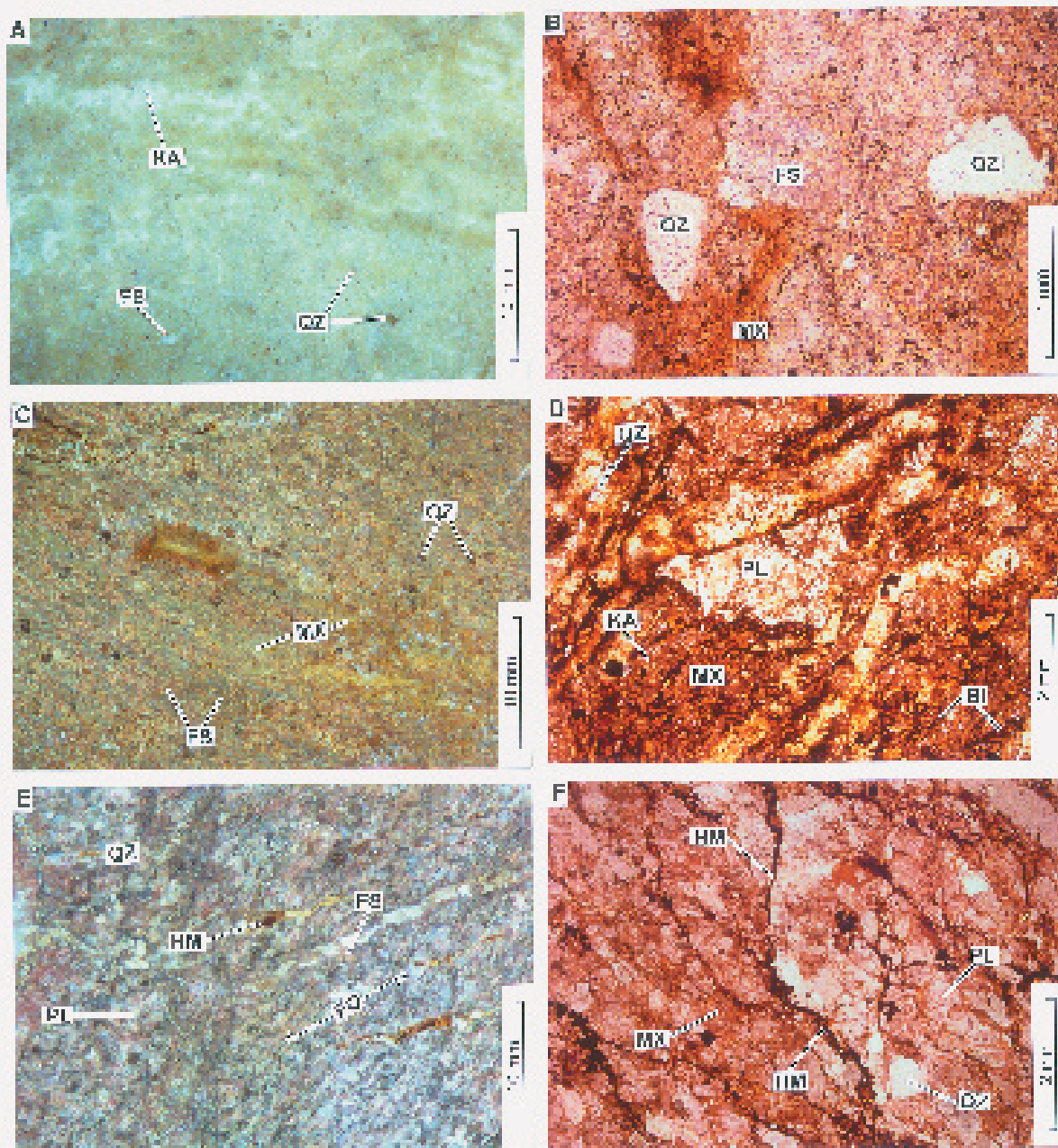


FIGURE 34

<p>A. WD32. 36.40 m. Unfoliated lower saprolite. Small anhedral quartz grains (QZ) and grey patches of partly-kaolinised Na- and K-feldspar (FS) are scattered in a white groundmass of kaolinite (KA) and minor quartz. Close up photograph of cut block in oblique reflected light.</p>	<p>B. WD32. 36.40 m. Grains of quartz (QZ) and patches of partly kaolinised feldspar (FS) are scattered in a kaolinised fine-grained quartzo-feldspathic groundmass (MX). Photomicrograph of thin section in transmitted plane polarized light.</p>
<p>C. WD33. 39.60 m. Ferruginous, schistose saprolite. Weathered Na-feldspar (FS) and quartz (QZ) are scattered in a kaolinised, quartzo-feldspathic groundmass (MX). Close up photograph of cut block in oblique reflected light.</p>	<p>D. WD33. 39.60 m. Weathered Na-plagioclase (PL) and fresh grains of quartz (QZ) (1 mm) are scattered in a kaolinised, granular quartzo-feldspathic groundmass (MX) with wisps of biotite (BI) and flakes of kaolinite (KA). Photomicrograph of thin section in transmitted plane polarized light.</p>
<p>E. WD34. 44.50 m. Fresh to very weakly weathered bedrock. A ribbon-like non-penetrative foliation (FO) cuts the fabric of Na-plagioclase (FS) and quartz (QZ). Close up photograph of cut block in oblique reflected light.</p>	<p>F. WD34. 44.50 m. Crystals of plagioclase (PL) and quartz (QZ) are distributed in a fine-grained, pinkish, slightly hematite-stained quartzo-feldspathic groundmass (MX). A braided non-penetrative foliation has been stained by secondary Fe oxides (HM). Photomicrograph of thin section in transmitted plane polarized light.</p>



ture. There may be some tabular, quartz-poor claystone clasts that are set in a more quartz-rich matrix. Parts show voids developed along cracks filled with a weakly banded very fine-grained clay. Parts are mottled with goethite and hematite, obscuring the clay and leaving the quartz. The detritus was probably locally derived.

WD29. 23.00 m: Mottled saprolite or pedolith - Figures 33A and B.

Equant to shardy and corroded anhedral quartz grains and patches of coarser, flaky kaolinite, possibly after feldspars, are set in a groundmass of fine-grained kaolinite. This groundmass has cracked into peds and the peds have been coated and filled with hematite and minor goethite. Parts of the clay structure has been mottled and stained by hematite and minor goethite. Although there are no visible quartz veinlets, there are some concentrations of small quartz granules. Originally, this rock could equally have been a quartz- and feldspar-phyric igneous rock with a fine-grained groundmass or a retextured metasediment. There is no visible foliation; this may not have been developed in the original bedrock or it has been obscured by subsequent pedoplasation.

WD28: 25.65 m: Mottled pedolith - Figures 33C and D.

A mat of coarse, flaky kaolinite contains scattered anhedral, in places, compound quartz grains. This mat is cracked into peds that are veined and coated with hematite. There are large patches of granoblastic vein quartz that has been penetrated by, and its grains separated by, clays and Fe oxides. There is no visible foliation. Originally this could have been either a quartz-phyric igneous rock, with a felsic groundmass, or a porphyroblastic feldspathic rock with metamorphic and vein quartz that has been modified by pedoplasation.

WD30: 29.40 m: Pedolith - Figures 33E and F.

Single and compound, strained grains of quartz are loosely packed in a goethite-stained fine-grained groundmass of flaky to fine-grained kaolinite. In some parts, the quartz forms single grains; in others it occurs as anhedral, cherty patches of granules. Remnants of quartz veins and lenses show separation of granoblastic grains by goethite-stained clay and goethite. The clays vary from lightly stained by goethite to intensely stained. The fabric appears to be palimpsest metamorphic that has been largely destroyed by pedoplasation. There is no visible foliation. The rock is part of the pedolith.

WD31. 34.55 m: Ferruginous, schistose saprolite of bedrock - Figures 33G and H.

This rock is strongly schistose with ribbons of flaky kaolinite. In this are set patches of granular cherty quartz and anhedral grains of strained quartz. The matted kaolinite ribbons have been intensely stained with goethite. Goethite is particularly intensely developed along a braided cleavage that follows the ribbon margins. Veins of granoblastic quartz cut the fabric. The rock is a saprolite.

WD32. 36.40 m: Unfoliated lower saprolite - Figures 34A and B.

Anhedral quartz crystals and a few remnants of partly kaolinised sodic and potassic feldspar are scattered in a groundmass of white, flaky kaolinite and minor quartz. Patches and lenses of granoblastic polygonal quartz meander in the fabric. There has been very minor staining of the kaolinite in patches and streaks. This rock lacks a significant foliation but the kaolinite seems to pseudomorph remnant feldspar grains. It is a lower saprolite.

WD33. 39.60 m: Ferruginous, schistose saprolite of bedrock - Figures 34C and D.

Roughly equant crystals of weathered Na-plagioclase and fresh grains of quartz (1 mm) are scattered in a kaolinised, yellowish, granular quartzo-feldspathic groundmass with wisps of biotite and flakes of kaolinite. The rock has been variably weathered. In some parts, the feldspars are partly kaolinised along cracks and the groundmass and biotite are stained with goethite. In other parts, ribbons of goethite-stained kaolinite form a foliation that has been extensively penetrated by weathering. This rock belongs to the lower saprolite and is probably a meta-arkose.

WD34: 44.50 m: Relatively fresh saprock - Figures 34E and F.

Anhedral, equant crystals of Na-plagioclase and lesser slightly strained quartz occur in a pinkish, fine-grained, very slightly hematite-stained quartzo-feldspathic groundmass with flakes and wisps of greenish-brown biotite and minor muscovite. A non-penetrative, braided foliation is formed by the biotite and minor kaolinite and has been slightly stained by secondary Fe-oxides. Small veins of granoblastic-polygonal metamorphic quartz wander through the fabric. This is very weakly weathered bedrock, close to the weathering front. It has a metamorphic fabric and is probably a meta-arkose.

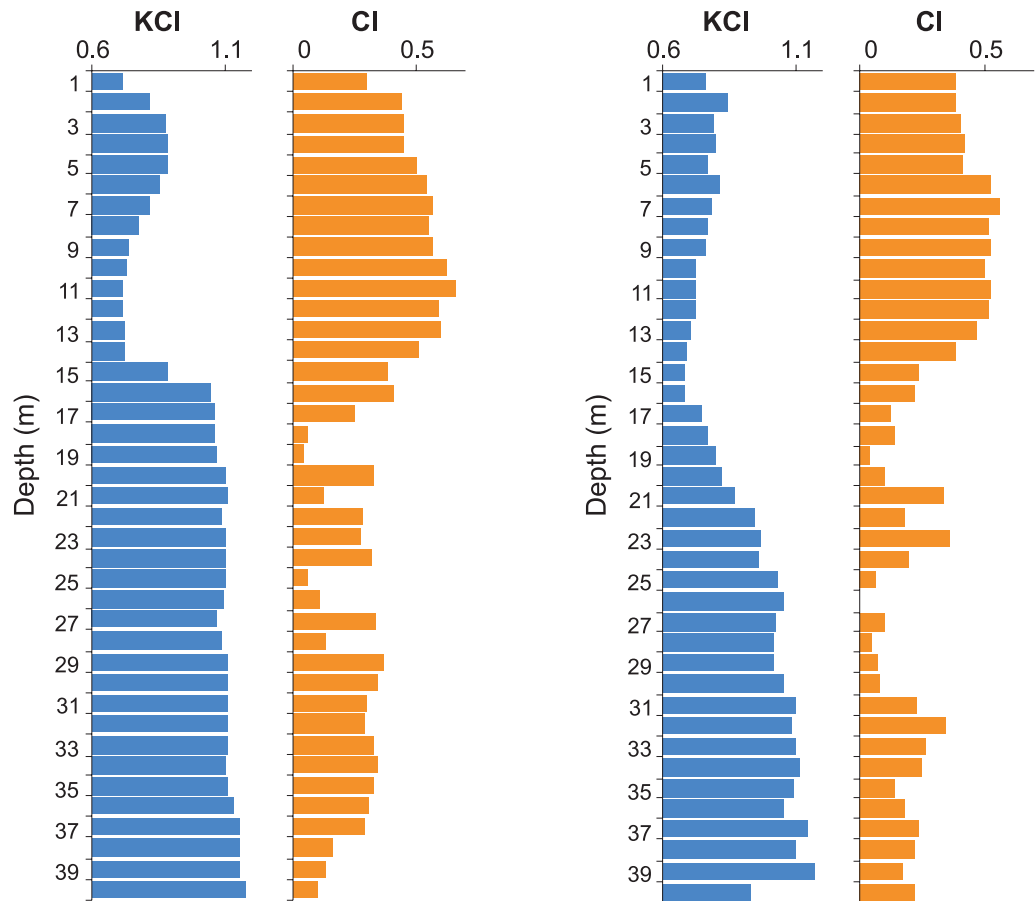


Figure 35. A comparison of colour and KCl profiles for a drill hole representing shallow sediment (left, WDAC004) and a drill hole with bleached zone beneath red clay sediment (right, WDAC007).

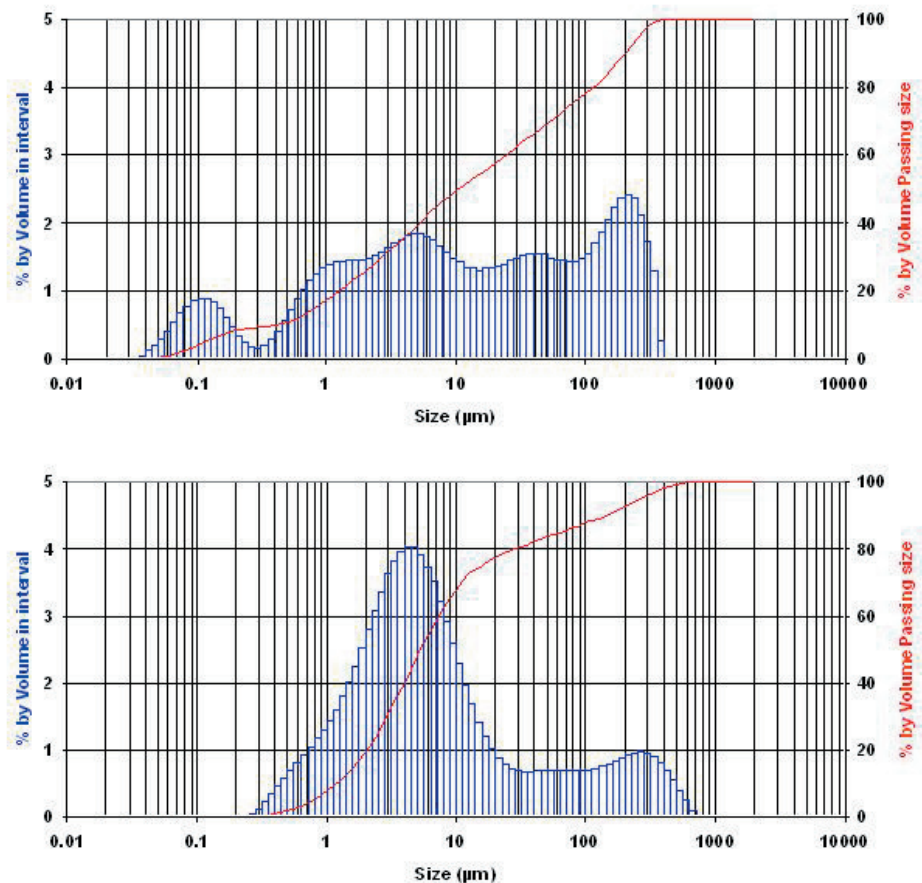


Figure 36. Particle size distribution of red clay sediment and underlying saprolite for drill hole WDAC004. The red clay sediment contains a very fine ($<0.2 \mu\text{m}$) clay fraction.

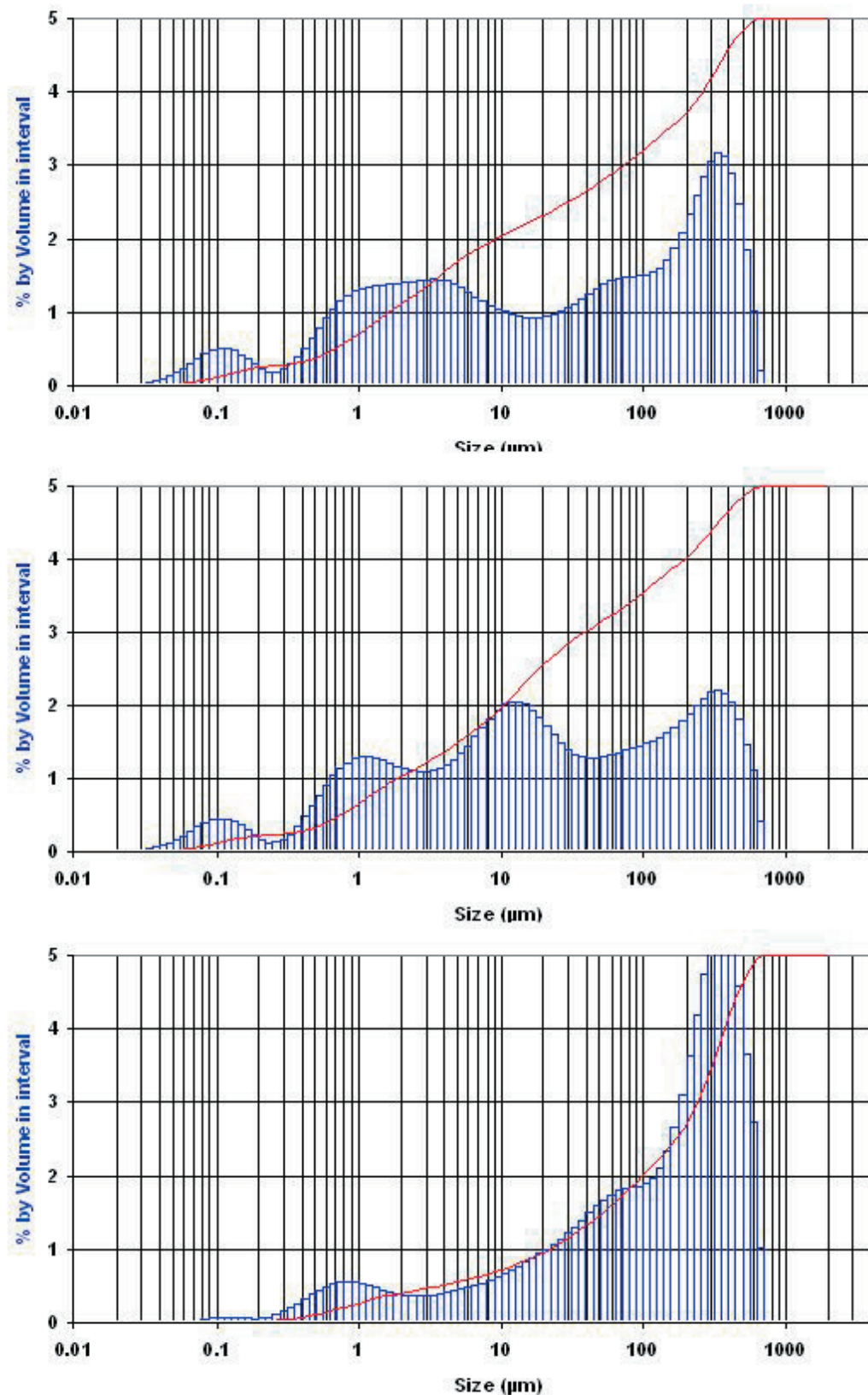


Figure 37. Particle size distribution of red clay sediment, bleached zone and underlying saprolite for drill hole WDAC007. The red clay sediment contains a very fine (<0.2 μm) clay fraction.

6.5 Distinction between transported and *in situ* material

The distinction between transported and *in situ* material was made by (i) visual inspection, (colour and fabric) and (ii) the kaolinite crystallinity index (measured by ASD). The infra-red spectrum of the transported kaolinite indicates it is generally poorly crystalline compared to *in situ* material. This difference can be determined by a kaolinite crystallinity index (KCI) to make an objective distinction.

Colour and KCI profiles of the Whirling-Dervish traverse are shown in Figure 28. Sediments at Whirling-Dervish consist mainly of red clays with magnetic nodules and overlie *in situ* saprolite,

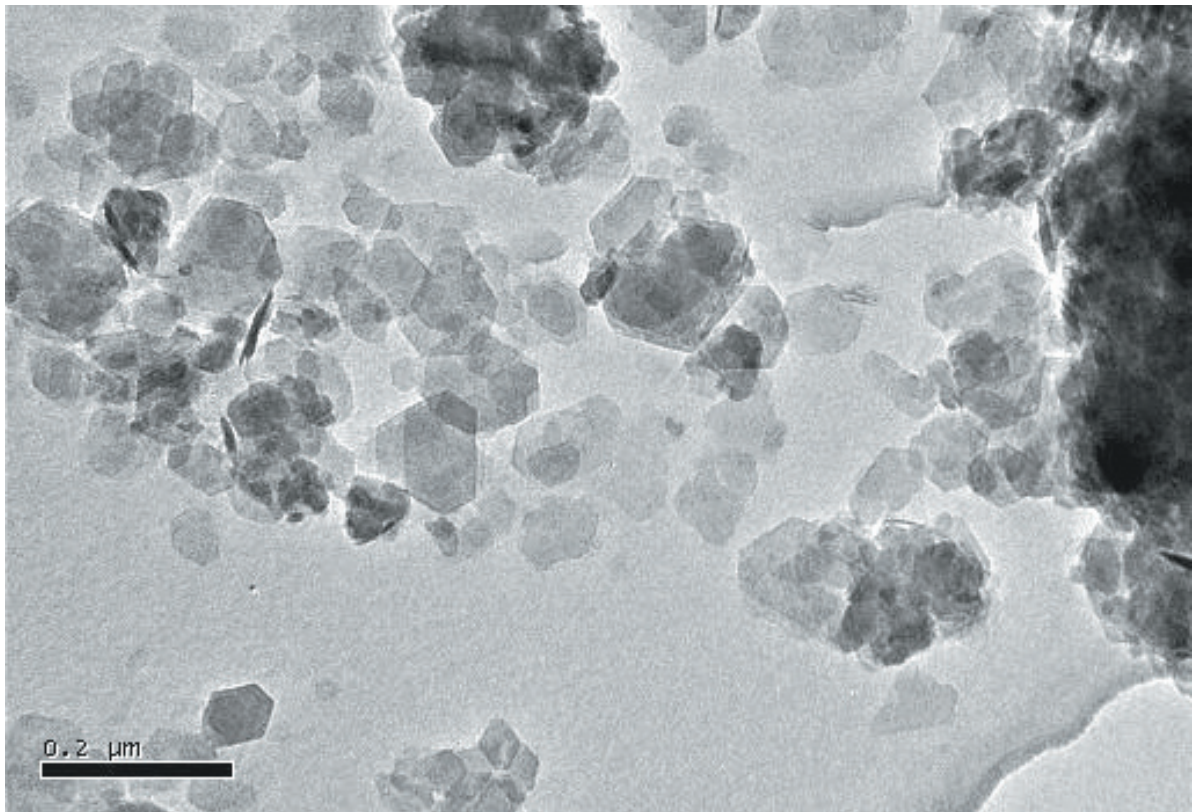


Figure 38. Transmission electron micrograph of red clay sediment from 16 m depth of WDAC007. The red clay sediment and bleached zone contain a very fine ($<0.2\ \mu\text{m}$) clay fraction.

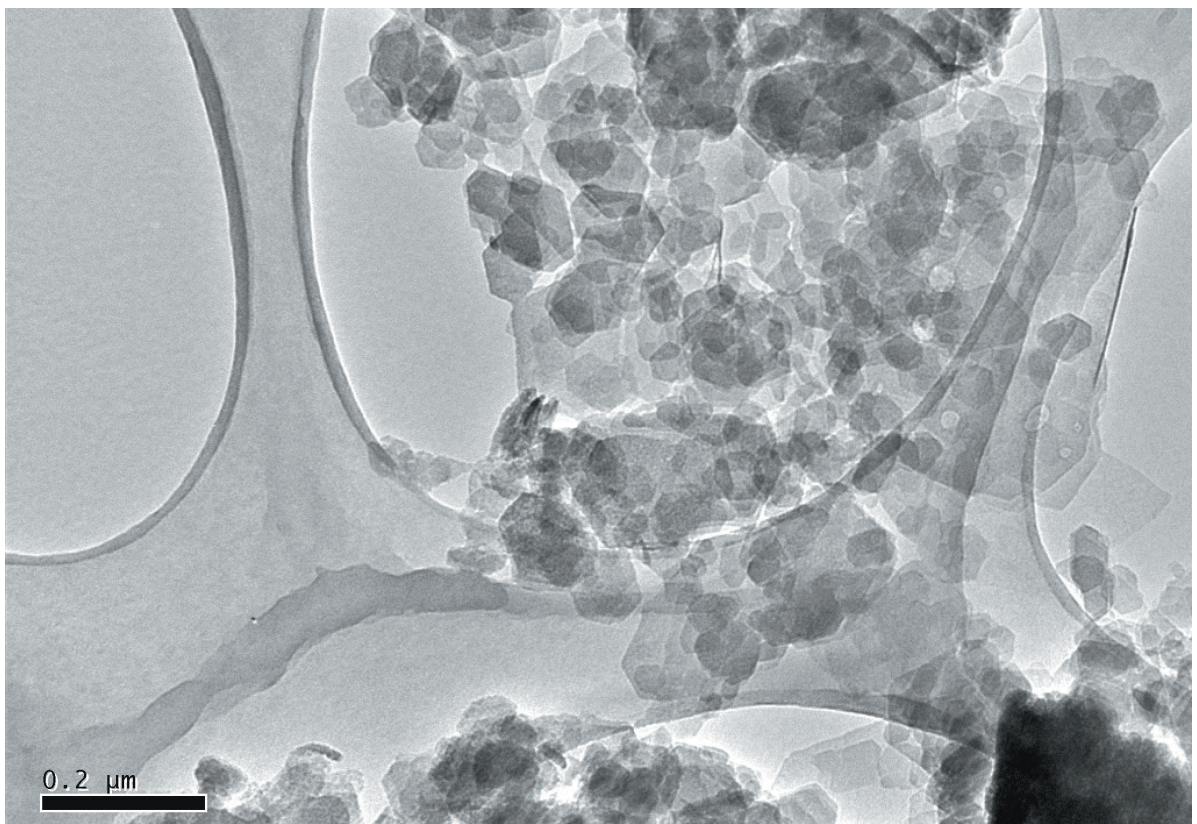


Figure 39. Transmission electron micrograph of bleached clay zone from 21 m depth of WDAC007. As with the red clay sediment, the bleached zone also contains a very fine ($<0.2\ \mu\text{m}$) clay fraction.

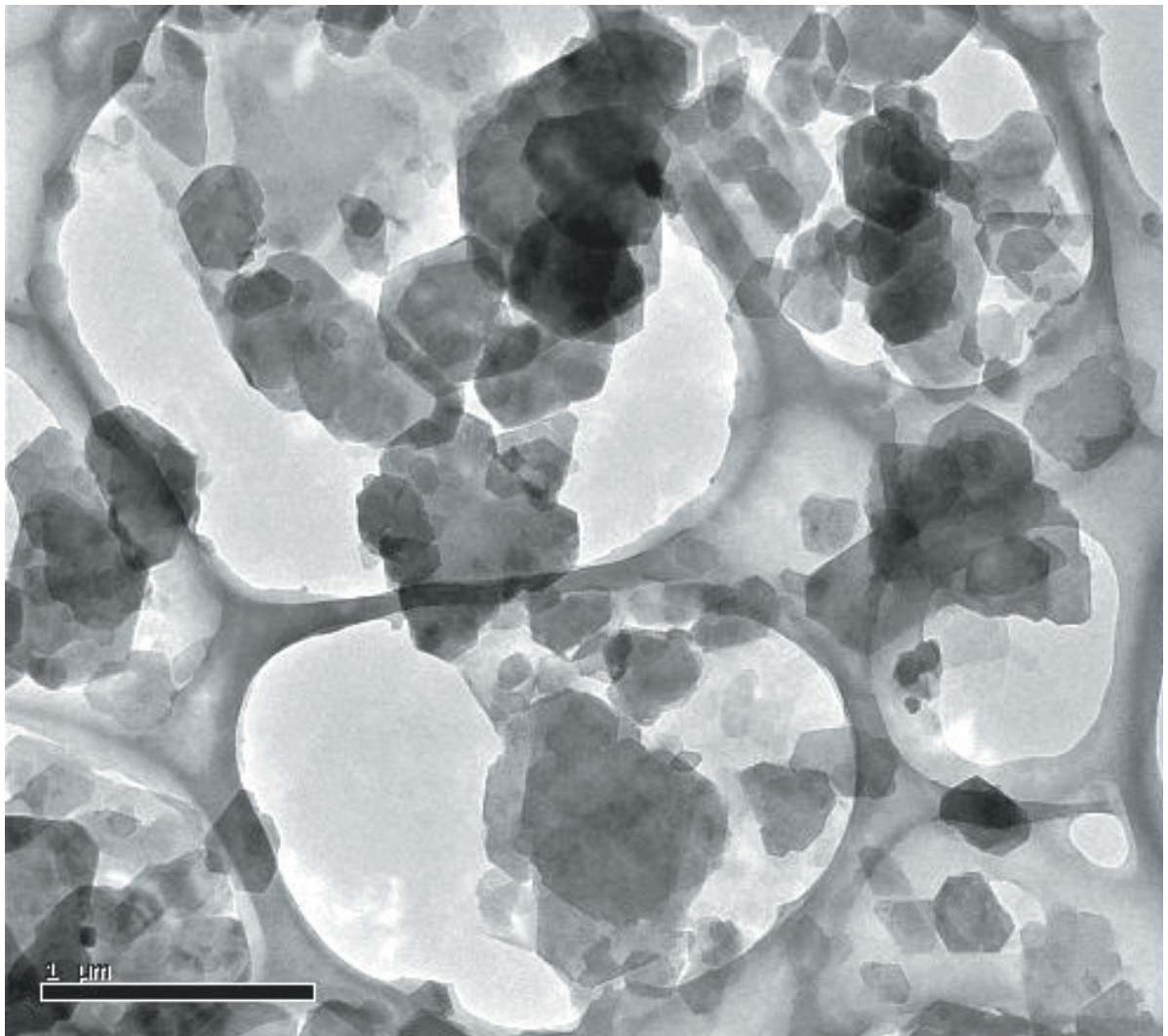


Figure 40. Transmission electron micrograph of saprolite from 25 m depth of WDAC007. The saprolite zone does not contain a very fine ($<0.2 \mu\text{m}$) clay fraction seen in the red clay and bleached zone material.

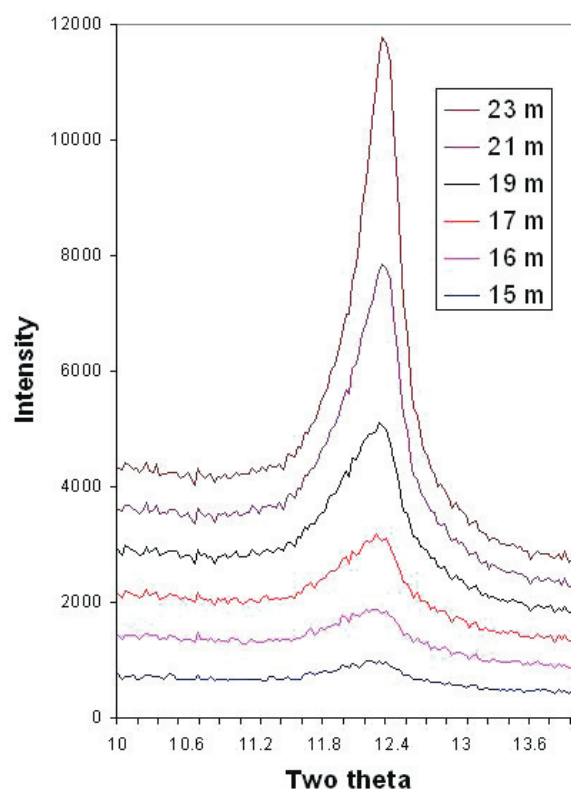


Figure 41. X-ray diffraction profiles of basal reflections of kaolinite from 15, 16, 17, 19, 21, and 23 m depth (stacked bottom to top) of drill hole WDAC007. The reflections become sharper and stronger

providing, in most cases, good contrast in colour, fabric and KCI. Shallow sediments are readily differentiated from the underlying light-coloured saprolite with high KCI. At the SW end of the traverse, where transported cover is shallow, the unconformity between transported and *in situ* material is marked by sharp change in colour and KCI (Figure 35A). In the NE, the colour change from red to white does not coincide with a sharp change in kaolinite crystallinity (Figure 35B). Below the colour boundary, the material lacks saprolitic fabric and the KCI increases gradually over several metres to reach levels typical of saprolite (Figure 35B). This transition between red clays and unambiguous saprolite, referred to as the bleached zone, is difficult to classify as sediment or saprolite on the basis of both field observation and KCI. It was studied further by conducting particle size analysis, X-ray diffraction and transmission electron microscopy to resolve this ambiguity.

Particle size distribution of drill hole WDAC004 (representing shallow sediment over saprolite) and WDAC007 (representing bleached zone over saprolite), determined by laser diffraction, is shown in Figures 36 and 37 respectively. The particle size distribution of red clay sediments for both drill holes show three modes in $<10\ \mu\text{m}$ material and contains a very fine fraction ($<0.2\ \mu\text{m}$). This fine fraction is absent in the saprolite, most of the material here being $>1\ \mu\text{m}$. The particle size distribution of the bleached zone of WDAC007 is more like the red clay sediment than the saprolite.

Transmission electron micrographs of red clay sediment, bleached zone and saprolite from drill hole WDAC007 are compared in Figures 38, 39 and 40 respectively. The red clay sediment contains very fine ($<0.2\ \mu\text{m}$), euhedral crystals of kaolinite. The kaolinite particles are very thin as indicated by poor contrast against the carbon film background. The fine fraction is consistent with particle size analysis provided by laser diffraction. However, the euhedral morphology of the kaolinite crystals was unexpected. Soil kaolinite is generally anhedral. The bleached zone consists of very fine, euhedral kaolinite crystals, similar to those of the red clay, but some larger particles ($>1\ \mu\text{m}$) also occur. The saprolite is devoid of very fine kaolinite and is dominated by thicker, larger ($>1\ \mu\text{m}$) kaolinite crystals; some appear to be pseudomorphs after primary minerals such as mica (Figure 41). These observations are consistent with the particle size analysis.

X-ray diffraction profiles of kaolinite basal reflections from 16-25 m depth are given in Figure 41. With increasing depth within the bleached zone, the basal reflections become sharper and stronger, indicating thicker and more crystalline kaolinite with increasing depth.

The TEM, ASD and XRD information suggest that the red clay sediments have been dissolved and recrystallised in the bleached zone leading to more crystalline kaolinite, (increased KCI with depth). Iron, both free and structural, in the Fe-oxides and kaolinite of the red clay sediments is also mobilised and removed, leading to the bleaching.

6.6 Soil geochemical survey

Four pits were excavated along line 49600N to sample roots, soil and calcrete above the main mineralized zones. Three pits tested the soil on non-mineralized bedrock. Other plant parts (bark, branchwood, phyllodes and litter) were sampled for comparison. Soil samples were analysed using total and partial/selective digests.

The results show Au concentrations are highest in calcrete (16-64 ppb), confirming earlier reports by Gray *et al.*, (2000) that calcrete provides an effective near-surface sampling medium in the Karari area. It appears the main direction of geochemical dispersion is to the NE. The only sample that was taken W of the main mineralized zone shows the lowest Au concentration (16 ppb) whereas Au-in-calcrete concentrations over the mineralization, and some 50-100 m to the NE range from 37-64 ppb.

Selective extraction of soil from approximately 50-150 mm depth using Na dithionite, enzyme leach, 0.1M hydroxylamine, 0.25M hydroxylamine at Whirling-Dervish (Appendix D) does not show any Au concentrations above the detection limit across the main mineralization.

6.7 Biogeochemical survey

As part of the biogeochemical pilot study, plant samples were taken at four sites along line 49600N. The haul road to the W and the tenement boundary to the E limited the lateral extent of this study. In addition, extensive surface disturbance across the deposit strongly limited the availability of sample sites and intact plants. Thus, it was impossible to collect a sufficient number of background samples. Sampled species include Acacia, Eucalyptus mallee, Eremophila and Grevillea.

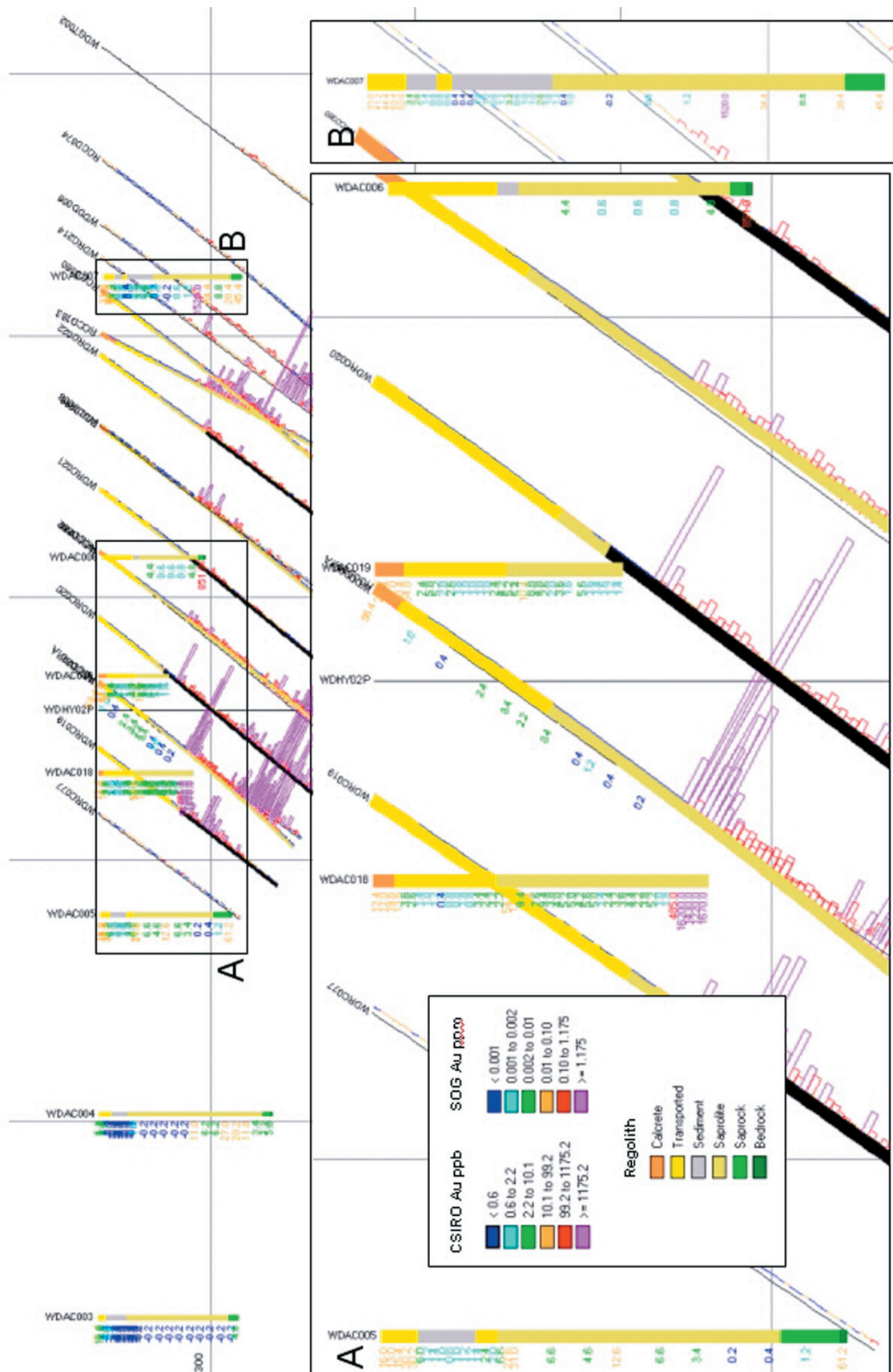


Figure 42. Cross section (49600N) showing Au concentrations (ppb) and Au histograms (SOG data).

The results (Appendix D) show measurable Au concentrations in all plant sample media with some higher concentrations in roots and branch-wood over parts of the mineralized zones. Concentrations of Mo, Bi, Ba, Cr, Mn and Ni are also elevated in some samples over the mineralization compared to samples over non-mineralized rocks. Although the results are only preliminary, they do not show a well-defined Au anomaly over the main mineralized zones.

6.8 Calcrete analyses

Soil carbonate occurs throughout the entire area, generally as a calcareous hardpan. Auger drilling

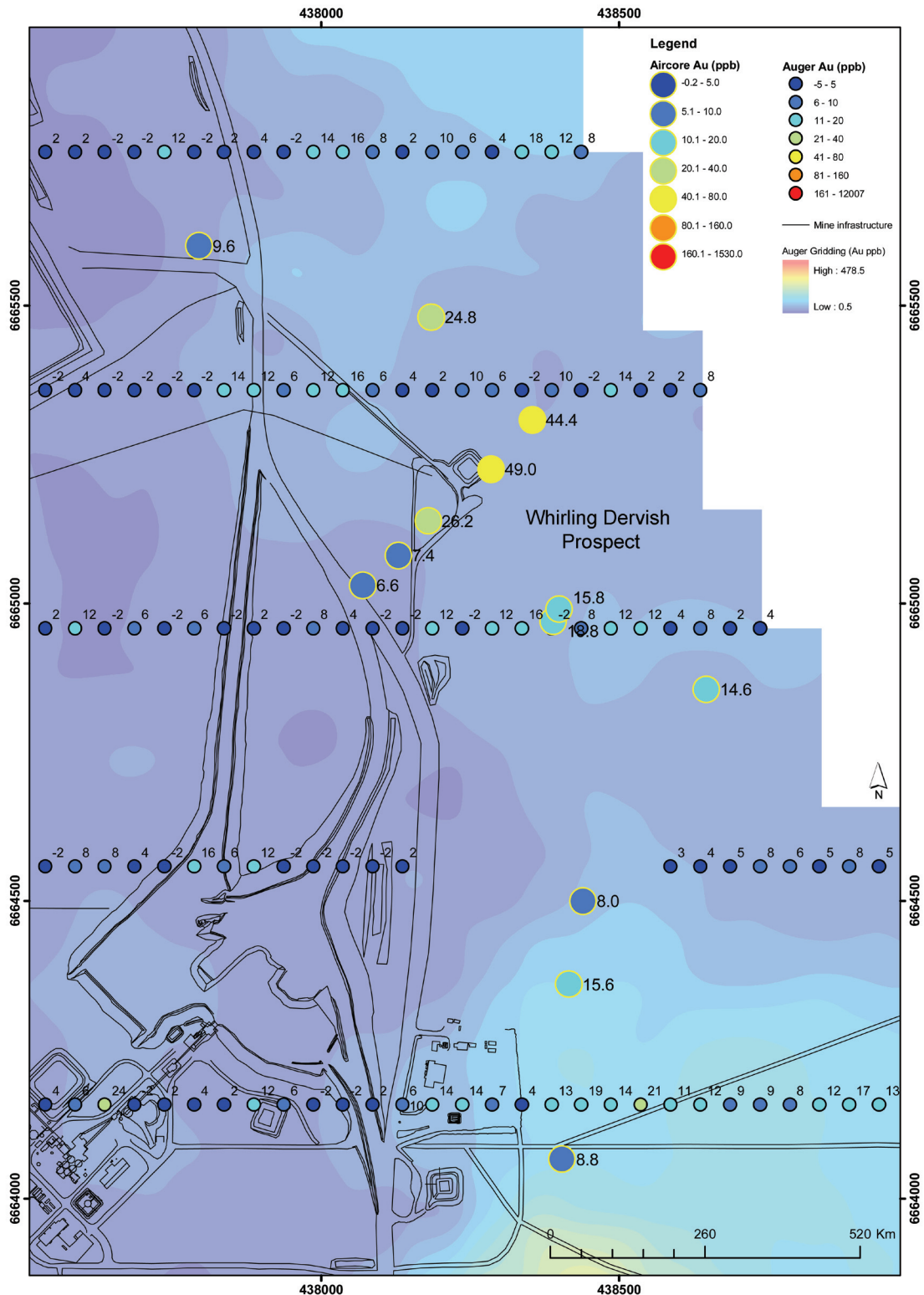
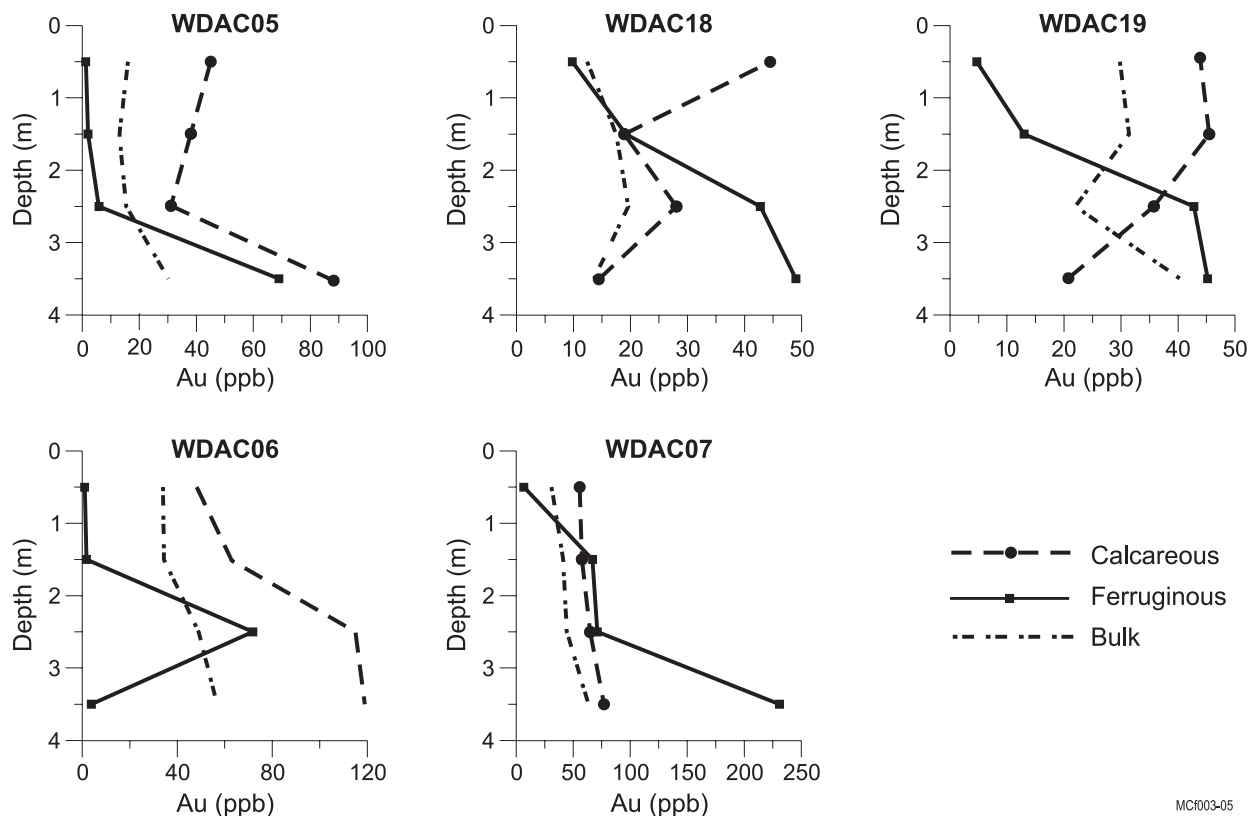


Figure 43 . Comparison of Au concentrations from auger drilling (Box-Cox normalized and kriged using ArcGIS) and from AC drilling (this project), 2-3 m intervals only. Note the absence of a discrete anomaly over Whirling-Dervish in the auger results and, by contrast, anomalous Au results from the AC drilling.

by previous explorers did not indicate a continuous Au anomaly over Whirling-Dervish. However, analyses of RC drilling provided by SOG (Figure 42) show widespread anomalous Au concentrations of 20-30 ppb in the top 3 m. To establish whether the calcrete was indeed anomalous in Au or whether the Au concentrations in RC samples were due to cross-hole contamination, further work was completed as part of this project. Independent studies by AC drilling and by pit face sampling confirmed the existence of a Au-in-calcrete anomaly at Whirling Dervish. It remains unclear why the earlier auger drilling did not identify the anomaly.



MC1003-05

Figure 44. Comparison of Au concentrations in the bulk sample, ferruginous and calcareous material in the upper 4 m AC profiles from Whirling-Dervish.

Sampling of the upper part of the regolith in AC drill samples (Figures 42 and 43) and soil pits (Figure 44) showed a well-defined Au anomaly in calcrete over the Whirling-Dervish mineralization, with Au concentrations ranging from 30-60 ppb (Figure 44). This Au-in-calcrete anomaly is located on 10-20 m of barren (<5 ppb Au) transported cover.

Results from Whirling Dervish show highest Au concentrations in the upper 4 m of the profile (Figure 42). In the upper 1-2 m, Au is generally associated with carbonate whereas from 2-4 m depth, carbonate and/or ferruginous materials host the anomalous Au (Figure 44). Similar relationships were observed at, for example, the Golden Delicious and Safari deposits (Lintern, 2002).

The results of our work at Whirling Dervish are of significance because of the considerable thickness of transported cover (10-20 m) that overlies Au-bearing saprolite. Both landform and palaeosurface suggest no lateral transport of Au has taken place from areas outside Whirling Dervish, for example Karari, to form the near-surface anomaly. It is therefore most likely that vertical transport of Au by, for example, biota, is the main mechanism by which this anomaly formed.

It would be most important to establish the maximum thickness of cover above which a Au-in-calcrete anomaly can form in this terrain and by what mechanism. Further studies along strike of Whirling Dervish are recommended. It is also feasible that bedrock Au targets in the Carosue Dam mine corridor remain undetected due to possibly ineffective testing by the earlier auger drilling program.

6.9 Laser ablation ICPMS and microprobe study

Method

In-situ geochemical analyses have been used to better constrain the minerals that act as significant hosts for Au and other important elements in the Whirling-Dervish regolith profile. *In-situ* geochemical microanalysis is a powerful method to search for specific mineral and regolith features that host indicator elements (Au, Cu, Pb, As and Zn). A preliminary electron-microprobe and laser ablation inductively coupled plasma mass spectrometry (LA-ICPMS) study has been completed on selected specimens from the WDDD001 core from Whirling-Dervish.

LA-ICPMS, in particular, is an increasingly useful technique in revealing the distribution of Au at thin section scale. It can detect >10 ppb Au through *in-situ* analyses at a spatial resolution of some 20 μ m,

given suitable specimen material and preparation. Two methods were used in this study of polished thin sections from Whirling-Dervish: -

Laser transects: These provide a rough indication of major and trace element distribution across the specimen. This creates large datasets as many elements can be collected simultaneously over a relatively long time scale. Although largely qualitative, it provides a rapid means of locating anomalous elements, including Au, in a heterogeneous specimen (e.g., regolith). Sensitivity is not as good as for *in-situ* spot analyses, due to shorter count times.

Spot analyses: These data are quantitative. A volume of the specimen is ablated by a single laser spot as small as 20 μm in diameter. Generally a spot size of 80 μm was a satisfactory compromise between spatial resolution and providing sufficient volume of ablated material to achieve good count rates from the mass spectrometer for the elements of interest.

Specimens

The core (WDDD001) was drilled from directly above mineralization. The profile comprised some 6 m of hardpanized colluvium, and 22 m of transported overburden that overlies residual saprolite and saprock with fresh bedrock at approximately 45 m depth.

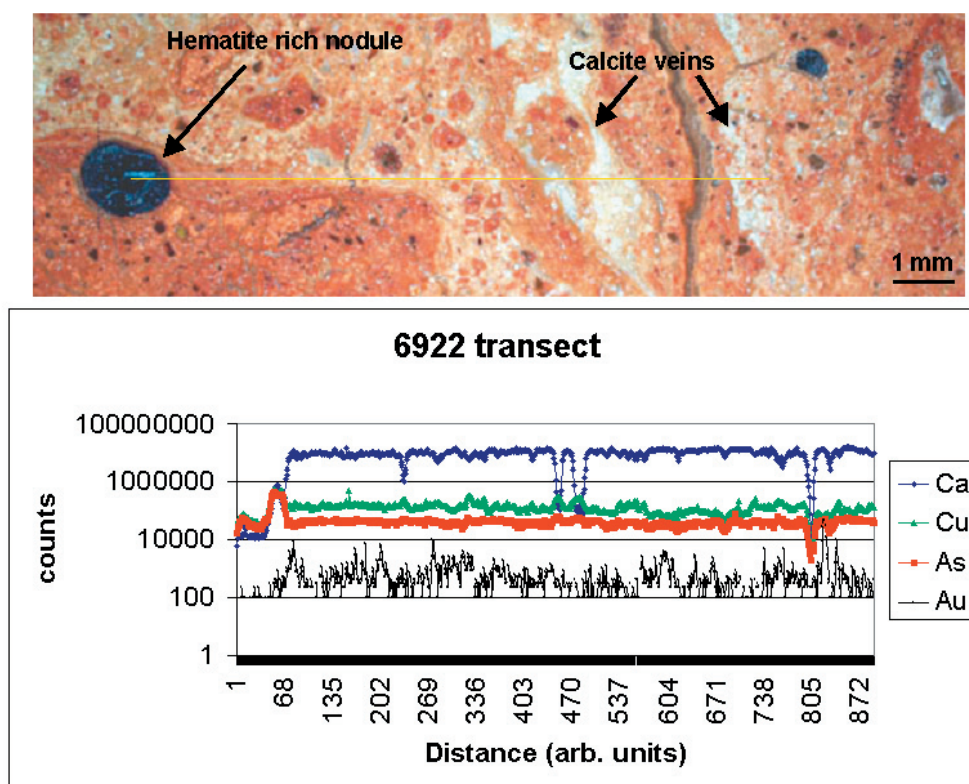


Figure 45. A. Optical micrograph of a hematite rich nodule set in a matrix of iron oxides, kaolinite and calcite, white calcite veins also penetrate the specimen. B. Laser ablation transect across the area marked in Figure 1A (yellow line).

Three specimens from the Whirling-Dervish core provided interesting results. They were: -

6922 Calcified, hardpanized colluvium from near surface (0.4-0.5 m) to identify the role of calcification and ferruginization in hosting anomalies in the colluvium near surface;

6929 Purple mottled *in-situ* clays form just below the unconformity (25.35-25.4 m) to precisely locate Au in the saprolitic clays below the unconformity;

6930 Red and purple mottled clays from deeper in the saprolite (27.7-27.82 m) to determine the level to which ferruginization had generally depleted clays in the saprolite and had created anomalies.

Results

Calcified, hardpanized colluvium from near surface (0.4-0.5 m) 6922.

A laser transect (Figure 45A) was ablated through a hematite-rich nodule, through its cutan and into a matrix of fine kaolinitic clays, Fe-oxides and calcite that also contained a few hematite clasts and

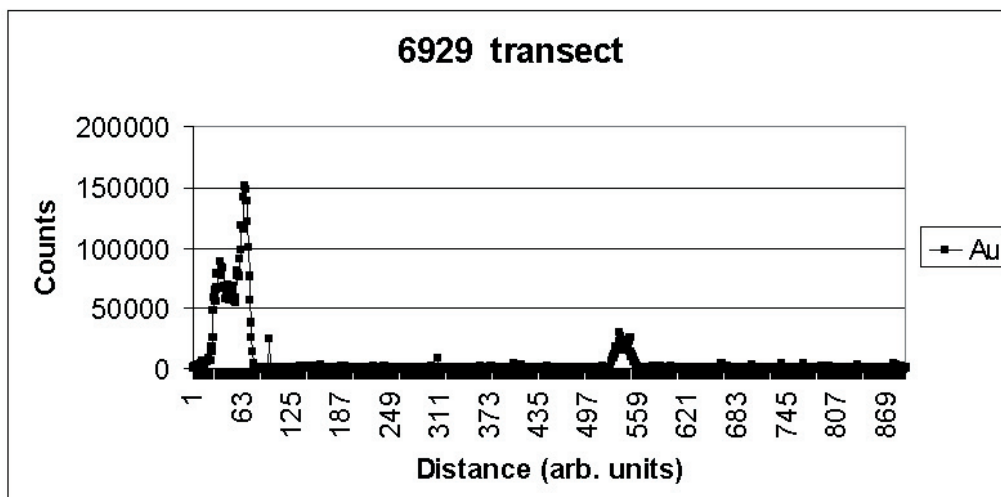
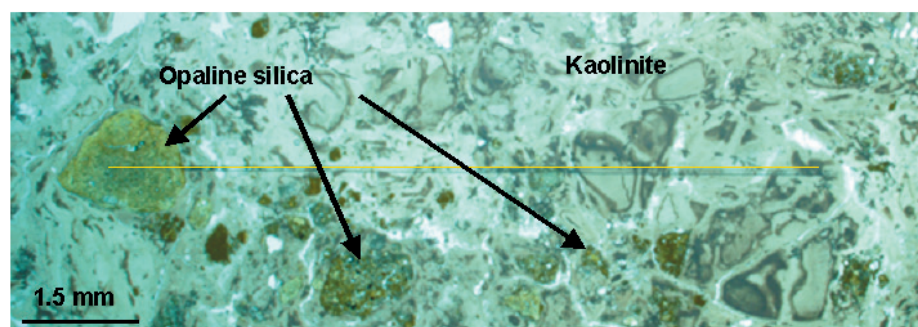


Figure 46. A. Optical micrograph of yellow opal clasts set in a kaolinite matrix. B. Laser ablation transect crossing Au bearing opal clasts in a kaolinite matrix (yellow line in Figure 46A).

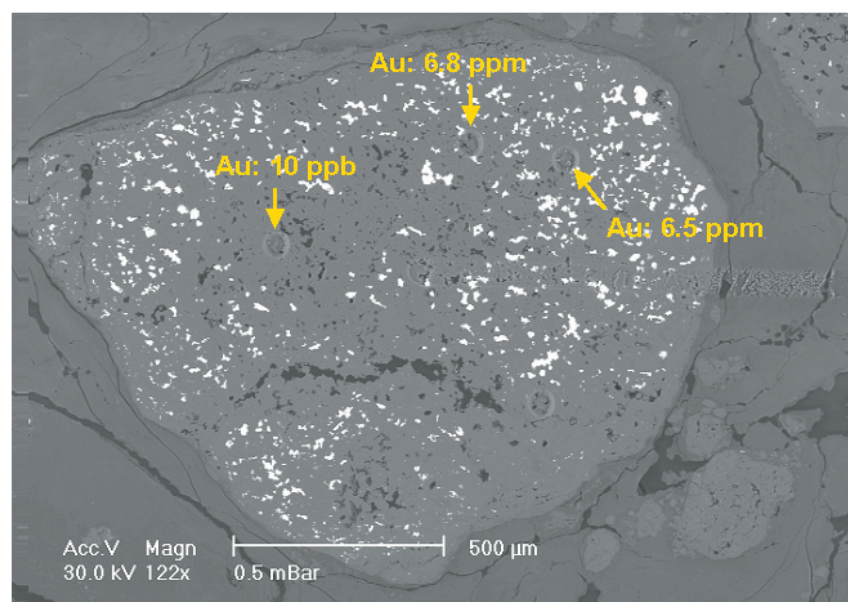


Figure 46C. Back-scattered electron image of opal clast with bright barite inclusions.

calcite veins. The transect (Figure 45B) reveals the hematite nodule has a cutan with more As and Cu than its core. Small Au spikes (up to 10 000 counts) can be seen throughout the matrix of the specimen; a larger spike occurs towards the end of the transect, coinciding with a calcite vein. This implies that calcite is a host for Au in the uppermost part of the profile.

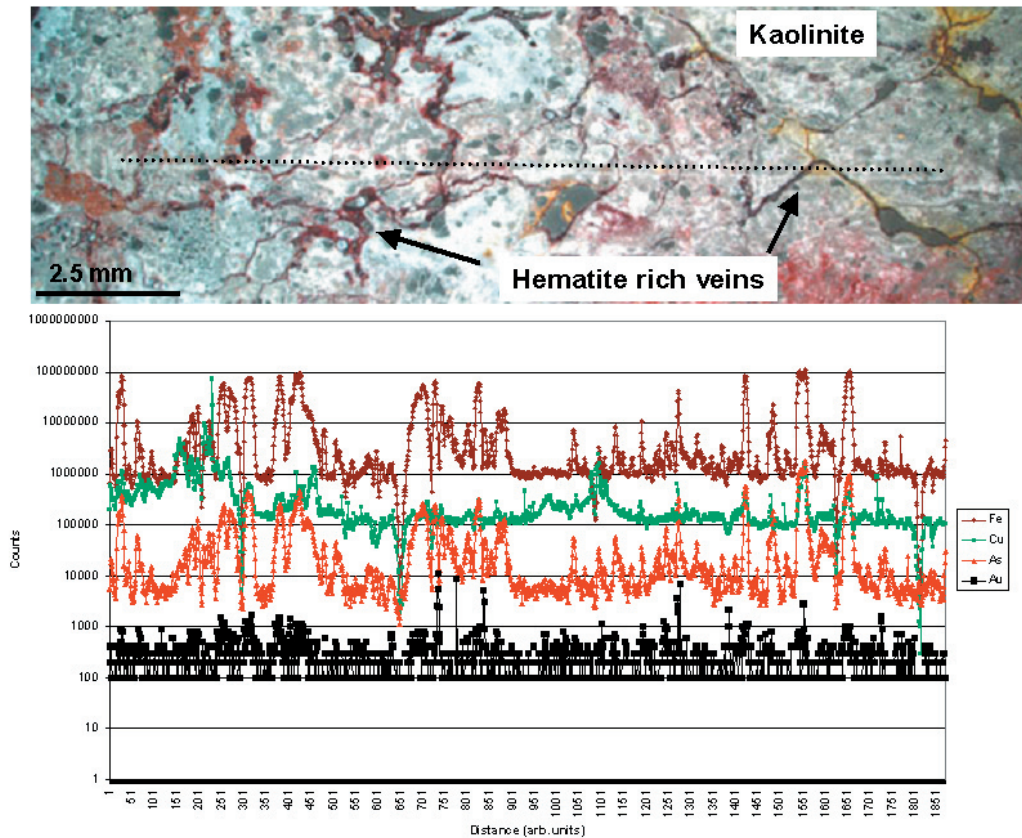


Figure 47. A. Optical micrograph showing the hematite rich veins penetrating dominantly kaolinitic clays with the laser ablation transect marked as a black dotted line. B. Laser transect across the dotted line in Figure 47A.

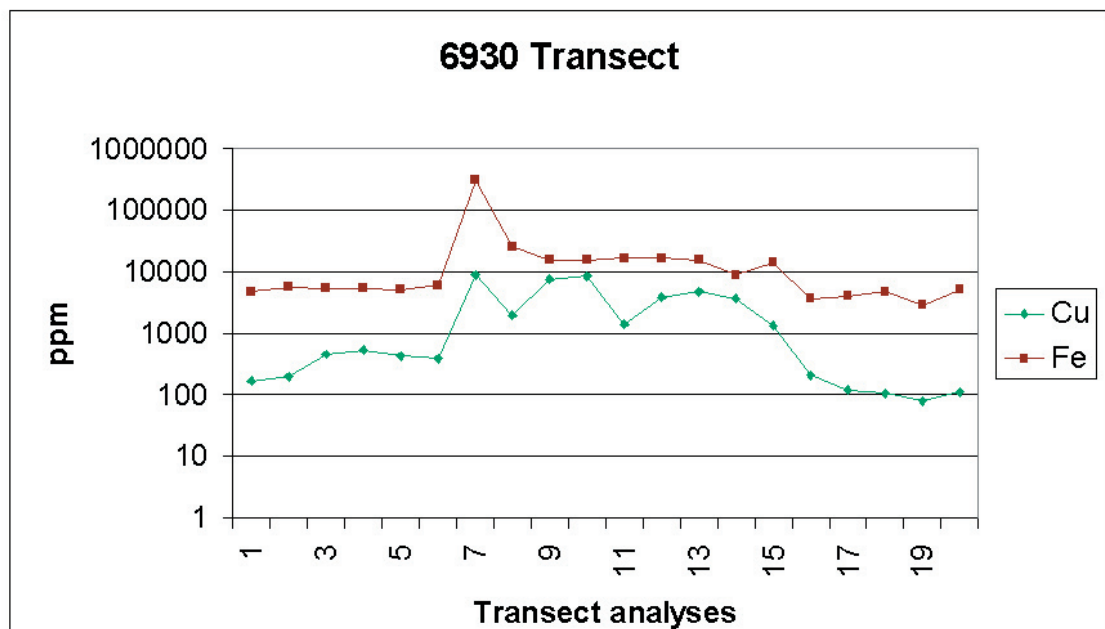


Figure 47C. Electron microprobe transect of hematite rich area in Figure 47D (yellow line).

Purple mottled *in-situ* clays from just below the unconformity (25.35-25.4 m) 6929.

In this specimen, a transect (Figure 46) was ablated in the bleached part of the mottled clays, going from a yellow, highly siliceous clast of opal (confirmed by SEM-EDS analyses) into the kaolinitic matrix. This transect intersects a second, much smaller opal clast about half way through the ablation traverse. The opal clasts contain appreciable Au anomalies; the large clast having two clear peaks.

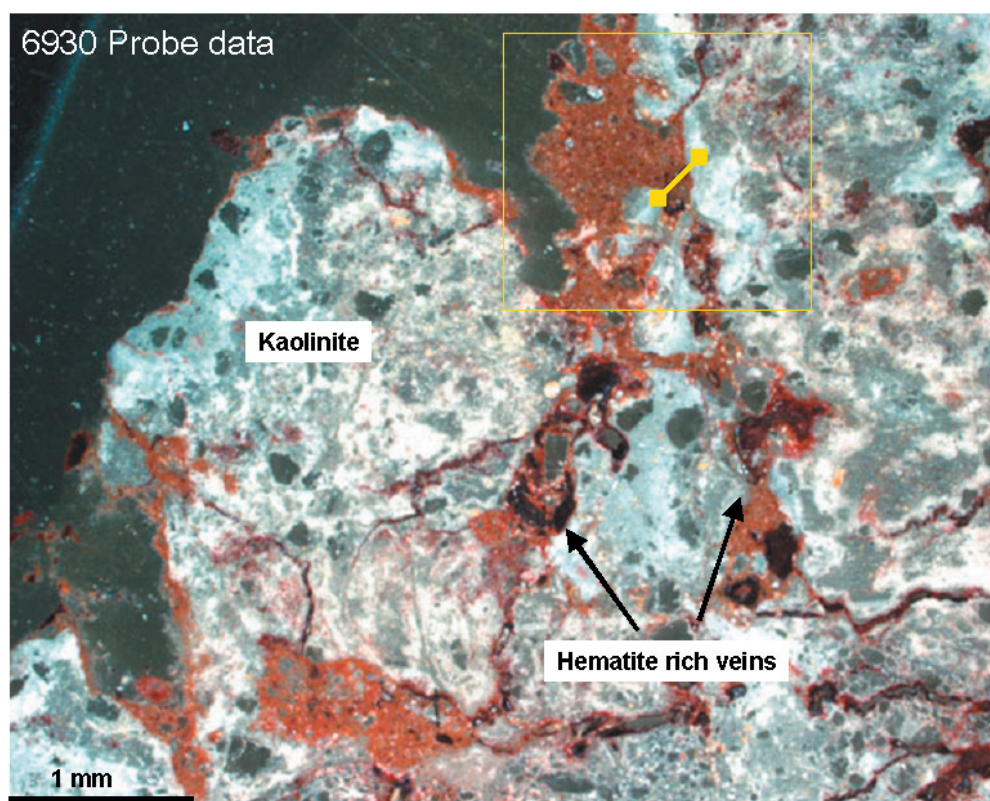


Figure 47D. Optical micrograph of specimen 6930, mottled kaolinitic clays showing location of the electron microprobe transect (Figure 48C) through a hematite rich vein.

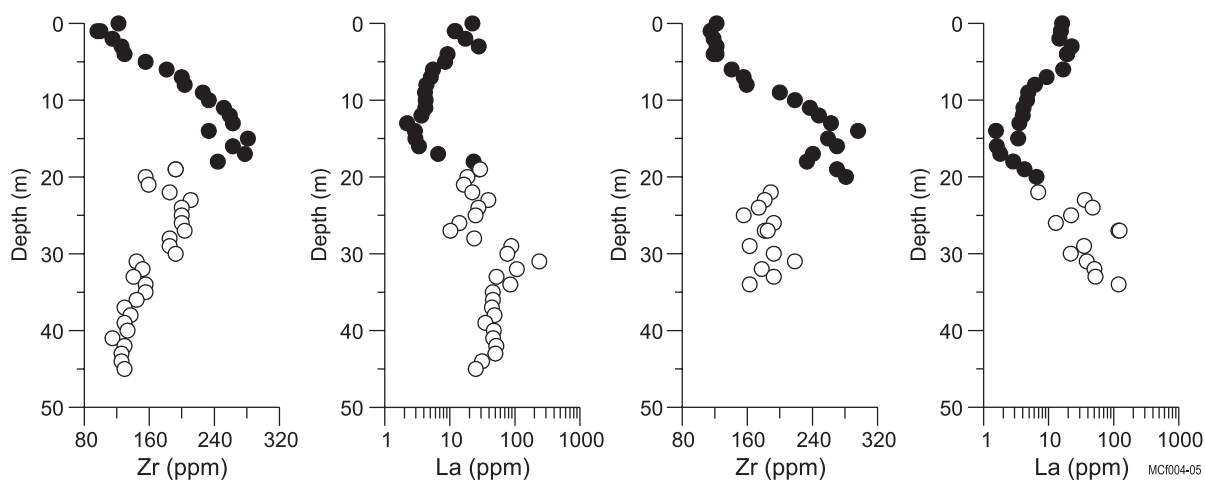


Figure 48. Zirconium and La profiles for WDAC18 (left) and WDAC19 (right). Light grey and red indicate the transported cover according to the ASD interpretation.

Further analyses using the SEM-EDS (Figure 46C) showed small barium sulphate (barite) inclusions within the opal and within all of the similar yellow clasts in the thin section. It is these sulphate inclusions that host Au. This was confirmed by laser ablation spot analyses (also marked on Figure 46C). The analyses show that, in the absence of sulphate, only 10 ppb of Au was detected. However, analyses of sulphate yielded 6.5 and 6.8 ppm (almost three orders of magnitude more). Three further spots giving 9, 10 and 29 ppm Au were obtained from sulphate inclusions in a separate yellow opaline clast.

Red and purple mottled clays from deeper in the saprolite (27.7-27.82 m) 6930.

This laser transect (Figure 47A) crossed at least two generations of hematite rich veins (dark brown and pale red-brown) that have penetrated the dominantly bleached kaolinitic saprolite. Arsenic abundance is closely linked to Fe throughout the transect, Cu behaves similarly in only a few cases and appears to be linked to more isolated occurrences of certain hematite-rich veins. The microprobe

transect (Figure 47C) of the area (boxed in Figure 47D) shows that the Cu concentration is typically around 1000 ppm in these veins but locally reaches nearly 10,000 ppm.

6.10 Regolith geochemistry and statistical analysis

Anomaly distinction

The geochemical data from Whirling-Dervish was to be investigated to distinguish a geochemical signature in regolith on or near mineralization from that in regolith on barren lithologies and to find vectors to mineralization to assist greenfields and brownfields exploration. The geochemistry of residual and transported regolith over the deposit were to be compared with a background population and samples from other prospects along strike within the Carosue Dam mine corridor. For this purpose, 177 samples from AC, RC and diamond drilling at Whirling-Dervish (residual and transported materials) were analysed for a suite of 52 elements, including low-level Au. Background samples and material from other prospects were to be provided by SOG as part of the companies' ongoing regional exploration. Analyses of regional end-of-hole samples by SOG did not provide adequate datasets due to differences in element suites and analytical techniques. So far, no suitable regional material has become available and it has therefore not been possible to perform the statistical analysis. All geochemical data are listed in Appendix D.

Distinguishing residual from transported materials

The geochemical regolith analyses assisted in defining the boundary between residual and transported materials at the Whirling-Dervish prospect. The element concentrations of, for example, Ti, Zr and the REE in residual clays in WDAC18 and WDAC19 differ from those in the overlying alluvium (Figure 48). Together with the ASD spectral data, this information can further improve the separation of these important regolith units.

In both holes, there appears to be a mixing zone between transported and residual rather than a sharp boundary. This confirms findings from the ASD survey. In the Whirling-Dervish/Carosue Dam area, a small number of Zr or La analyses across a poorly defined unconformity could assist in better determining the boundary, particularly if combined with the KCI from an ASD survey.

6.11 Geophysical surveys

Tests using Time Domain Electromagnetic methods (TEM) and Refraction Seismic were completed to study their application for mapping regolith units, in particular the interface between transported and residual materials, and the fresh rock-regolith boundary. This work was by Ralf Kriege, as part of his MSc course work at Curtin University of Technology, Western Australia. The following three paragraphs are, with minor changes, extracts from his thesis, submitted in November, 2004.

Ten TEM transects across the Whirling-Dervish prospect with a 50 m x 50 m transmitter loop configuration show a resistive upper layer, approximately 5-10 m thick. Below is a fast transition into a 30-70 m thick highly conductive layer. The conductivity then decreases slowly to a basement value at depths of 60-100 m with a lower basement at the western part of each transect.

To further resolve the upper layers, 10x10 m and 20x20 m transmitter loop surveys were conducted. Results show that the surface layer (5-10 m) displays a high conductivity layer due to ferruginous materials. Both small loop datasets also display a deep high conductivity layer below the transported cover that was identified as saprolite.

A seismic refraction survey was conducted in the centre of the prospect, partly coinciding and parallel to the TEM lines. The refraction seismic data mapped the interface between colluvium and alluvium, indicating a depth of 2-10 m across the centre transect.

The results show TEM surveys are suitable as a first pass regional tool, designed to broadly distinguish between areas of shallow, medium and thick cover. TEM surveys also seem to provide reasonable estimates of the saprock-fresh rock boundary. On the other hand, the use of seismic refraction surveys with a weak shot signal appear less useful as the colluvium-alluvium boundary generally is of less interest to exploration than the transported cover-residual interface. A greater shot signal, e.g., by a thumper, may improve the depth reach and this warrants further work.

7. SUMMARY OF RESEARCH OUTCOMES

Whirling-Dervish – mineralogical studies

- Calcite veins and the calcite-rich matrix of the near surface calcified, hardpanized colluvium hosts Au.
- Kaolinite-rich saprolite just below the unconformity contain clasts of highly siliceous material, probably opal, that contain small inclusions of barite that are rich in Au (6.8-29 ppm). These need further investigation to identify their distribution both vertically in the profile and laterally in other drill holes.
- Hematite-rich veins that penetrate the clays deeper in the profile contain high concentrations of Cu, some reaching 10 000 ppm.
- Laser ablation ICPMS analysis using both transect and spot techniques, is a powerful method to determine the location of Au and pathfinder elements within the regolith.
- As the LA-ICPMS technique can supply isotopic analyses, it could determine the provenance of anomalies using Pb isotopes.
- The transported materials in the Whirling-Dervish area consist of red clays with magnetic nodules. Red clay contains a very fine grained (<200 nm) kaolinite fraction.
- In areas of shallow cover (<16 m), transported material overlies *in situ* saprolite and is readily distinguishable by colour and kaolinite crystallinity index (KCI).
- In areas of deeper cover, the transported material below about 16 m has undergone diagenetic transformation leading to (i) mobilisation and removal of iron oxides and (ii) dissolution of transported kaolinite and formation of more crystalline and stable kaolinite.
- The neo-formed kaolinite is more crystalline than transported kaolinite and therefore tends to mask the unconformity as determined by KCI.

Whirling-Dervish – geochemical studies

- In the Carosue Dam mine corridor, pedogenic carbonate (calcrete) is an effective regional (a few hundred metre spacing) surface exploration medium for Au. Gold concentrations of >20 ppb in calcrete corroborate the presence of the Whirling-Dervish ore body with an average of 28 ppb Au for all analyses (CRC LEME A/C drilling) of the one-metre intervals between 0 and 4 m depth. In contrast, the geometric mean for calcrete at the neighbouring Karari prospect is 60 ppb (Gray *et al.*, 2000).
- Biogeochemical sample media may assist in delineating drill targets within larger Au-in-calcrete anomalies using pathfinder elements such as Mo and Bi.
- Plants and possibly other biota (e.g., microbes) may play an important role in the formation of surface and near-surface anomalies. Plants could provide a mechanism of transporting Au and associated elements from the residual regolith to the upper part of the transported overburden. Depth to ground-water, thickness of the transported cover and the types of present and past vegetation are likely to control the extent and strength of any geochemical surface signature.

McGrath – geochemical studies

- In areas of thick transported cover, ferruginous materials, in particular magnetic detrital gravel beds at or near the base of the cover, may indicate the presence of a regional geochemical anomaly, e.g., Sb and As at McGrath. Ferruginous gravels near the base of transported cover, overlying Au mineralization in fresh rock, may also act as a sink for transported Au, Cd, Hg and other pathfinder elements. The near-basal gravels therefore not only carry a regional geochemical signature but also point to nearby bedrock mineralization.
- Selective sampling of ferruginous nodules and pisoliths, either by magnet or by manual separation after sieving, is recommended.

8. ACKNOWLEDGEMENTS

The project was logistically supported in a generous manner by Sons of Gwalia and we particularly acknowledge support by K. Watkins, D. Hammond, W. Witt and staff at the Karari and Tarmoola mine sites, in particular, I. O'Grady, I. Snell and B. Love. CRC LEME sponsored the project financially. R. Davis of the WA Herbarium assisted with plant identification. Professor P. Greerson of UWA assisted with plant collection and identification in the field. Both M. Pirlo and D.J. Gray reviewed drafts of this report. T. Naughton drafted several figures. W. Robertson took 3D photographs of the Karari pit and processed them using CSIRO Sirovision software. S. Rogers of CSIRO Land & Water investigated soil samples for microbes. A. Kepic of Curtin University supervised two students, R. Kriege and B. Bayat, who undertook geophysical fieldwork at one of the sites as part of their degrees. T.J Munday supported planning of the geophysical work. S. Welch and A. Usher of ANU, Canberra, sampled and appraised samples for microbial studies. M. Norman of ANU, Canberra, provided assistance with laser ablation ICP-MS. All this assistance is acknowledged with much appreciation.

9. REFERENCES

- Anand, R.R. & Paine, M. 2001. Regolith geology of the Yilgarn Craton, Western Australia: implications for exploration. *Australian Journal of Earth Sciences*, **49**, 3-162.
- Andersson, A., 1979. Mercury in soils. In: J.O. Nriagu (ed.), *Biogeochemistry of mercury*. Elsevier, Amsterdam, 79-106.
- Butt, C.R.M. 1988. Major uranium provinces: Yilgarn Block and Gascoyne Province, Western Australia. In *Recognition of uranium provinces*. International Atomic Energy Agency, Vienna. 273-304.
- Butt, C.R.M., Horwitz, R.C. and Mann, A.W. 1977. Uranium occurrences in calcretes and associated sediments in Western Australia. CSIRO Division of Mineralogy. Report FP16. 67p.
- Carr, G.R. and Wilmshurst J.R., 2000. Mercury. In: M. Hale (ed.), *Geochemical Remote Sensing of the Subsurface*. In: G.J.S. Govett (ed.), *Handbook of Exploration Geochemistry*, **7**.
- Geological Survey of Western Australia, 1998. Laterite geochemistry of the Yilgarn Craton and Albany-Fraser Orogen: digital data from CSIRO-AGE. Western Australia Geological Survey, Record 1998/8, 13p.
- Gray, D.J., Sergeev, N.B. and Porto, C.G., 2000. Characteristics of gold distribution and hydrogeochemistry at the Carosue Dam Prospect, Western Australia. CRC LEME – AMIRA Project 504. CRC LEME Report 121R / E&M Report 664R, Perth.
- Kriege, R, 2004. Determination of interfaces within the regolith using near surface geophysical and petrophysical methods at the Whirling-Dervish gold prospect, Western Australia. Report No.: GPM 1/04. Department of Exploration Geophysics, Curtin University of Technology, Western Australia, unpublished thesis, 100p.
- Lintern, M.J., 2002. Calcrete sampling for mineral exploration. In: X.Y. Chen, M.J. Lintern and I.C. Roach (eds): *Calcrete: characteristics, distribution and use in mineral exploration*. CRC LEME, Perth.
- Robertson, I.D.M. and King, J.D., 1998. Prospecting beneath colluvial-alluvial cover at Quasar in the Boogardie Synform – Mt Magnet, WA. Geological Society of Australia Abstracts No 49. (14th Australian Geological Convention, Townsville), 382.